

**POLITECNICO DI TORINO**

**Corso di Laurea Magistrale  
in INGEGNERIA MECCANICA**

Tesi di Laurea Magistrale

**Design with Additive Manufacturing of a  
steering knuckle in AlSi10Mg**



**Relatore**

Prof. Giovanni Belingardi

**Corelatori**

Dr. Mo Elbestawi (McMaster University)

Ing. Roberta Sampieri (FCA)

Ing. Carlo Carcioffi (Maserati)

**Candidato**

Antonio Suavo Bulzis

**A.A. 2019/2020**

*A chi c'è*

*E a chi avrebbe tanto voluto esserci.*

# Contents

1	Introduction .....	2
1.1	FCA - McMaster University – PoliTo Project .....	3
2	Materials and Methods .....	5
2.1	Additive Manufacturing .....	5
2.1.1	Advantages and disadvantages of AM.....	7
2.1.2	Selective Laser Melting (SLM) .....	9
2.1.3	AlSi10Mg.....	13
2.2	Topology optimization .....	15
2.3	Component Selection .....	19
3	State of art .....	46
4	Results .....	62
4.1	Preliminary Finite Element Analysis .....	63
4.2	Topology optimization of the complete component .....	78
4.3	Final Finite Element Analysis .....	82
5	Conclusions .....	101
5.1	Conclusions .....	101
5.2	Future developments .....	102
	Bibliography .....	103

# 1. Introduction

The objective of this master thesis is the study of a complete Additive Manufacturing (AM) engineering and production process of a metal automotive component. Every step in this work is aimed at demonstrating that this technology can be a competitive solution and it is almost ready to be included in the industrial production.

Additive manufacturing has significant advantages: higher complexity of geometries, shorter lead times and possibilities of weight reduction [1]. One major problem is often faced: adapting the component and the process for additive manufacturing. Thanks to topology optimization, it could be more convenient to produce this part with AM instead of traditional manufacturing.

Additive manufacturing is strongly linked with design because this technology allows freedom of design and costs and production times can be decreased [2].

Topology optimization is a mathematical method invented some years ago, [3] considered useful in a wide range of branches but in particular with the use of Additive Manufacturing because it could be used for designing complex geometries, with the help of modern software [4]. It is possible to recognize the advantages topology optimization and design changes bring, especially when there is a significant saving in decreasing the weight of the component (e.g. aerospace industry, automotive industry, medical industry).

Altair's HyperWorks or Inspire are the most used programs for optimizations (topology, shape, sizing). Some other software used are Abaqus-Tosca from Dassault Systèmes, NX Frustum or NX Nastran from Siemens, MSC Nastran from MSC Software, Ansys Mechanical from Ansys or Inventor from Autodesk.

The final purpose of this thesis is to highlight the advantages that AM could have in industrial production, focusing on the weight reduction of this automotive component in order to improve the performances of the vehicle and to decrease the fuel consumption.

The body of this thesis is made up of 5 chapters: chapter one provides a general introduction on AM and to topology optimization.

The second chapter contains a general description of additive manufacturing and, in particular, of Selective Laser Melting: this is the process the redesigned component is thought for. Once the production process is defined, this chapter explains the main characteristics of the Aluminum alloy

chosen for the manufacture of the component. Paragraph 2.2 explains in detail the theory of topology optimization, from the concepts to the mathematical theory. Paragraph 2.3 is focused on the initial component and to all steps of preprocessing, necessary to do in order to perform a FE analysis of the initial component and after a topology optimization.

The third chapter collects the experiences of other researchers about the necessity of a weight reduction.

The fourth chapter is organized in the following way:

- Preliminary Finite Element Analysis (FEA): the results of a preliminary FEA will be observed and commented in order to realize which kind of stresses the component is facing;
- Topology optimization of the complete component: the shape of the optimized component will be shown;
- Finite Element Analysis of the optimized component: the results of a final FEA will be shown in order to determine if the component can resist to the applied loads.

Finally, the fifth chapter shows the conclusion of this work and some hypotheses about future developments.

## 1.2 FCA - McMaster University – PoliTo Project

This master thesis is the result of a cooperation among three different institutions: Politecnico of Turin, McMaster University of Hamilton (Ontario, Canada) and FCA.

The main topic of this work is the redesign of an automotive component; in particular, this component belongs to the suspension assembly. Its redesign has been developed with the help of professionals of FCA and the research group of Prof. Elbestawi from McMaster University.

The software used for CAD modelling and modifications was Siemens NX 12.0 while, to perform Finite Element (FE) analysis ABAQUS CAE has been used and, thirdly, to perform the topology optimization Tosca has been used.

From a temporary point of view, this thesis has been divided in two periods:

- June/July 2019: component selection and CAD modelling and modifications at FCA PD EMEA AM Centre in cooperation with Maserati.
- September 2019/February 2020: redesign of the component at McMaster University.

## 2. Materials and Methods

### 2.1 Additive Manufacturing

Additive Manufacturing (AM), most commonly known as 3D Printing, was born in 1984, when Charles Hull first invented Stereolithography [5].

The original production technology known as Stereolithography uses a pool filled with a liquid photopolymer that solidifies with UV (Ultraviolet) laser beam through a process called photopolymerization [7]. Thanks to this process, it was possible, for the first time, to build the whole component layer by layer [7].

In 1987, Rapid Prototyping became a reality with the first commercially available AM machine in the world produced by 3D Systems [5].

Start-up DTM (now a part of 3D Systems) produced the world's first Selective Laser Sintering (SLS) machine only in 1992, using, instead of a liquid, a powder: this powder melted thanks to the energy provided by a laser source and, after the deposition, it solidified creating a solid component [5].

AeroMet developed, from 1997 to 2005, a process called laser additive manufacturing (nowadays known as Laser Beam Melting - LBM) that used a high-power laser and powdered titanium alloys [5].

More than one hundred of new processes were invented in the AM field only in the 21st century [8]. Most of their names are trademarks of different machine manufacturers. At the beginning this technology was far from perfection, but the idea of manufacturing something without the constraints of the traditional manufacturing technologies, only having its STL (Standard Triangle Language) file was revolutionary [9]. STL file describes only the surface geometry of a three-dimensional object without any representation of colour, texture or other common CAD attributes [10]. They only state the coordinates of triangular surfaces vertexes and their normal, according to a Cartesian coordinate system [10].

During the following years, different types of Additive Manufacturing technologies were born [8]. Each kind has its own advantages and disadvantages, but the most important advantage consists in adding material instead of eliminating it with machining. Figure 2.1 shows the essential steps of

the process to follow in order to obtain a tangible object from a 3D model with Additive Manufacturing technology.

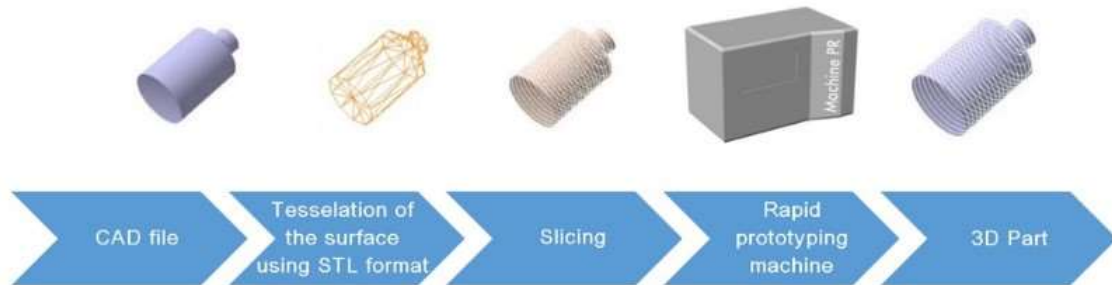


*Figure 2.1 – Additive Manufacturing steps [6].*

The first important use of this technology was prototyping: it was faster than the traditional way, but at the beginning it was too much expensive because machinery was patented [11]. With time, there were a lot of innovations that helped the development of these technologies, so prices became more affordable and, at the same time, the accuracy of products increased [8].

Nowadays, it is possible to print in many different materials, still a short list when compared to all the materials available for the traditional manufacturing. However, the main materials can be identified by dividing them into different classes: metallic, polymeric and ceramic materials. For what concern metals, the set of common commercially available alloys is essentially limited to pure Titanium, Ti6Al4V Titanium alloy, 316L stainless steel, 17-4PH stainless and 18Ni300 maraging steels, AlSi10Mg aluminum alloy, CoCrMo 625 and Nickel based superalloys Inconel 718 and Inconel 625 [12]. Obviously, the AM processes are studied all over the world in order to prepare other alloys with the aim of decreasing costs and increasing mechanical properties.

Polymers are considered the most common materials in the 3D printing industry due to their diversity and ease of adaption to different 3D printing processes. Polymers for additive manufacturing are found in the form of thermoplastic filaments, reactive monomers, resin or powder [13]. Among polymeric materials there are ABS, Polyamide, PEEK, PMMA, Polycarbonate, ULTEM, Polyphenylsulfone and Filled PA [14].

It is also possible to print ceramic materials such as Alumina, Mullite, Silicon Carbide, Zirconia, Plaster and Graphite [14]. There are also a few organic materials as waxes and tissue or cells [14].

The main reasons why AM technologies developed so quickly are:

- AM allows industries the possibility to produce a prototype for completely new products: in this way they can test the component and realize how convenient it is;
- AM gives the possibility to produce highly complex and highly performance pieces, thanks to the layer-by-layer deposition process;
- AM gives the possibility to have a full customization of every product.

As reported in literature, AM techniques for metal parts manufacturing can be summarized in two main parameters:

- input raw material: metal powder or wires;
- energy source: laser/electron beam or arc.

It is also possible to classify AM techniques as:

- Powder Bed Fusion based technologies (PBF): powder is spread on the building plate in order to be melted partially or totally by the laser;
- Directed Energy Deposition (DED): while the deposition nozzle is working, an energy source melts the powder or the wire. The most common technologies are Direct Metal Deposition (DMD) and Laser Engineered Net Shaping (LENS).

### 2.1.1 Advantages and disadvantages of AM

AM offers a wide range of advantages but also some disadvantages; there are a lot of pros and cons that need to be considered, when comparing this technology to the conventional one.

Considering the quick development of AM, it is possible that in the future the pros will increase, and the cons decrease. This development will make this technology attractive even to industrial businesses where it is considered inconvenient nowadays. The main advantages of AM comparing to conventional manufacturing are:

- Complex design: there are no constraints linked to design. In fact, it is possible to design every kind of shape, including complex geometries, hollow shapes and undercuts. Obviously, this complexity in design does not represent an additional cost since all the costs are related to the volume of the component;

- Simpler process: this technology takes only one step to manufacture a certain component and all the process is automatized, so it needs an operator just for the setup and post-processing phases. Compared to AM, conventional manufacture may take more processes in sequence and it may need an operator for each of them.
- Customization: one of the most important advantages is the customization. With AM it is possible to customize the components according to the customer's needs.
- Multi material component: with some processes it is possible to combine different materials in a single printing thanks to specific nozzles. This is an important advantage because it is possible to create multi material components that can be used in different industrial applications, decreasing the cost of assembly and maintenance.
- Single machine: AM needs a single machine to manufacture a high number of components even with different shapes, while with conventional manufacturing it is necessary to organize a new production chain for different components.

The major limitations to AM, compared to the traditional manufacturing processes, are:

- Low speed: AM can be considered slower when compared to conventional manufacturing, even if AM needs less planning and setup time;
- Less accuracy: due to layering process, the superficial roughness may not satisfy the customer's requests. In these cases, it is necessary a post-processing operation;
- Limited volume of the component: this limitation is referred to all the processes where the machines have a building chamber. In fact, in these cases, the volume of the component to be manufactured is limited by the size of the building chamber;
- Defects: in addition to the worst surface finishing, there is a wide range of defects that can be faced with this technology. In fact, cracks and voids may be found inside the components. Of course, it is possible to limit the presence of these defects with some techniques (e.g. preheating of the building plate, where possible). Furthermore, there might be the problem of the component anisotropy or the not perfect bondage of two adjacent layers;
- Materials: there is not a wide range of available materials and the cost of materials is still high. This is clearly a disadvantage in comparison with the conventional manufacture, where it is possible to use almost all the materials:

- Higher system costs: all the available machines have, at present, a high cost. Due to the development of this technique, prices might drop.

After having considered all the advantages and disadvantages of AM, we can say that the only real advantage that makes it more convenient than conventional manufacturing is the complexity of the geometry; when the geometry is very complex, using AM is advisable.

### 2.1.2 Selective Laser Melting (SLM)

The Selective Laser Melting process belongs to the class of powder bed fusion technologies; it uses a high intensity laser as an energy source to melt and fuse selective powders, layer-by-layer, according to the .STL (abbreviation of “stereolithography”, lossy file format) file. The .STL representation of the solid model is no longer a mathematical equations, but it is a surface geometry made by triangular elements, called facets. Each facet is defined by three vertices and a normal vector. Each closed set of facets includes a shell, and multiple parts can be represented inside a .STL file by including multiple shells. Of course, this kind of file does not have a volumetric information [6].

SLM process can be divided in several steps: except the first and the last steps, the process is automated:

- CAD data are uploaded to the SLM machine in order to manufacture the component;
- STL file is processed by specific software to provide the appropriate support structures in order to avoid any kind of failure during the printing phase and to generate slice data for laser scanning of every layer;
- Lay of the first thin layer of metal powder on the building plate in the building chamber;
- Use of the high energy density laser to melt and fuse specific zones of the powder thin layer according to the input STL file;
- Move downward the building plate to lay a new layer of powder on top and then to scan the new layer with the laser.
- Step repetition until the component is manufactured;

- Loose powder removal;
- Component separation from the building plate (manually or with EDM).

In figure 2.2 the steps of this process are shown.

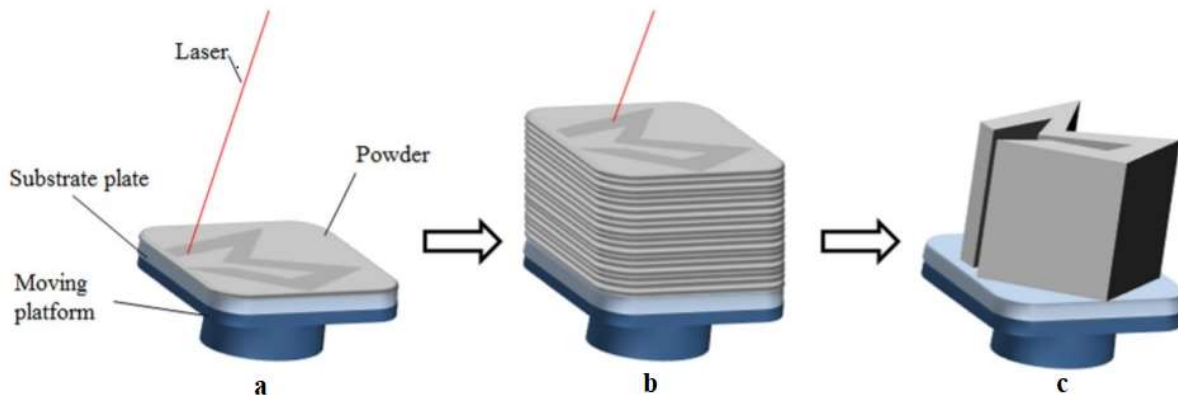


*Figure 2.2 – Concept of SLM process. (a) High-power laser melts selective areas of the powder bed. (b) Process is repeated for successive layers. (c) Loose powder is removed, finished part is revealed [15].*

This process may present different problems because of the use of metal powders:

- High conductivity of metals;
- Rapid oxidation;
- High reflectivity of metals when hit by the laser.

Due to these problems, it is preferred to use Nd – YAG or fiber laser than CO<sub>2</sub> laser, in order to have a higher absorptivity of emitted energy.

There are several process parameters. They can be classified in those depending on the machine and those depending on the powder. In the first class, the main process parameters are:

- Laser power;
- Scanning speed;

- Hatch spacing;
- Layer thickness.

In the other class there is only one parameter that is the absorptance of powder to the laser irradiation.

All these parameters affect the volumetric energy density that is available to heat up and melt the powders. Moreover, there are other two parameters that need to be taken into account:

- Heat capacity;
- Latent heat.

These two parameters are heavily dependant on the material and on the mass to be melted [15].

During the entire process, the building chamber is filled with an inert gas; it could be nitrogen gas or argon gas in order to provide an inert atmosphere to protect the component from the oxidation.

Some machines can provide pre-heating to the substrate plate or to the building chamber.

The thickness of the layer can range between 20  $\mu\text{m}$  and 100  $\mu\text{m}$ ; in this way it is possible to have an effective control on the resolution and build tolerance.

The mechanical properties result even better than those obtained through more traditional processes, since it is possible to use single phase metallic powders without the addition of organic binders or elements with low melting point. High cooling rates are achieved (103-108 K/s) in the melting pools. In this way, the crystalline grains do not have time to grow and a very fine microstructure is obtained. There is anisotropy of mechanical properties because of the crystals grow along the direction of heat flow. Moreover, the reached densities are often close to the theoretical values (99.5-99.8%) [16].

The SLM process is used to make component with complex geometry, with thin walls and empty spaces. Obviously, to manufacture complex component it is necessary to have support structures. In this process, it is possible to have only supports made of the same material of the component; the need to eliminate the supports makes the post-processing more time-consuming and more expensive economically.

This technique is not appropriate to a big volume of production; usually it is better to limit the number of components to manufacture.

There are several materials that can be used with SLM process: different metals and alloys, including stainless steel, nickel-based super alloys or cobalt-based super alloys and light alloys. Among the light alloys the most used are titanium alloys such as Ti6Al4V, aluminum alloys like AlSi10Mg and Maraging steel. EOS, one of the most important producer of AM machines, focuses the attention on aluminum alloys. These aluminum alloy components find many applications in automotive and aeronautic fields [17].

Since not all the powder is used during the process, it is possible to recycle this powder. This represents a huge saving from an economic point of view. Despite this, it is necessary to recycle in a reasonable way: in fact, the recycled powder has been subjected to a thermal history, so its mechanical properties may have changed. Due to this, it is necessary to adopt a reasonable proportion of new powder and recycled one.

It is possible to make a comparison between traditional manufacturing techniques and SLM process: SLM shows a higher cost per part (mostly because it is a time-intensive process), so it is advisable if only very few parts are to be produced. Traditional techniques, instead, show higher set-up costs.

### 2.1.3 AlSi10Mg

The aluminum alloy AlSi10Mg is a widely used alloy for aluminum castings. The hypoeutectic alloy is near the eutectic composition (12.5% Si) which is responsible for the excellent casting properties. In Figure 2.3 the phase diagram of Al–Si is shown. The red line corresponds to the adopted alloy composition. Minor additions of magnesium (0.3–0.5% are most beneficial) allow hardenability by natural or artificial ageing [18]. Table 1 reports the typical chemical composition of the AlSi10Mg alloy.

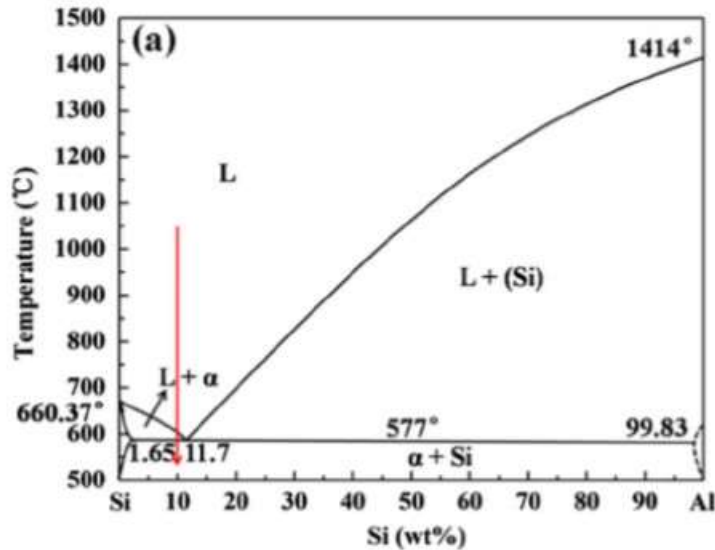


Figure 2.3 – Phase diagram of Al-Si [14].

Al	Si	Fe	Cu	Mn	Mg	Zn	Ti
Balance	9.0-11.0	0.3	0.03	0.001-0.4	0.2-0.5	0.1	0.15

Table 1 – AlSi10Mg Chemical Composition.

The material is used as a powder. The particle size of the AlSi10Mg is in the range of 25-45  $\mu\text{m}$ .

The AlSi10Mg is a hypoeutectic alloy and it is considered convenient for AM processes because of its internal characteristics. Furthermore, this alloy has a good castability and a small solidification temperature range.

The main average mechanical properties, referred to the “As Built condition”, are:

- Young’s Module:  $E = 75 \text{ GPa}$ ;
- Yield strength:  $\sigma_y = 240 \text{ MPa}$ ;
- Poisson ratio:  $\nu = 0.33$ ;
- Density:  $\rho = 2.67 \text{E-6 kg/mm}^3$ ;
- Fatigue endurance limit (R=-1):  $\sigma_F = 160 \text{ MPa}$ .

The mechanical properties are provided by the website of EOS Gmbh [19].

## 2.2 Topology optimization

The optimization field concerns everything related to the research of an optimum solution with computational methods. Generally speaking, there are three different kinds of methodologies, that are adopted according to the type of design problem:

- Topology optimization;
- Size optimization;
- Shape optimization.

In this work topology optimization has been used, taking into account that the considered design problem is to redesign the assigned component for additive manufacturing; in fact, the result obtained from this technique is a piece with a very complex geometry, almost impossible to manufacture with conventional manufacturing.

Topology optimization is a well-established numerical design methodology. This method is most famous for its ability to generate lightweight mechanical components for the automotive and aerospace industries [21].

The optimization works by iteratively redistributing the available material converging towards a better solution [21], the solution is calculated without violating constraints. Setting a topology optimization problem requires, as a preliminary data, the definition of a design domain [20]. This domain must have a definite shape and it represents the space within which the structure is bound to exist [20]. The definition of load and constraint conditions completes the definition of the problem [20]. The optimization process leads to the identification of the material optimal location, looking for the configuration characterized by minimum weight, in order to avoid waste of material and, contemporary, to give the correct shape that is strictly indispensable [20]. In figure 2.4 a topology optimization design problem is shown.

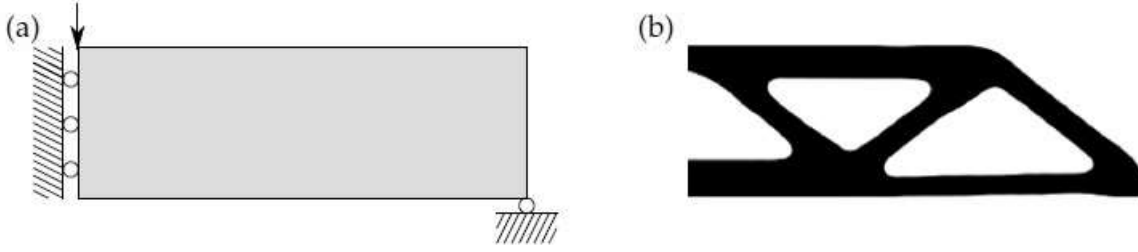


Figure 2.4 – Example of topology optimization design problem. (a) Design domain, including applied loads and constraints, (b) Optimized design [21].

Once loads and constraints are defined, there are other two parts that need to be defined:

- Objective function: this states the targets that must be achieved. For structural optimization problems, the most common are weight, displacement or stresses [20];
- Design variables: parameters whose can be varied within a defined range [20].

The application of optimization methods on structural field involves the use of objective functions and constraints defined basing on state variables of the analyzed structure [20]. The evaluation of state variables and, indirectly, of the abovementioned functions, is generally assigned to finite element numerical codes [20]. With every modification of the structure proposed by the optimization method, the finite element code evaluates its new state and the optimization process guides the solution toward the targets [20]. In this way, a too large number of infinitesimal voids are created inside the structure and it follows that more design variables per element are required than when using the density method. Moreover, one important limitation of this approach, is that can be applied only using the compliance as a constraint or cost function [32].

In this way it is possible to penalize these intermediate densities through the Solid Isotropic Material with Penalization (SIMP) method; the SIMP model was developed with the aim of reducing the complexity of the homogenization approach, improving the capability of the algorithm to reach the convergence with a solution made only by 1 and 0 densities.

The design variables  $x$  are collected in the vector  $x$ . These design variables are related to variables  $\rho$ , i.e.  $\rho = \rho(x)$ . The latter variables will be called the filtered variables and they can be considered physical variables, as they define the stiffness and enter the mass calculation. The equilibrium equation in terms of stiffness for a design  $\rho(x)$  is shown in Eq. 1.

$$K(\rho(x))u = F \quad (1)$$

Where  $\mathbf{K}(\rho(\mathbf{x}))$  is the global stiffness matrix of the structure,  $\mathbf{u}$  is the vector of global nodal displacements and  $\mathbf{F}$  is a vector of known external loads.

There is another way to write Eq. 1 where the displacement vector is seen as a given function of the design variables and it solved for in the finite element analysis [23]. For a given design  $\rho(\mathbf{x})$  and for an invertible stiffness matrix, the displacement vector is calculated as shown in the Eq. 2.

$$\mathbf{u} = \mathbf{u}(\mathbf{x}) = \mathbf{K}^{-1}(\rho(\mathbf{x}))\mathbf{F} \quad (2)$$

Obviously, there are several formulations for the topology optimization problem; the one used in this work is the stress constraint formulation. Eq. 3 shows the mathematical approach to the problem.

$$(\mathbb{P}_1) \begin{cases} \min \sum_{e=1}^{n_e} m_e \rho_e(\mathbf{x}) \\ \text{s. t. } \begin{cases} \sigma_i^{PN}(\mathbf{x}) \leq \bar{\sigma}, \quad i = 1, \dots, n_c \\ \mathbf{x}_e \leq \mathbf{x}_e \leq \bar{\mathbf{x}}_e, \quad e = 1, \dots, n_e, \end{cases} \end{cases} \quad (3)$$

Where:

- $n_e$  is the number of design variables, typically the number of elements in the design space;
- $m_e$  is the solid element mass for the element related to design variable  $e$ ;
- $\rho_e(\mathbf{x})$  is the  $e$ :th filtered variable;
- $\mathbf{x}_e$  is the  $e$ :th design variable;
- $\bar{\mathbf{x}}_e$  is the upper limit of  $\mathbf{x}_e$  and its value is 1;
- $\mathbf{x}_e$  is the lower limit of  $\mathbf{x}_e$  and its value is  $\varepsilon$ ;
- $\varepsilon$  is a small positive number used to avoid the stiffness matrix becoming singular;
- $\sigma_i^{PN}(\mathbf{x})$  is a modified P-norm based on Von Mises stresses for cluster number  $i$ ;
- $n_c$  is the number of clusters or constraints;
- $\bar{\sigma}$  is the stress limit.

In order to create a black-and-white structure, a penalization factor is introduced that makes intermediate design variable values expensive.

The SIMP penalization function,  $\eta_K(\rho_e(x))$  is inserted when the global stiffness matrix  $\mathbf{K}(\rho(x))$  is assembled from the solid material element stiffness matrices  $\widehat{\mathbf{K}}_e$  as shown in Eq. 4.

$$\mathbf{K}(\rho(x)) = \sum_{e=1}^{n_e} \eta_K(\rho_e(x)) \widehat{\mathbf{K}}_e \quad (4)$$

The SIMP penalization function is given by the Eq. 5.

$$\eta_K(\rho_e(x)) = (\rho_e(x))^q \quad (5)$$

Where  $q > 1$ ; in this case the intermediate densities are penalized and hence 0-1 solutions are favored. Usually a value as 3 is set for this penalization factor [22].

Figure 2.5 shows the SIMP interpolation scheme. As it can be noted, the densities are linked to the penalization parameter  $q$ , and it shows that the use of SIMP model forces the topology design to stay toward the values 0 and 1.

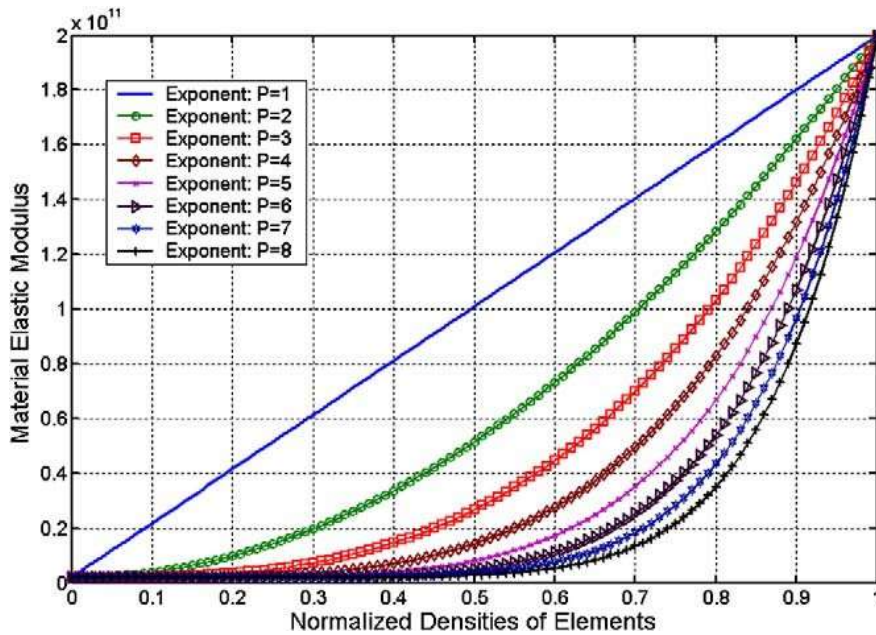


Figure 2.5 – SIMP interpolation scheme.

## 2.3 Component Selection

AM processes need a properly conceived evaluation in order to select the suitable component. Maserati gave FCA PD EMEA AM Centre an appropriate part for this thesis project.

The chosen part is an anterior mounting or steering knuckle of a suspension. This component is a part which contains the wheel hub and bearings and attaches through the steering arm the steering mechanism component to the suspension. In figure 2.5 an example of steering knuckle is shown.



*Figure 2.6 – Example of a steering knuckle.*

The main advantage expected from the use of additive manufacturing for this part is to reach a lower weight without losing the structural properties.

Performing a topology optimization can be advantageous for this component because of its high potential for weight reduction. It can lead to a reduction of weight of the entire vehicle, considering that there are four mounting in a car. To produce this component in AM can bring advantages on the whole system with the reduction of fuel consumption and CO<sub>2</sub> emissions.

Figures 2.7, 2.8, 2.9 and 2.10 show the entire volume of the original part, modeled with Nx Siemens; using AlSi10Mg, the total weight of this component is 23.6 kg.

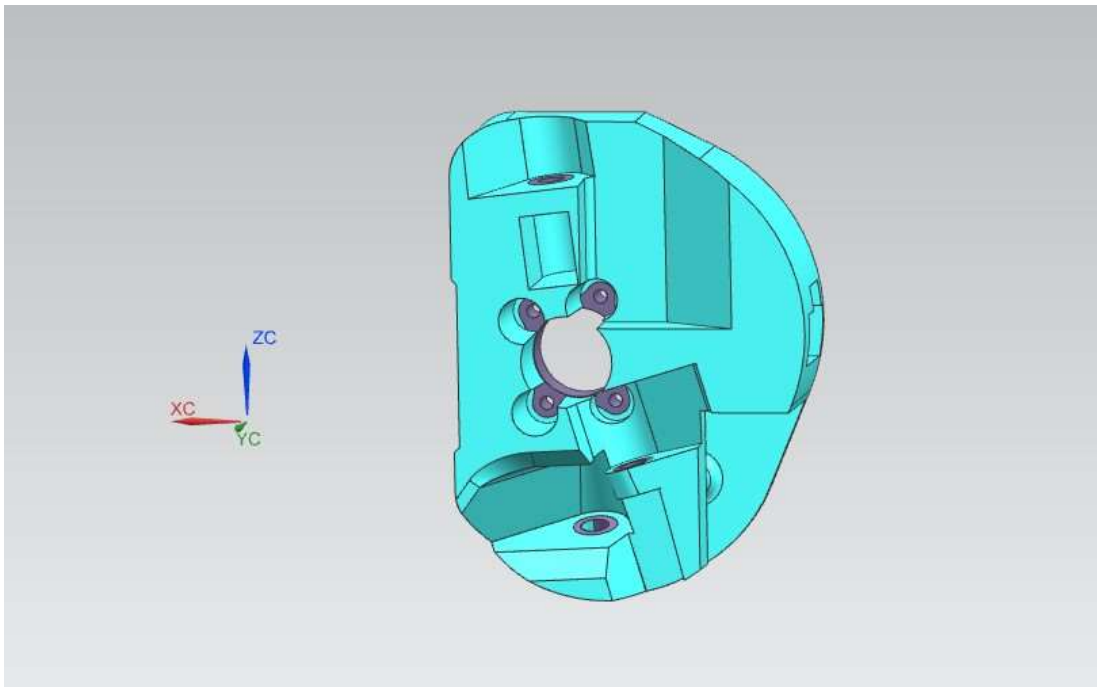


*Figure 2.7 – Original component entire volume, view 1.*

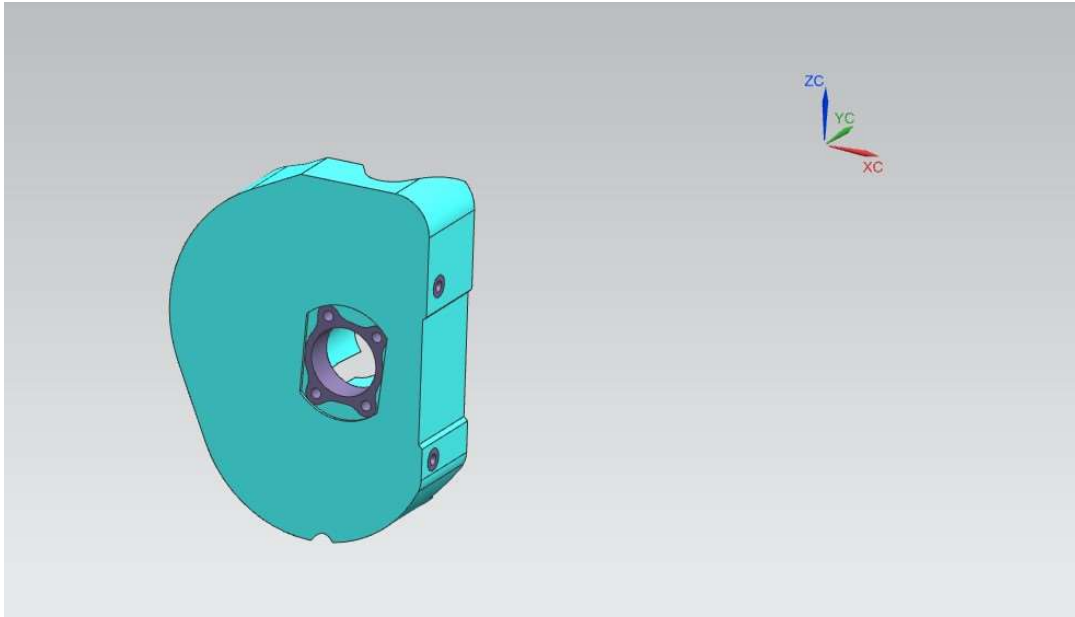


*Figure 2.8 – Original component entire volume, view 2.*

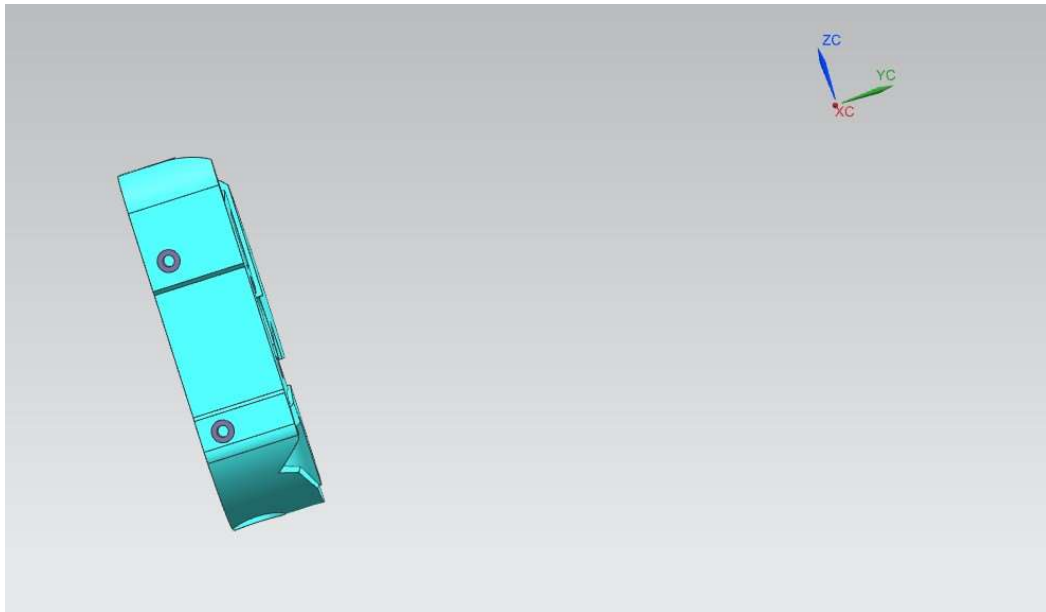


*Figure 2.9 – Original component entire volume, view 3.*

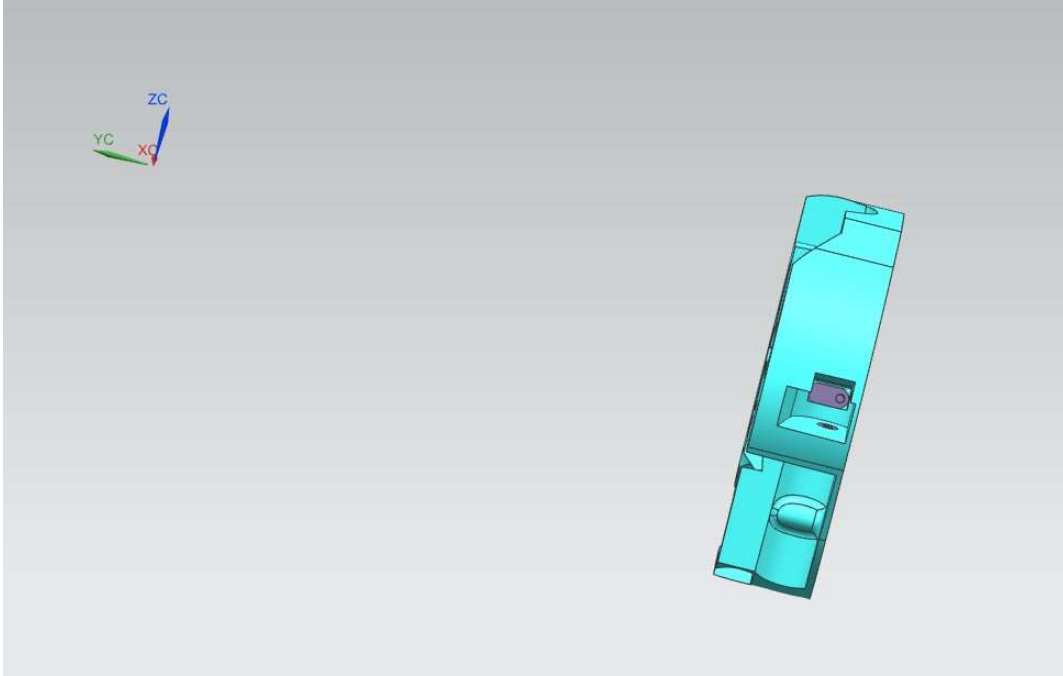


*Figure 2.10 – Original component entire volume, view 4.*

It is possible to identify two different parts: the green part represents the volume to be optimized, while the grey parts are the non-design spaces, i.e. the not editable parts of the component. In figure 2.11 the non design spaces are represented. From now on, the design space might also be indicated as “central part”.

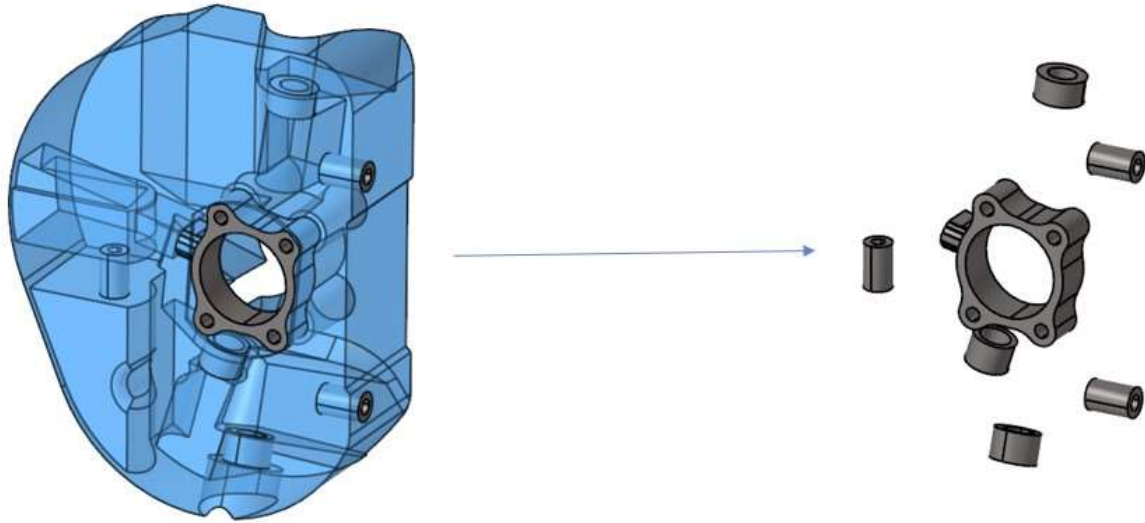


*Figure 2.11 – Design space and non design space.*

From now on, the software Abaqus was used to perform the FE analysis and achieve the final results of this work.

Abaqus/CAE is an application software used for both modelling and structural analysing of mechanical components and assemblies and visualizing the FEA results; it means that it is possible to use this software both for pre-processing and for the post-processing.

There is a drop-down menu where there are several modules:

- Part module: it is possible to create or to import different parts. A part can be defined as a building block of an Abaqus/CAE model. Each part can be modified with the tools provided by the software;
- Property module: it is possible to define materials. Once the material is defined, it is possible to create a “section”, which contains information about the properties of the materials assigned to a part or to a part region;
- Assembly module: it is possible to assembly each part from the model in order to define a global coordinate system. In this way every part will be positioned according to the global coordinate system;

- Step module: it is possible to create analysis steps and to specify output requests, adaptive meshing and analysis controls. The most used function is the creation of analysis steps, where a sequence of one or more analysis steps are defined;
- Interaction module: it is possible to set different types of interactions and constraints.
- Load module: it is possible to define loads, boundary conditions, predefined fields and load cases;
- Mesh module: it is possible to generate meshes on parts and assemblies;
- Optimization module: it is possible to create optimization tasks, defining as well objectives and restrictions of the topology optimization;
- Job module: it is possible to create and manage analysis. It is also possible to check the status of one job while it is still running;
- Visualization module: it is possible to see graphically the results of the finite elements analysis or the topology optimization results;
- Sketch module: it is possible to create sketches that can be used in different ways.

In this thesis, almost all of them were used.

Once the geometry of the original part was provided, the .STL file was imported in Abaqus/CAE. It can be observed that the geometry is very complex. In fact, a geometry simplification of the component was needed.

## PART MODULE

In the part module it is possible to use several tools in order to change the geometry, avoiding warnings and errors in the part model. In figure 2.12 the modified geometry is shown.

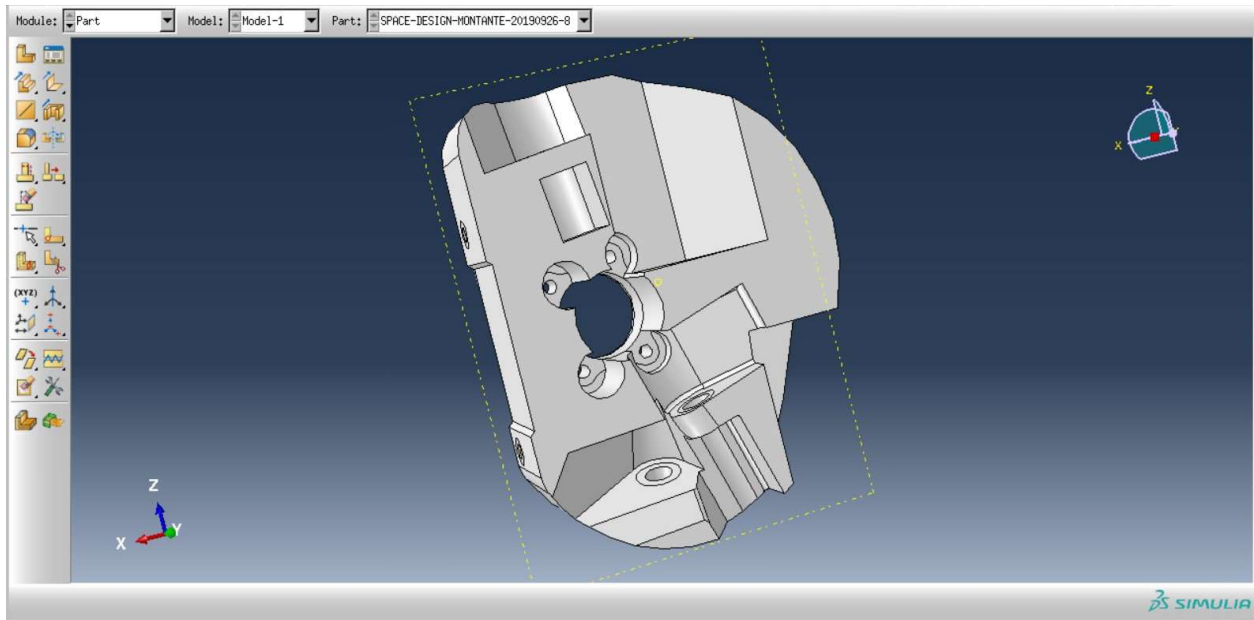


Figure 2.12 – Modified geometry, view 1.

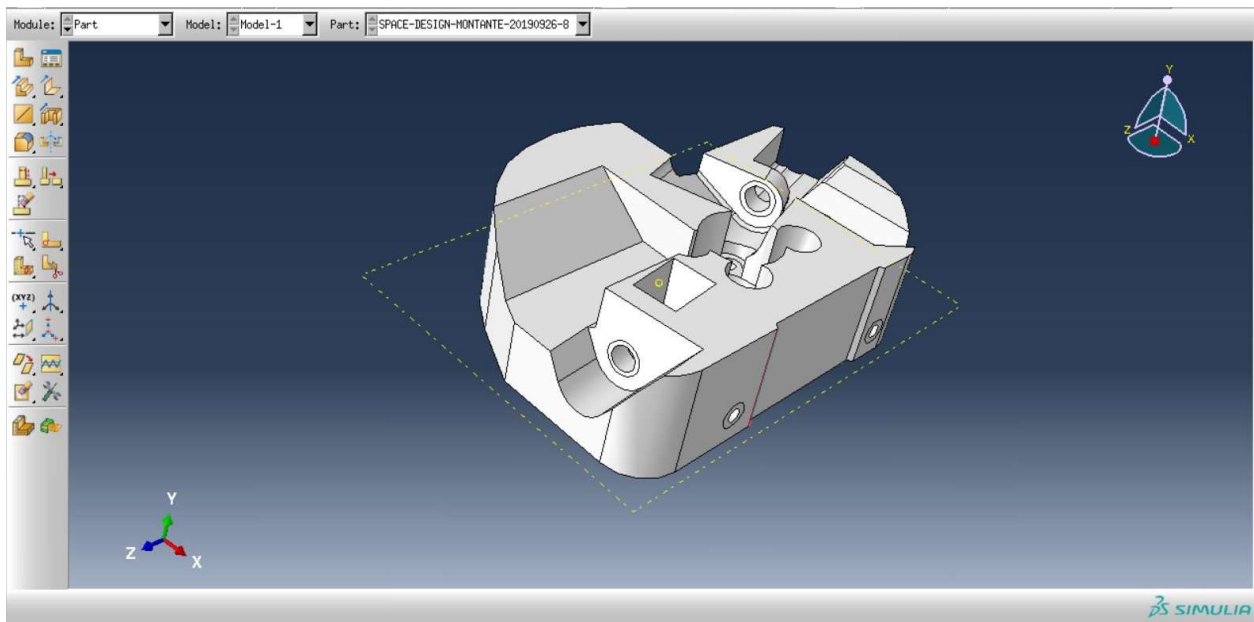
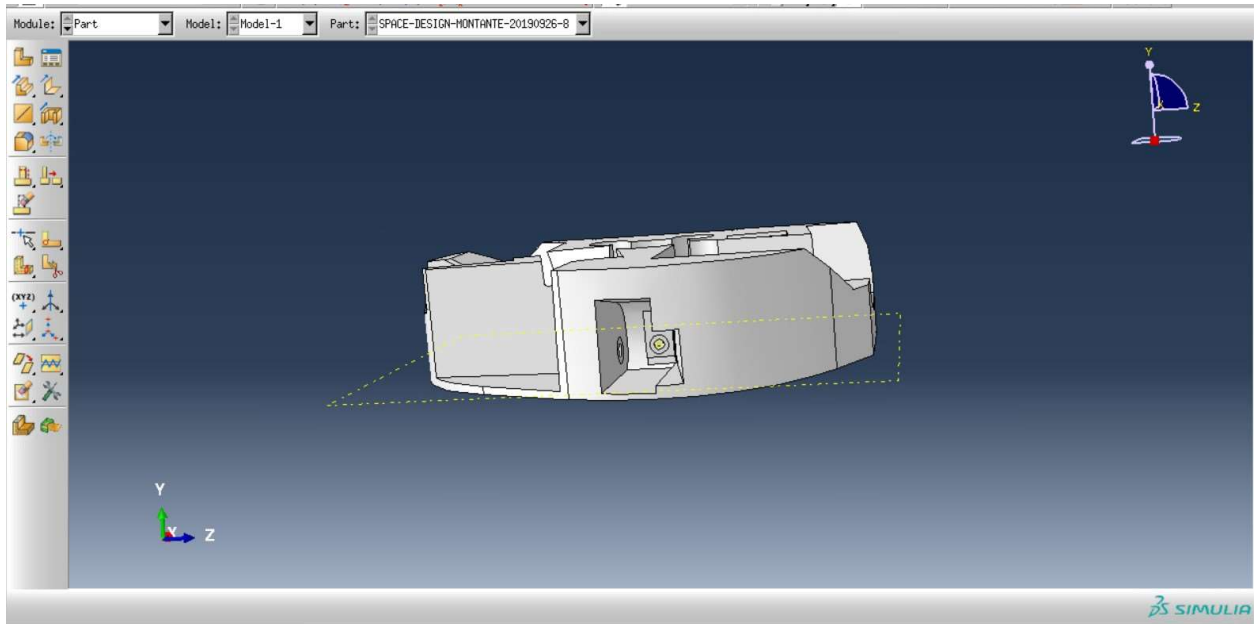
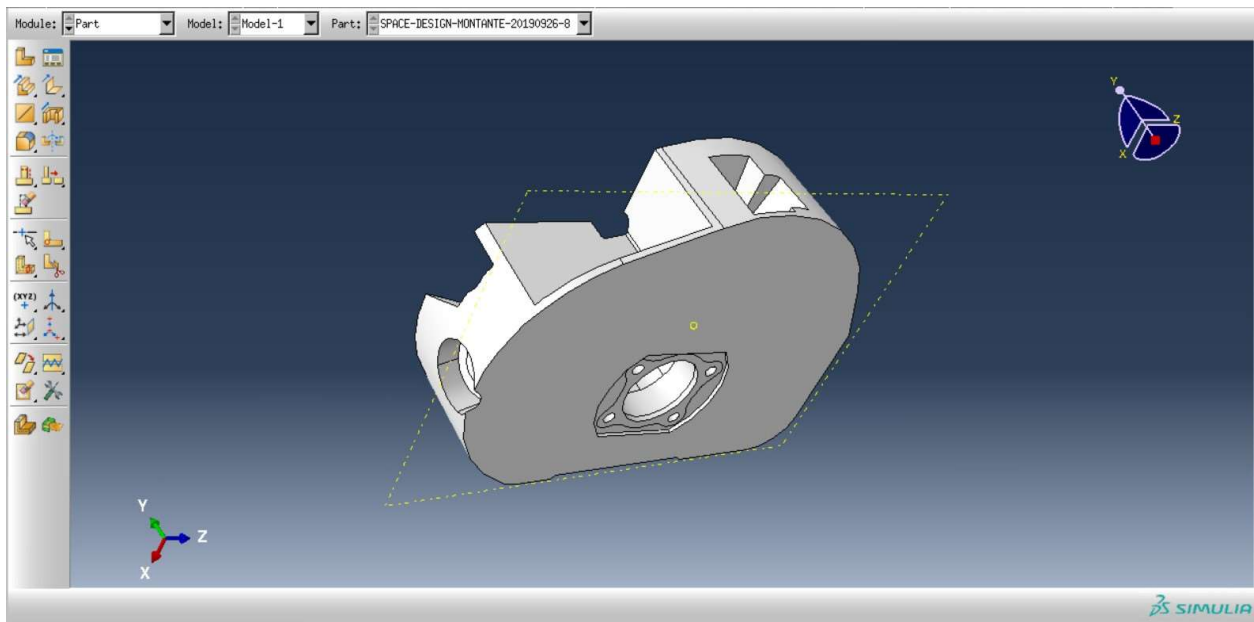


Figure 2.13 – Modified geometry, view 2.



*Figure 2.14 – Modified geometry, view 3.*



*Figure 2.15 – Modified geometry, view 4.*

In figures 2.12, 2.13, 2.14 and 2.15 it is possible to observe that all the bushings have been obtained directly from the biggest part of the component. The geometry is thus less complex because, in this way, the constraints among bushings and central part were avoided. This

expedient decreases the computational cost; in fact, the software will have to solve less equations. Furthermore, other parts were modified in order to make the component as simple as possible, without changing the main aspects.

## PROPERTY MODULE

In the property module the material was defined. Since the topology optimization works only with the linear characteristic of the material, Abaqus CAE needed just a few data: density, Young's modulus and Poisson's ratio, all of them have been reported in Chapter 2.1.2. After that, it was necessary to create a section. In figure 2.16 the section card is shown, selecting the red circled icon in the menu.

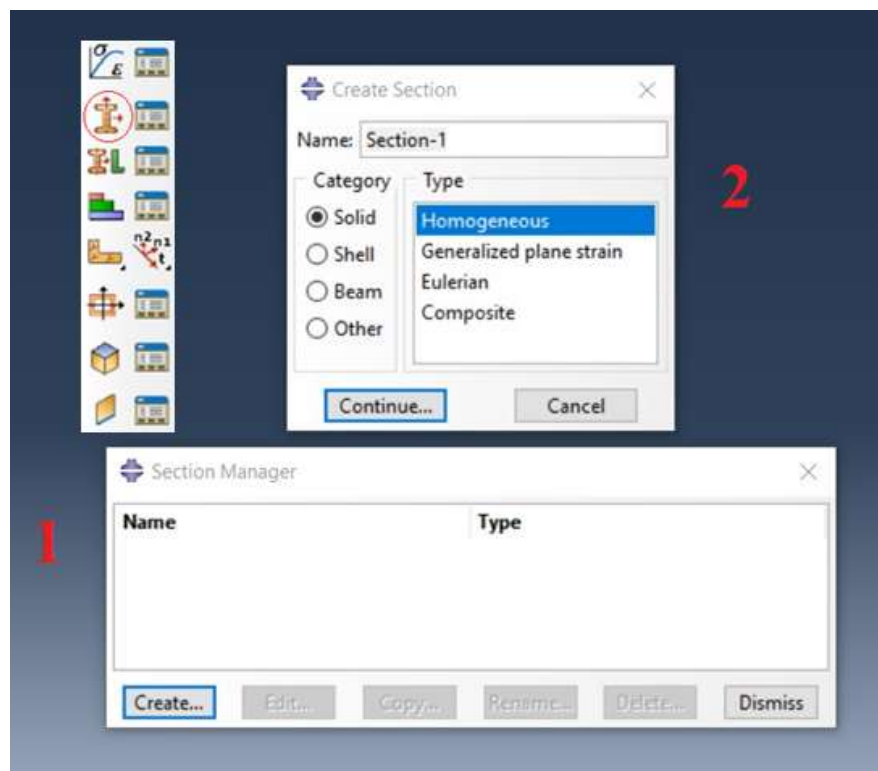
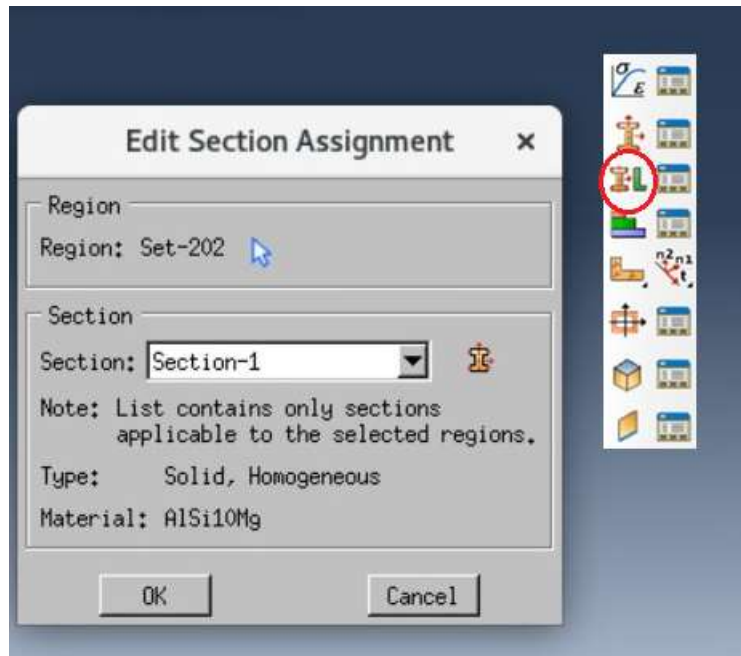


Figure 2.16 – Steps to follow in the section assignment.

As it is shown in the figure 2.16, in the step 1 the software asks for a name of the new section and in the step 2 it asks for a category and type. In this thesis work a Solid Homogeneous section has been chosen.

After that, the material (in this case AlSi10Mg) is assigned to the section.

Finally, the section is assigned to the part. In Figure 2.17 the assign section card is shown, selecting the third icon in the menu.



*Figure 2.17 – Section Assignment Card.*

## ASSEMBLY MODULE

In this case there is only one part in the assembly, so the central part with all the bushings integrated has been assigned to the assembly.

## STEP MODULE

In this thesis work FCA provided several steps for different tests. The provided loading conditions were:

- Fatigue loading conditions;
- Buckling;
- Braking.

Each one of them has been defined with loads, constraints and limits. The fatigue loading conditions are shown in Table 2.

1. Stabilization #2	8. Bump	15. ax+ay 3
2. Vertical load 1	9. Rebump	16. ax+ay 4
3. Vertical load 2	10. Acceleration 1	17. ax+ay 5
4. Cornering 1	11. Braking 1	18. ax+ay 6
5. Cornering 2	12. Braking 2	19. ax+ay 7
6. Cornering 3	13. ax+ay 1	20. ax+ay 8
7. Cornering 4	14. ax+ay 2	

*Table 2 – Fatigue loading conditions.*

In Figure 2.18 the step creation card is shown. The relative icon is circled in red.

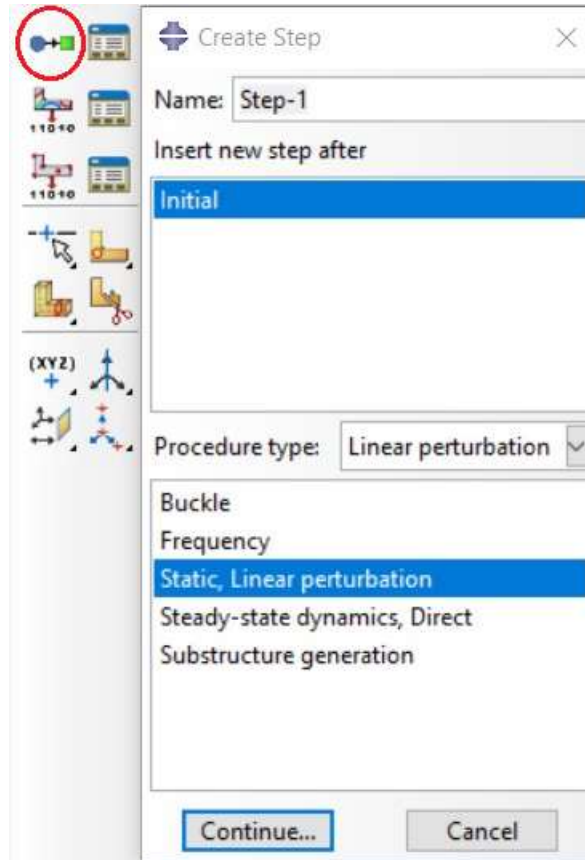


Figure 2.18 – Create step card.

In this module twenty-two steps have been defined. Each one of them has been defined as a static linear perturbation step with a direct method of resolution.

After that, a field output and a history output have been created in order to visualize stresses and displacements at the end of the optimization.

#### INTERACTION MODULE

In this module, several couplings have been created according to what FCA requested. In fact, all the loads have been applied on different points external to the component because, theoretically, the load is applied on the physical coupling and then transferred to the bushing, not directly on the bushing. In this way the situation described has been recreated.

The reference points have been created using the tool circled in red in Figure 2.19.

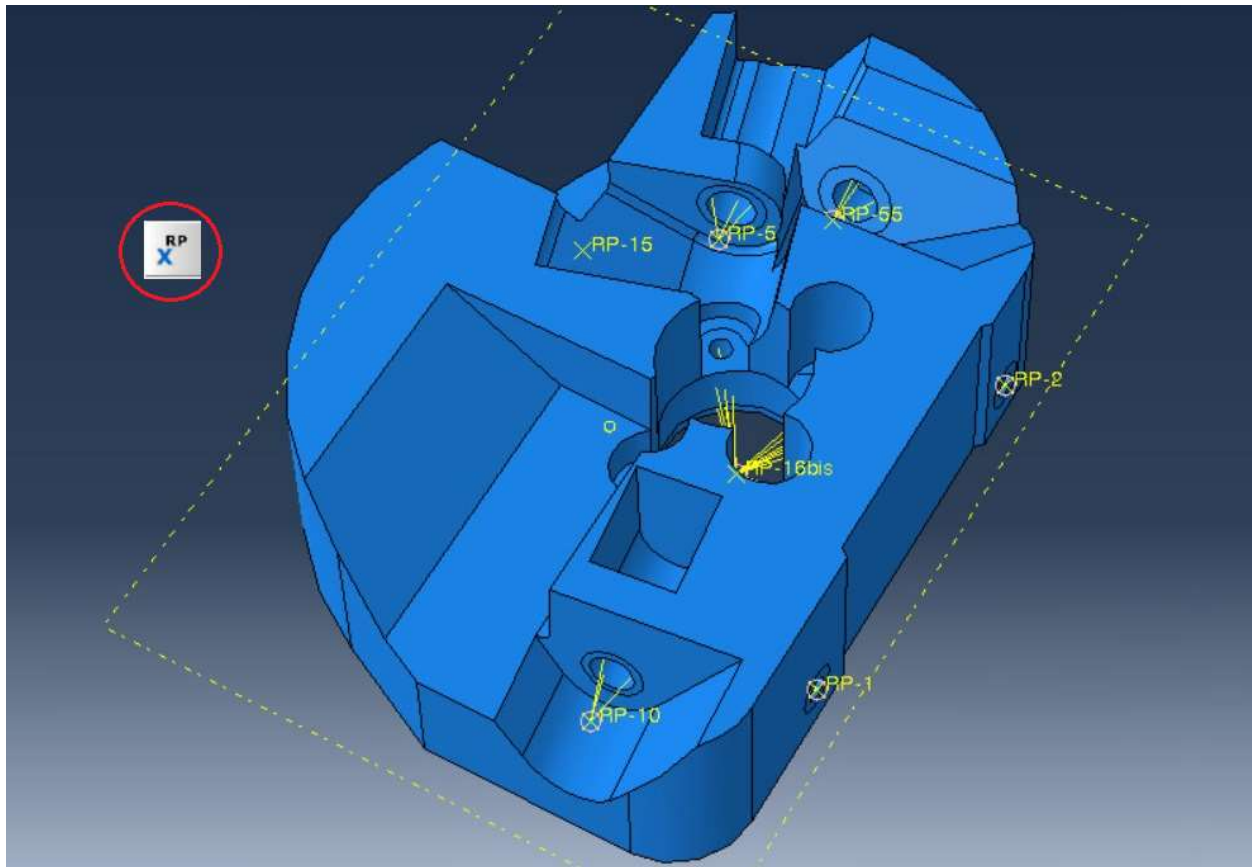


*Figure 2.19 – Representation of reference points.*

There are 8 different reference points with different purposes:

- Point 5 and 55: linked to the bushing where the inferior arm of the suspension is located;
- Point 15: linked to the bushing where the steering arm is located;
- Point 10: linked to the bushing where the superior arm of the suspension is located;
- Point 1 and 2: linked to the bushing where the brake caliper is coupled;
- Point 16 and point 16bis: linked to the bushing where the bearing housing is located.

Each point is related to the internal surface of the bushing with a “coupling” connection. In figure 2.20 the coupling card is shown, selecting the red circled icon.

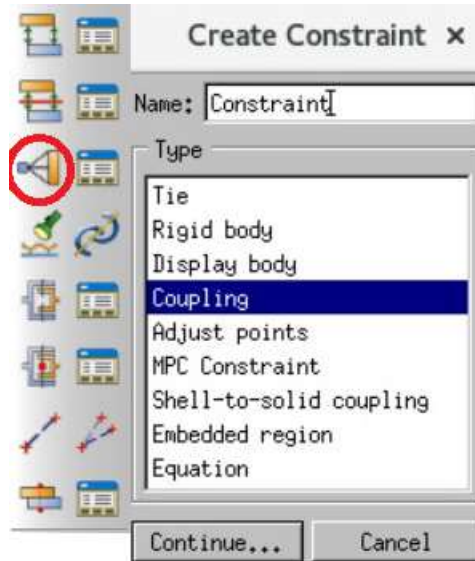


*Figure 2.20 – Connections creation card.*

Once coupling constraint is selected, the chosen coupling type is the “Continuum distributing”, completely bounded. A Continuum distributing coupling has been chosen in this thesis work because all the couplings were symmetrical (no need for Structural distributing) and the coupling could not be a rigid connection. In figure 2.21 the edit constraint card is shown.

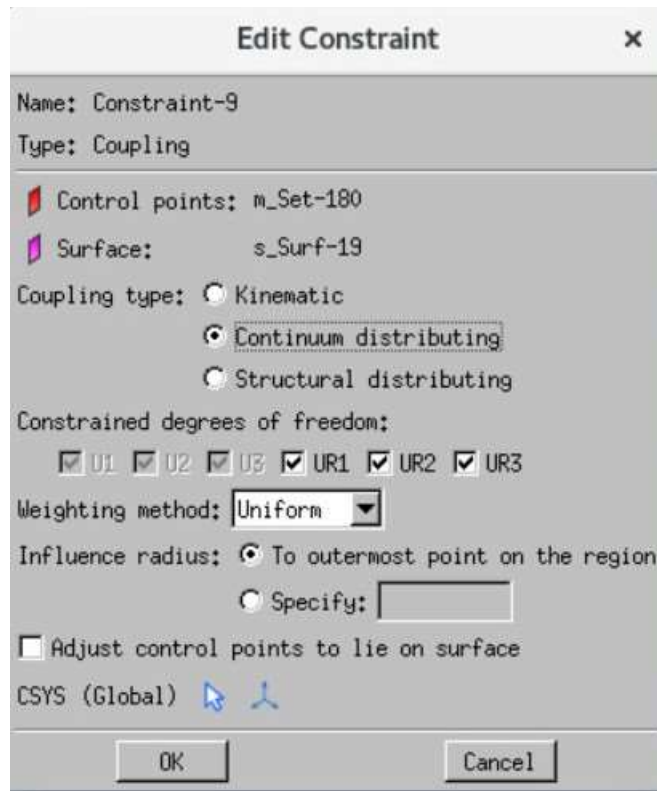


*Figure 2.21 – Edit constraint card.*

There are 8 different constraints:

- Constraint 1: connection between control point 16 and the internal surfaces of the four screw holes for the flanged connection of the bearing. Furthermore, the control point is connected also to four millimeters on the bottom of the bearing housing, where there is the contact between the bearing and its housing. In figure 2.22 this constraint is shown;

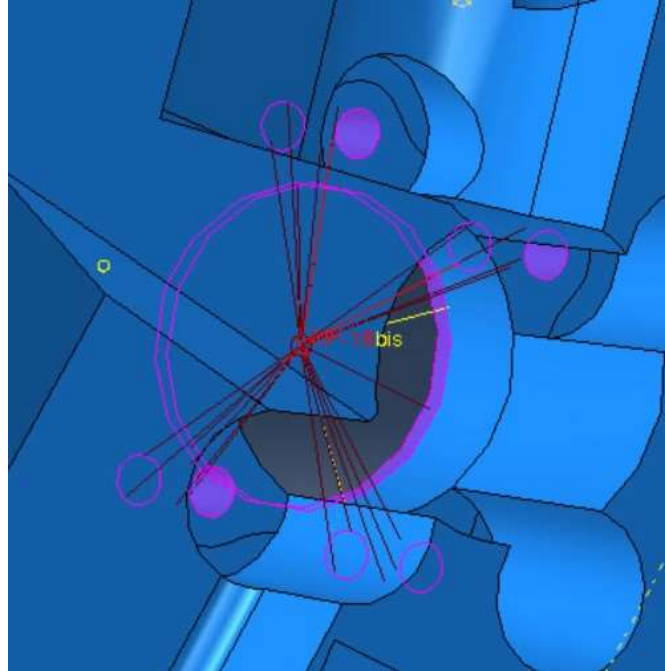


*Figure 2.22 – Constraint 1.*

- Constraint 2: connection between control point 2 and the relative internal surface of the bushing. In figure 2.23 this connection is shown.

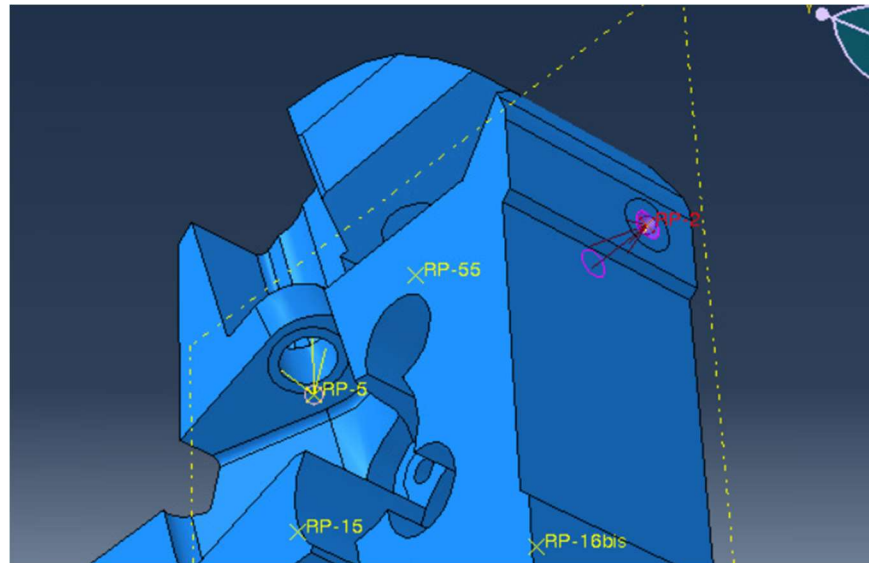


*Figure 2.23 – Constraint 2.*

- Constraint 3: connection between control point 1 and the relative internal surface of the bushing. In figure 2.24 this connection is shown.

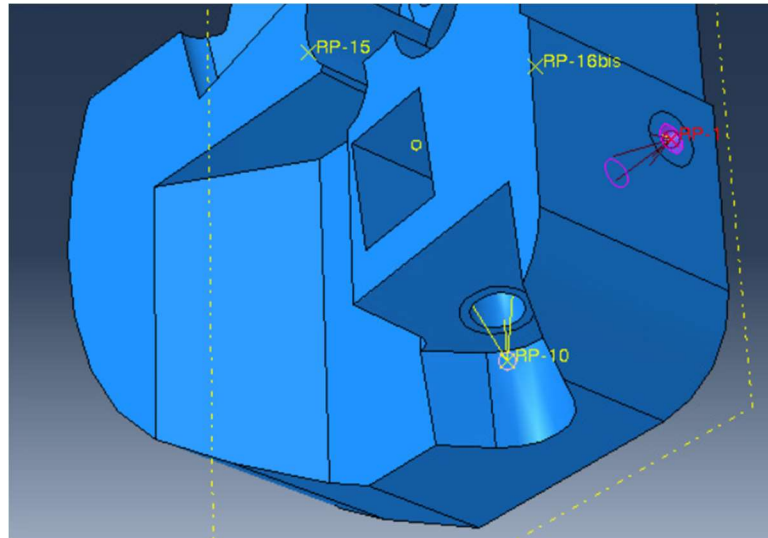


*Figure 2.24 – Constraint 3.*

- Constraint 4: connection between control point 10 and the relative internal surface of the bushing. In figure 2.25 this connection is shown.

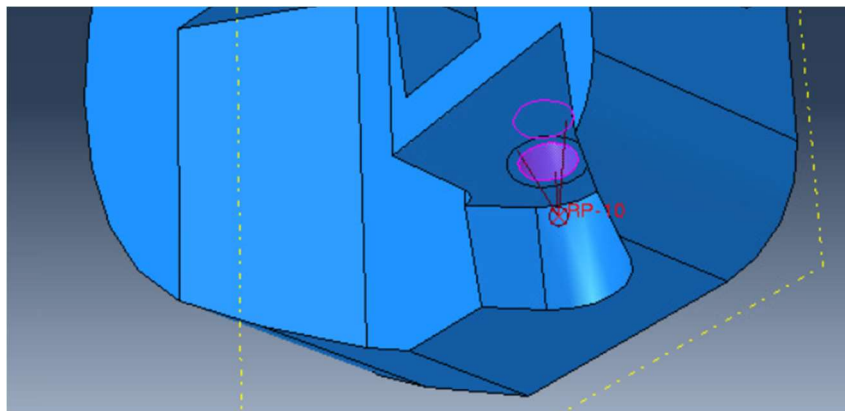


*Figure 2.25 – Constraint 4.*

- Constraint 5: connection between control point 15 and the relative internal surface of the bushing. In figure 2.26 this connection is shown.

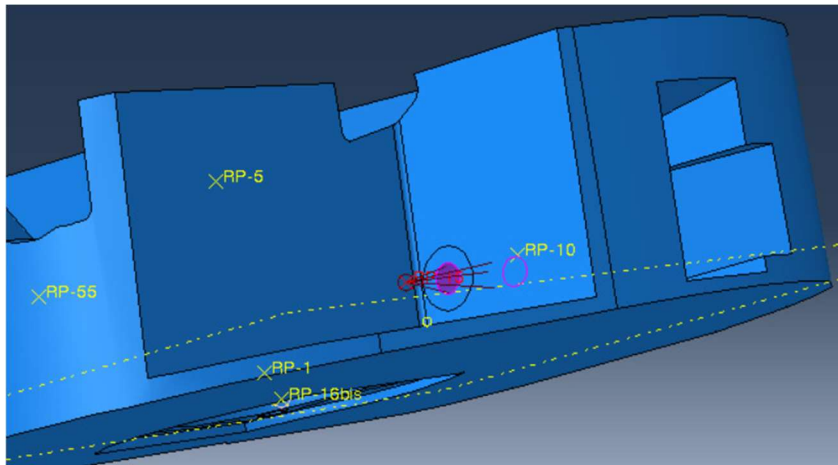


Figure 2.26 – Constraint 5.

- Constraint 6: connection between control point 55 and the relative internal surface of the bushing. In figure 2.27 this connection is shown.

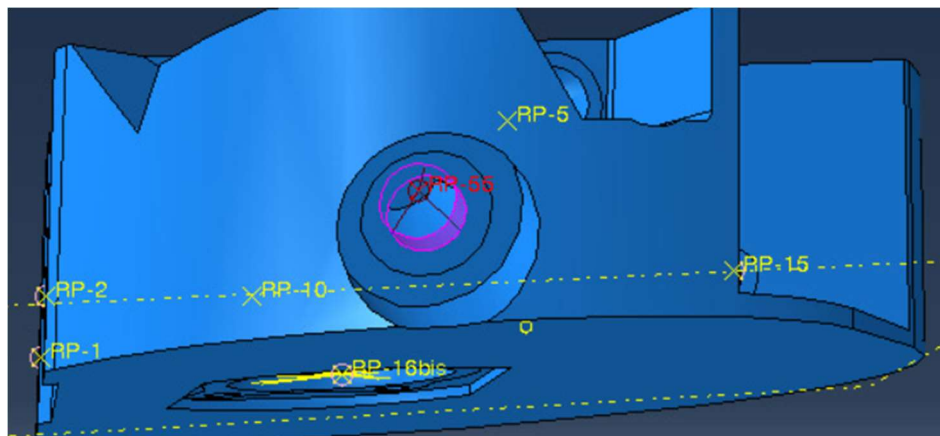


Figure 2.27 – Constraint 6.

- Constraint 7: connection between control point 5 and the relative internal surface of the bushing. In figure 2.28 this connection is shown.

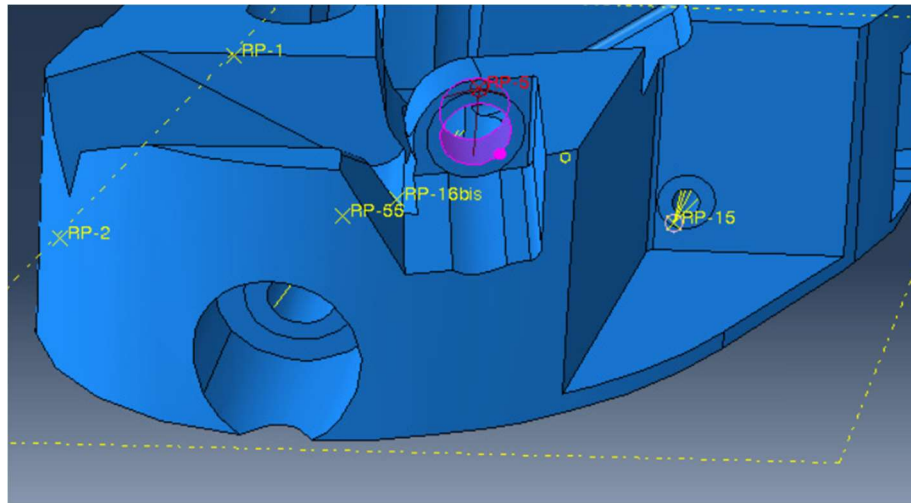


Figure 2.28 – Constraint 7.

- Constraint 8: connection between control point 16bis and points 1 and 2. This is a specific coupling used for Braking step. In figure 2.29 this connection is shown.

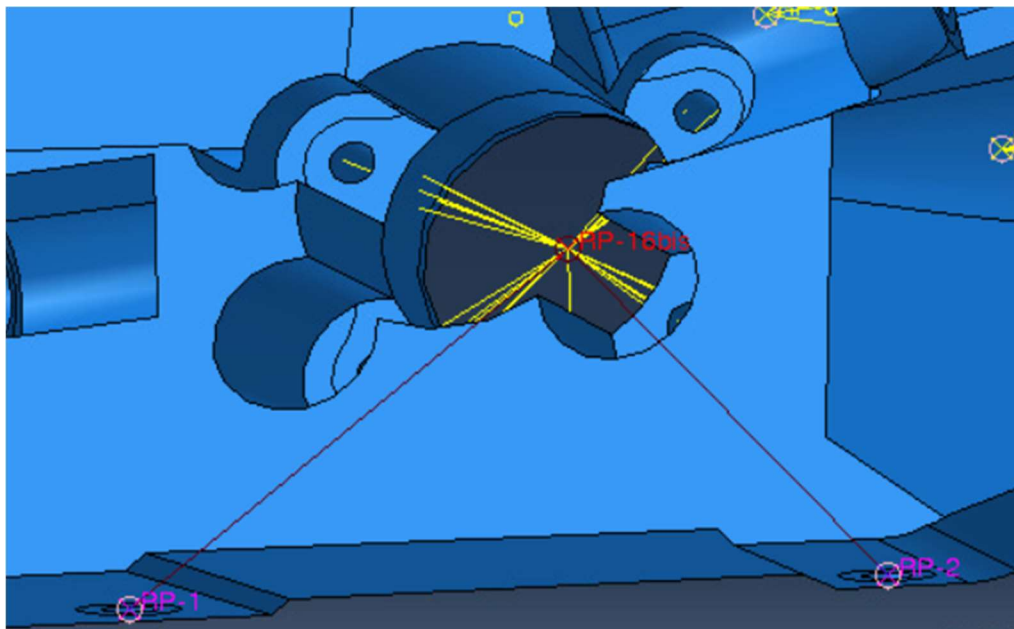


Figure 2.29 – Constraint 8.

## LOAD MODULE

Each step has five different loads for points 5, 15, 55, 10 and 16 and just one moment applied on point 16. The first step has been to define the boundary conditions; in particular, the constraints have been set to bound translations and rotations. Regarding Fatigue loading conditions and Buckling loading condition the point 16 has been bounded, while for Braking loading condition the constraints have been applied on points 5,15, 55 and 10. The constraints have been set as encastre and they have been defined for each step. Figure 2.30 shows an example of boundary condition card with some of the already discussed features.

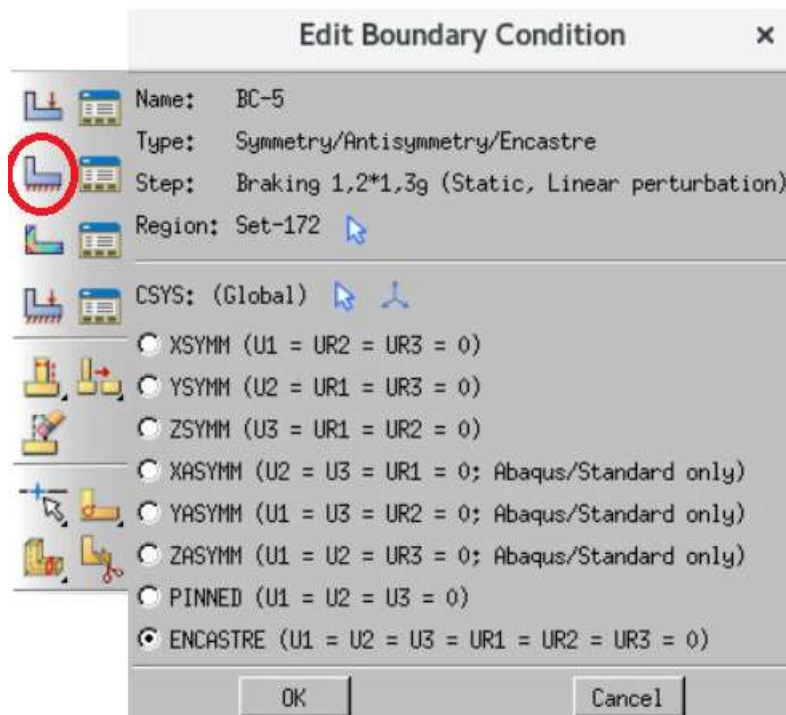


Figure 2.30 – Example of boundary conditions card.

Once all the boundary conditions are defined, the loads can be set.

All the loads have been set as concentrated forces on the reference points for each step. Figure 2.31 shows an example of load creation card.

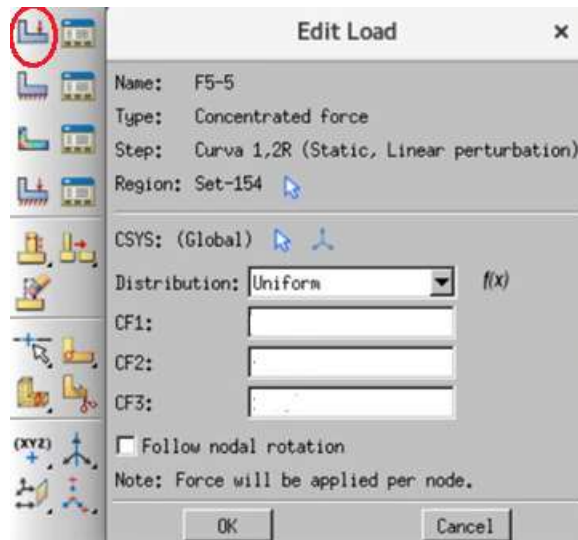


Figure 2.31 – Example of a load creation card.

In the end, one loadcase for each step has been created. A loadcase means a set of loads and boundary conditions that define a specific loading condition. In figure 2.32 the loadcase edit card is shown. It is possible to notice that both load and boundary condition have been assigned to a loadcase, in order to create the loading condition for a particular step.

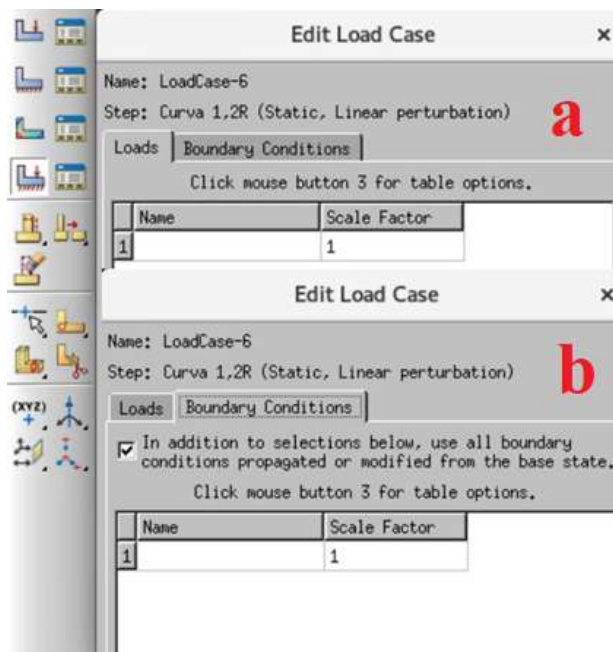


Figure 2.32 – Example of a loadcase card: a) Load creation, b) boundary condition creation.

The three loading conditions have been created with different loads:

- Braking: there is only one moment applied on point 16;
- Fatigue: there are several loads applied on points 5, 10, 55 and 15;
- Buckling: there is only one load applied on point 15.

## MESH MODULE

In this module the meshed part has been created. The global size and the deviation factor have been set after several iterations, in order to have a meshed part with less errors and warnings. The figure 2.33 shows the global seeds card, where it is possible to see the real values used in this work.

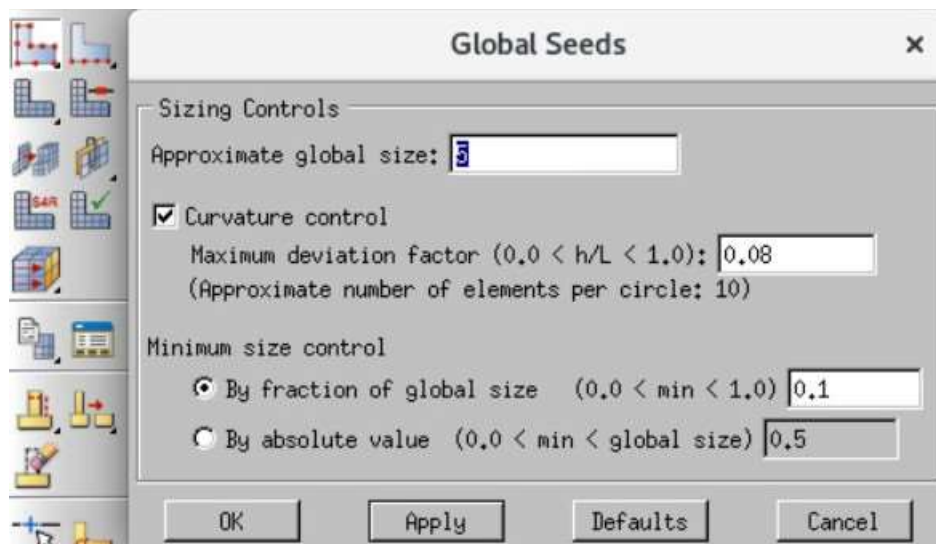
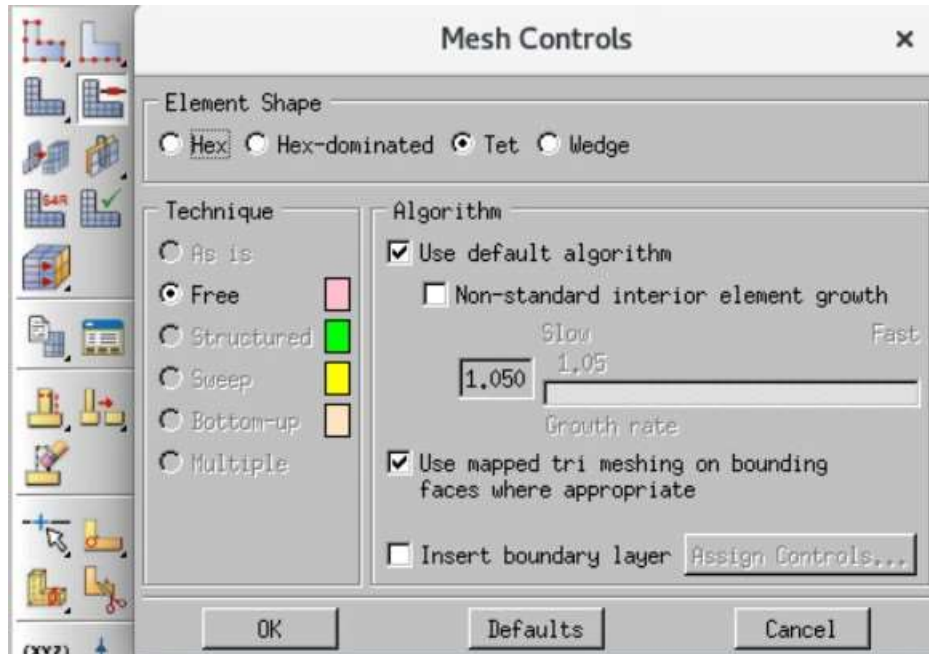


Figure 2.33 – Global seeds card.

Once the element size has been chosen, the shape needed to be set. In fact, a tetrahedral element has been used everywhere. Figure 2.34 shows the mesh controls card and all the values and settings used in this thesis.



*Figure 2.34 – Mesh controls card.*

Finally, the part has been meshed and in Figure 2.35 it is possible to observe the final result.

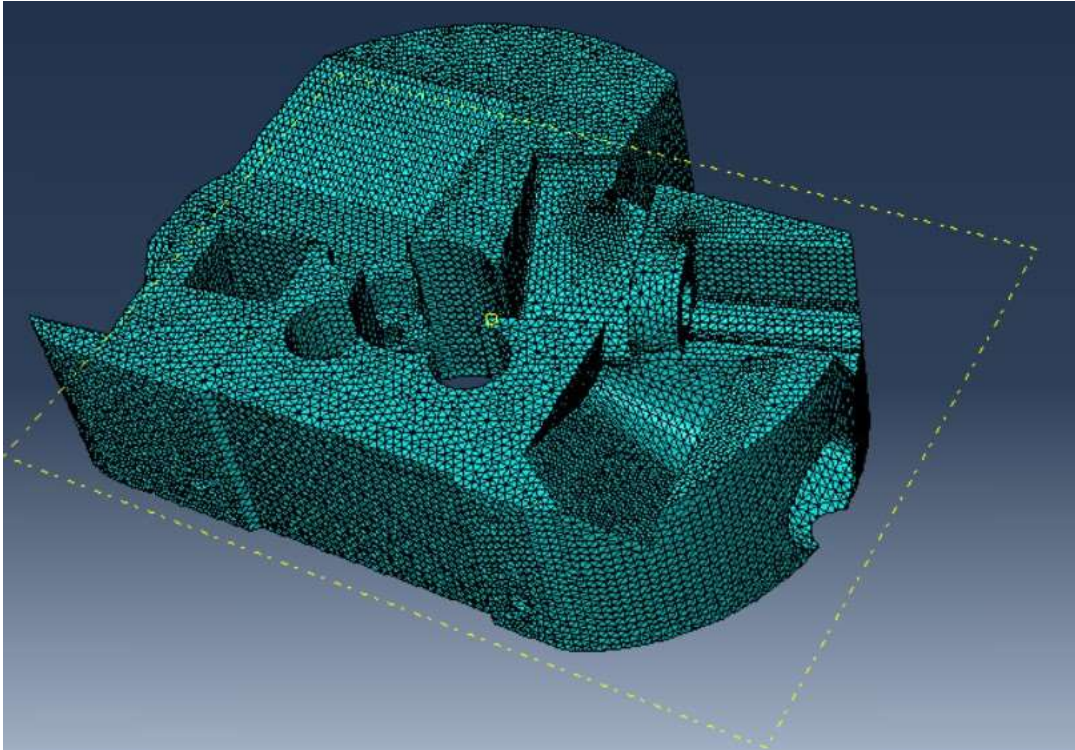


*Figure 2.35 – Meshed design space.*

Once the component is meshed, several checks have been done in order to find and fix every warning and error.

In this work elements Abaqus C3D10 were used; C3D10 are second-order tetrahedral elements, each element is a 10-node quadratic tetrahedron. These elements are recommended for this type of analysis.

## OPTIMIZATION MODULE

In this module the topology optimization task has been created. The software gives the user several possibilities:

- Topology optimization modifies the design area removing and adding materials in order to find the optimal design;

- Shape optimization modifies the coordinates of the surface nodes in order to modify the part surfaces;
- Sizing optimization modifies the thickness of the shell elements in the design region;
- Bead optimization modifies moments of inertia of a shell structure in order to modify the stiffness and eigenfrequencies.

In this work topology optimization has been used. The first step to obtain an optimized structure is to create the optimization task. After choosing the topology optimization option, the design area has been identified. Figure 2.36 shows the part where it is possible to make changes in order to progress in the optimization; in fact, it is possible to observe that all the internal parts of the bushings are excluded because their design should not be modified.

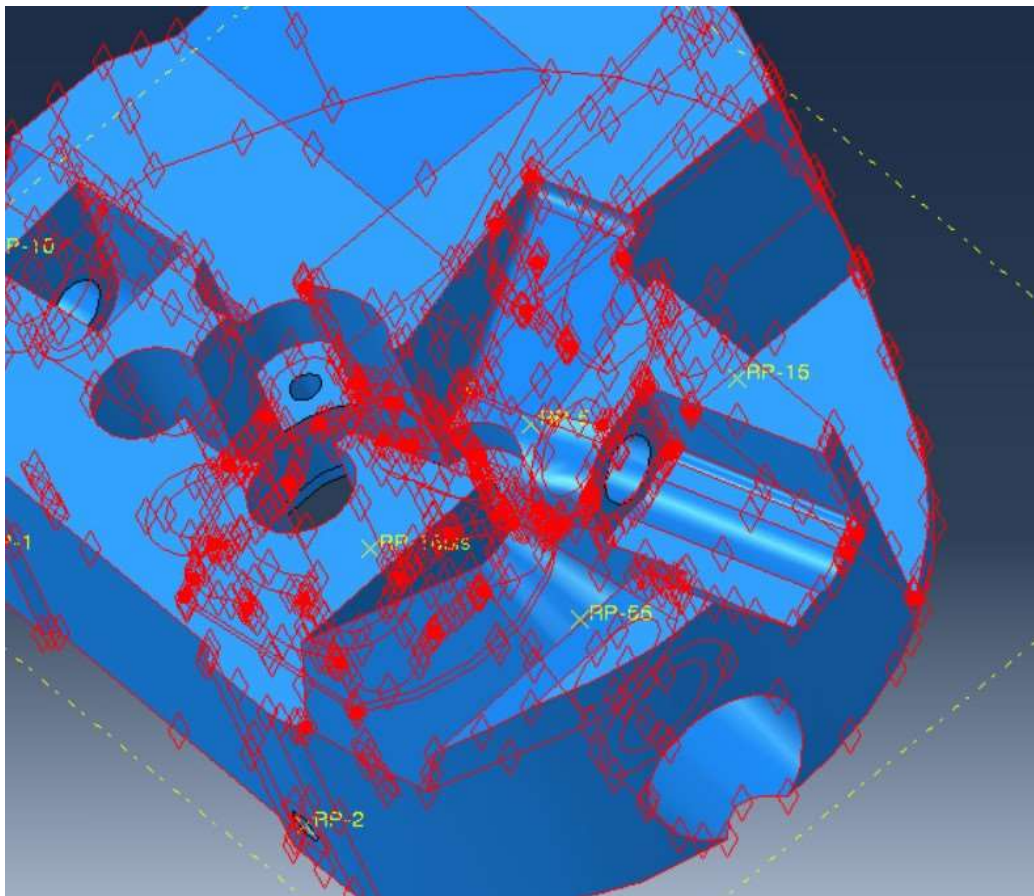


*Figure 2.36 – Optimization design, internal part of the bushings is excluded.*

Once the design space is identified, it was necessary to define the design responses, which are values referred to objective functions and constraints. In this work three design responses have been set:

- Volume;
- Fatigue stress;
- Yield stress.

To set them, it was necessary just to select the design.

After defining design responses, an objective function has been defined; in this work the final aim is to reduce the volume of the component. In fact, the objective function is to minimize the volume (i.e. the part weight), as shown in figure 2.37.

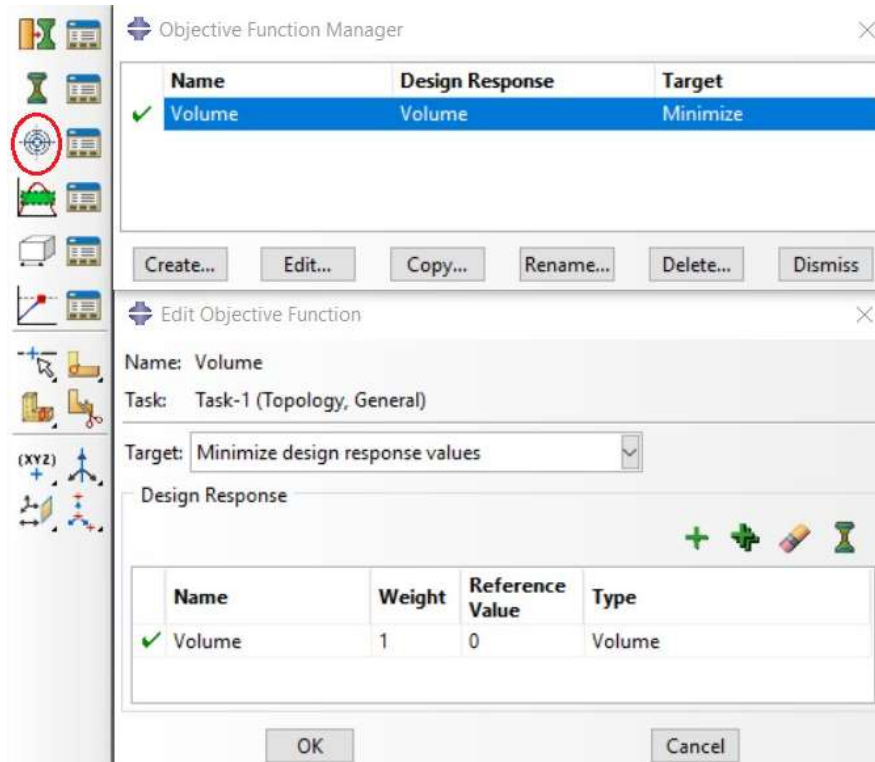


Figure 2.37 – Creation of the objective function.

Subsequently, the topology optimization constraints have been created. In this case only two constraints have been determined:

- Fatigue stress: all the fatigue loading conditions defined in the STEP MODULE needed to be limited at the fatigue stress. The value used for this constraint was 160 MPa;
- Yield stress: the buckling and braking loading conditions needed to be limited at the Yield stress. The value used for this constraint was 240 MPa.

## JOB MODULE

In this module the complete job has been run. In figure 2.38 the optimization process manager is shown, where model 1 is the component and task 1 is the task set in OPTIMIZATION MODULE.

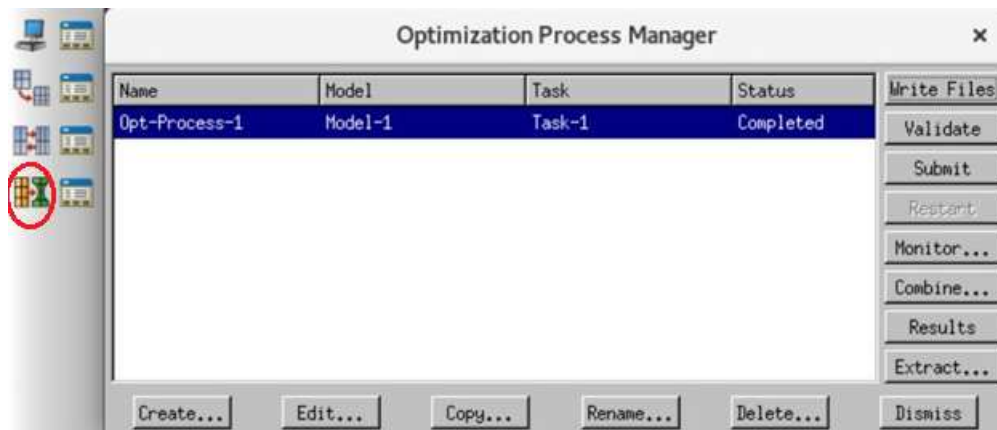


*Figure 2.38 – Optimization process manager.*

Once the process was set, the optimization has been run.

### 3. State of art

The steering knuckle is a structural part of the suspension system of the vehicle; during its whole life, this component is subjected to a wide range of loading conditions [25]. Furthermore, this part guarantees a good road holding, absorbing the vibrations from road irregularities, while the vehicle is travelling [25]; in fact, the steering knuckle is subjected to time varying loadings during its service life. For this reason, the design of this component is submitted to a lot of constraint conditions and combination of loads. Any kind of failure in the steering knuckle leads to a loss of road holding [31].

Figure 3.1 shows one example of assembled steering knuckle system.

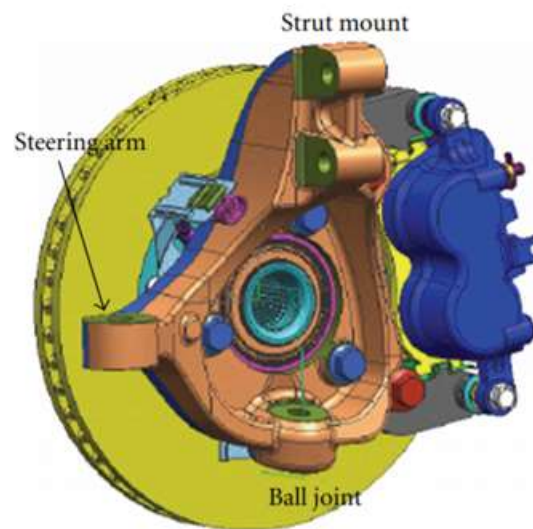


*Figure 3.1 – Example of assembled steering knuckle system [25].*

From a technical point of view, the steering knuckle represents the connection among the wheel hub, the suspension and the steering rod; the wheel hub is connected to the knuckle through a bearing, the hub housing is connected to the knuckle through a pin. The main function of this component is to convert the linear motion of the steering rod into angular motion of the hub. Of

course, it would be a significant improvement to make the steering knuckle lighter because, in this way, there would be less vibrations and a better road holding.

Steering knuckle for automobile applications is typically manufactured by the following ways:

- Casting: in this way it is possible to manufacture valuable parts even if the components could have blow holes which might lead the component to an early damage;
- Forging: in this way it is possible to manufacture better parts than casting. This is the reason why it is always preferred to produce these components by forging.

Due to the large volume production of the steering knuckle, a lot of car manufacturers invested in manufacturing a lighter steering knuckle in order to reduce vehicle weight and improving vehicle performances and decrease fuel economy [24]. To obtain all these achievements, it has been thought to use the AM technology instead of forging the component. As already said, it could be more expensive for some reasons, but AM can bring a lot of advantages. Nowadays, it is possible to say that AM needs more improvements in terms of technology and costs before it can be included in the large-scale industrial production.

During the past 10 years, some researchers have understood that usually the steering knuckle is overdesigned; they introduced different kinds of design optimization in order to avoid this overdesigning. As already said a heavier steering knuckle results in heavier vehicles; generally, a vehicle weight reduction leads to a decrease in fuel consumption and to improvements in performances. Finally, these researchers were and, still, are trying to make improvements in this way using design optimization and sometimes AM.

*Gore et al.* studied the weight distribution of a front wheel vehicle during 4 different maneuvers in order to define proper load conditions applied on the knuckle. Each load condition contained load components along X, Y and Z axes, while the torques were around the X axis. In this work, all the loads were applied on the bushing of the steering arm and on the bushings of the superior and inferior suspension arms, while the constraints were applied on the screw holes around the bearing location.

The loading conditions were:

- Bumping: the wheel load components along X, Y and Z axes and the moment around the X axis were considered. Figure 3.2 shows the loading and constraint conditions.

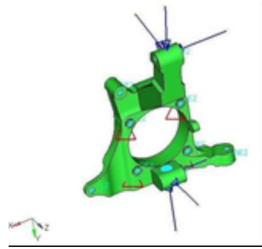


*Figure 3.2 – Loading and constraint conditions of bumping [27].*

- Braking: two brake force components along X applied on the brake caliper were considered. Figure 3.3 shows the loading and constraint conditions.

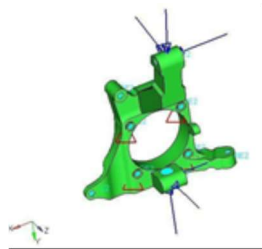


*Figure 3.3 – Loading and constraint conditions of braking [27].*

- Steering: the loads considered are steering loads along X, Y and Z axes. Figure 3.4 shows the loading and constraint conditions.

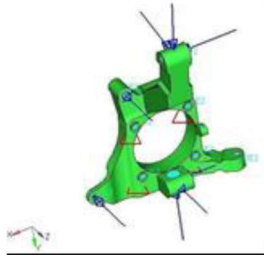


*Figure 3.4 – Loading and constraint conditions of steering [27].*

- Combined loading: all the three previous loading conditions are applied simultaneously. Figure 3.5 shows the loading and constraint conditions.

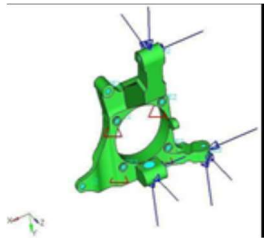


*Figure 3.5 – Loading and constraint conditions of combined loading [27].*

Figure 3.6 shows the original steering knuckle.

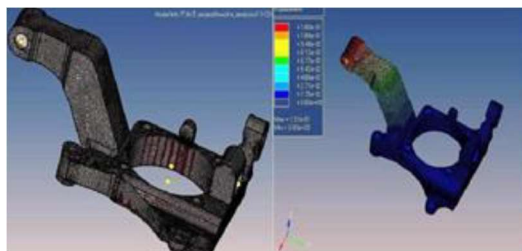


*Figure 3.6– Steering knuckle [27].*

A FE analysis has been performed in order to know if the component resists to the loading conditions already defined. All the analyses were preprocessed with Hypermesh and performed with the help of Optistruct.

After the preliminary analysis, a changing in the design of the steering knuckle has been performed in order to achieve a weight reduction. The component initially weighted 5.320 Kg. Once the component has been redesigned, it was necessary to perform another FE analysis in order to verify stresses and displacements induced in the final steering knuckle for each loading condition: the final component had the same shape of the initial one, but with a lighter structure. It can be observed that the structures are almost the same because the weight reduction was quite small: the optimized structure weighted 4.600 Kg, with a mass reduction of 13.20% [27].

The results of this work were satisfactory: the final component is lighter even if it is just a little more stressed [27]. The results are shown in table 3.1.

<b>Steering Knuckle</b>	<b>Bumping</b>	<b>Braking</b>	<b>Steering</b>	<b>Combined loading</b>
<b>Maximum Stress</b>	171.2 MPa	168 MPa	171 MPa	255.4 MPa
<b>Maximum Displacement</b>	0.223 mm	0.209 mm	0.229 mm	0.328 mm
<b>Optimized Steering Knuckle</b>				
<b>Maximum Stress</b>	150.9 MPa	155.6 MPa	150.9 MPa	251.7 MPa
<b>Maximum Displacement</b>	0.177 mm	0.182 mm	0.177 mm	0.289 mm

*Table 3.1 – Comparison between the initial steering knuckle and the optimized one [27].*

It is possible to observe that the design optimization does not compromise the safety features for the component [27].

*Srivastava et al.* [28] studied the mass reduction of a steering knuckle using the Finite Element Analysis. A FEA on the component has been done and then, after a re-design of the same component, a finite element analysis on the optimized component has been performed. An iterative process has optimized a CAD model of steering knuckle: the unnecessary material has been

removed from the original steering knuckle where induced stress was negligible and necessary material has been added to the region where induced stress was maximum. The CAD model has been developed using Solidworks, choosing S.G. Iron material. The CAD model has been imported in ANSYS as STEP format for meshing and FEM analysis. The initial weight was 2.631 Kg [28].

The loading condition has been calculated from empirical relations, considering the mass of the vehicle as  $m = 1340 \text{ Kg}$ ; these relations are shown in table 3.2.

<b>Loading conditions on the knuckle</b>	
<b>Breaking Force</b>	$1.5 * m * g$
<b>Lateral Force</b>	$1.5 * m * g$
<b>Force on knuckle hub in X-axis</b>	$3 * m * g$
<b>Force on knuckle hub in Y-axis</b>	$3 * m * g$
<b>Force on knuckle hub in Z-axis</b>	$1 * m * g$

*Table 3.2 – Loading condition [28].*

Once the FEA has been performed, a conceptual design has been accomplished Solidworks. Once again, the STEP model has been imported in Ansys in order to perform a FEA on the optimized component. Figure 3.7 shows the points where loads and constraints were applied; obviously, the two views have been taken from different points of view. As it is possible to observe, the shape of the initial component has been optimized in order to reduce its own weight. In this case the shape has been totally changed because it was a design optimization, focused on re-designing the component instead of using optimization algorithm.

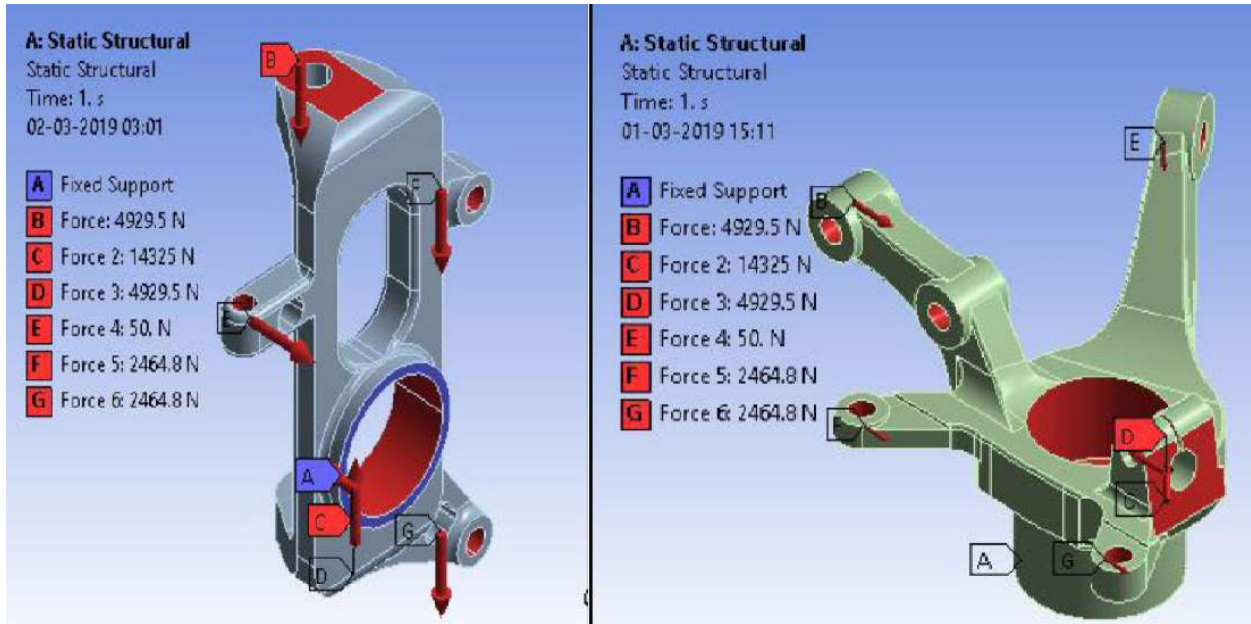


Figure 3.7 – Applied loads and boundary conditions of the initial and the optimized component [28].

Figure 3.8 shows the mesh of the initial steering knuckle and the optimized one.

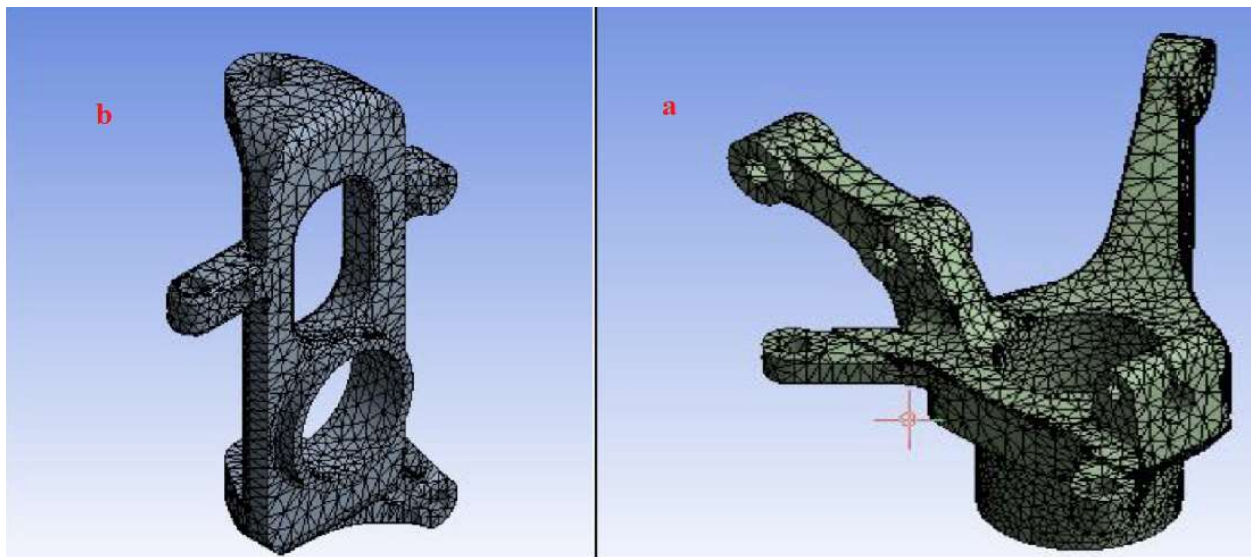


Figure 3.8 – (a) View of the meshed initial component; (b) View of the meshed optimized component [28].

Figure 3.9 shows the results of the two finite element analyses.

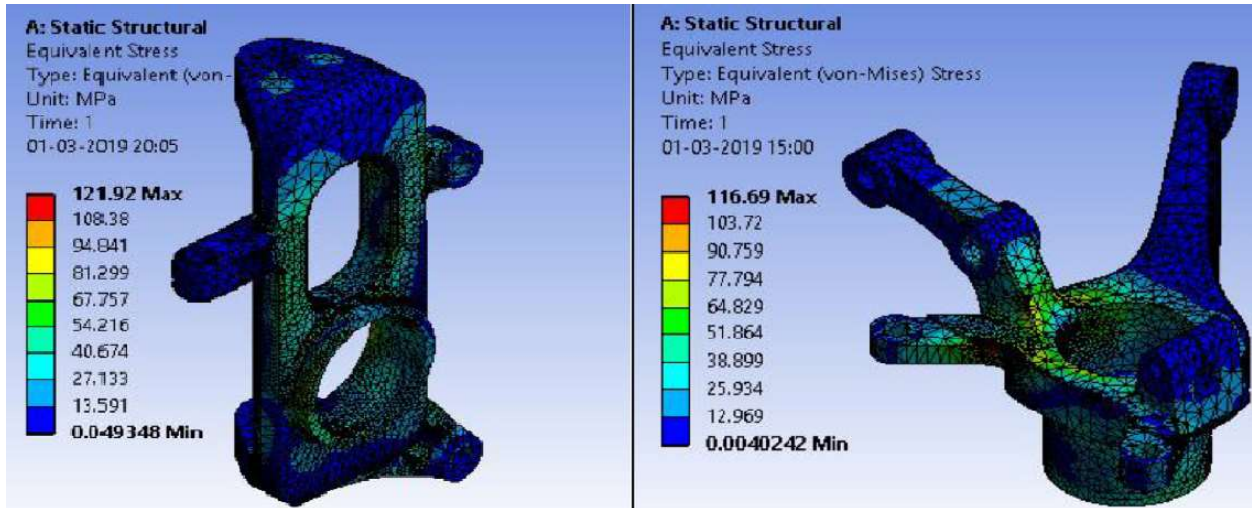


Figure 3.9 – Resultant stresses of the initial and the optimized component [28].

Table 3.3 shows a comparison between the results of the initial and the optimized component.

	Initial Design	Optimized Design	Reduction
Displacement	0.264 mm	0.320 mm	
Stress	116.69 MPa	121.92 MPa	
Mass	2.631 Kg	2.1394 Kg	19 %
Safety factor	2.65	2.54	4.15%

Table 3.3 - Comparison between the initial steering knuckle and the optimized one [28].

Even in this case the design optimization did not compromise the safety of the structure. Of course, there was a reduction of the safety factor because deformations and induced stresses were slightly higher in the optimized component than in the initial one [28]. Anyhow, the decrease of the safety factor can be considered negligible [28].

*Dumbre et al.* also investigated the mass reduction of a steering knuckle; different software were used:

- Finite element modeling was done using Hypermesh;
- Setup was solved using Radioss solver;
- Optimization was performed with Optistruct;
- CAD modeling was done using CATIA V5;
- Meshing was done using Abaqus workbench.

Figure 3.10 shows the meshed component and the points where the loads were applied. In this work only one loading condition has been used [26].

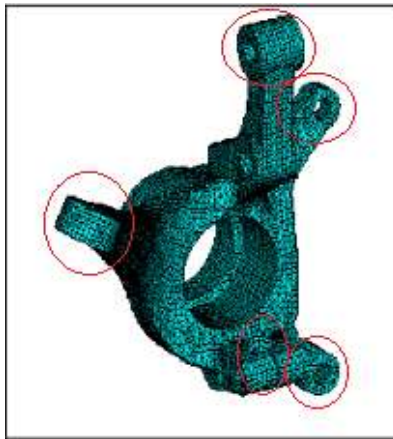


*Figure 3.10 – Meshed steering knuckle [26].*

The FE analysis has been performed and figure 3.11 shows the results of the finite element analysis and the material density distribution, in order to establish which areas could be removed [26].

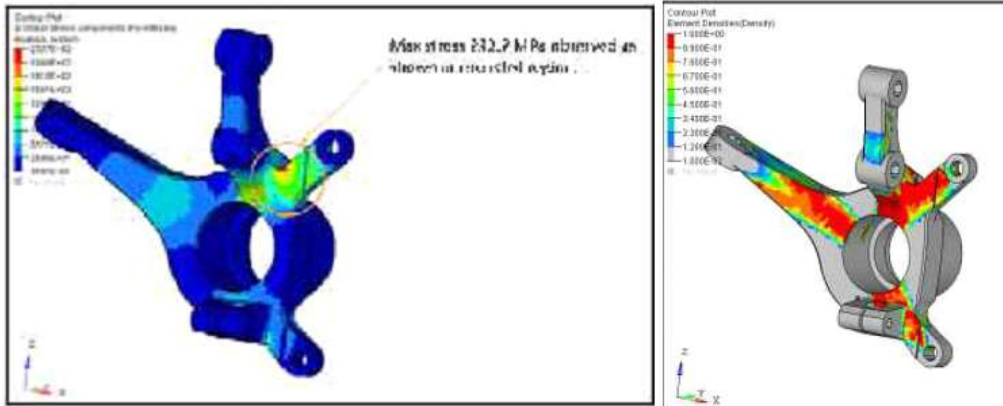


Figure 3.11 – FEA results and material density distribution [26].

Figure 3.12 shows the modified geometry, taking to account the material density distribution; in fact, the material that could be removed is highlighted in green [26].

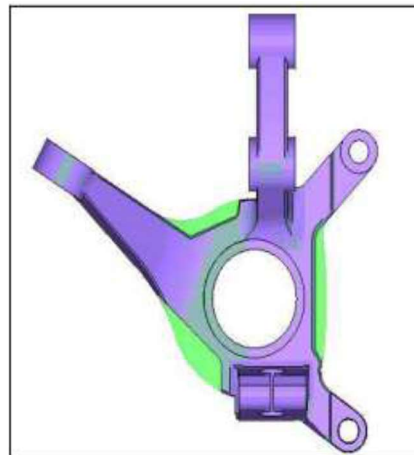


Figure 3.12 – Steering knuckle modified geometry [26].

Once the optimized component has been obtained, a new FE analysis was performed in order to guarantee the structural integrity of the component after the loads have been applied [26]. Table 3.4 shows a comparison between the results of the component before and after the optimization.

	<b>Initial Design</b>	<b>Optimized Design</b>	<b>% Reduction</b>
<b>Displacement</b>	0.2 mm	0.21 mm	
<b>Stress</b>	232.7 MPa	223 MPa	
<b>Mass</b>	2.91 Kg	2.6 Kg	11%

*Table 3.4 - Comparison between the initial steering knuckle and the optimized one [26].*

Even in this case, there was a mass reduction and the results could be considered satisfactory. In this way the overall weight of the vehicle can be reduced to achieve less fuel consumption, less pollution and better performances; all these improvements lead to a decrease of the costs [26].

*Sharma et al.* studied another steering knuckle with the aim of mass reducing; in this case a shape optimization has been performed in order to achieve this final goal. The chosen material to manufacture this component was Aluminum 2011 T3 alloy. The methodology followed by the authors was the same of other papers:

- 3D modeling: in this work CAD model has been developed in CREO 2.0 environment;
- Meshing: CAD model has been converted into STEP file and after imported in Ansys Workbench simulation [29].
- Results: the first results of the FEA have been obtained [29]. The loading and constraint conditions are shown in figure 3.13;
- Shape optimization: the purpose of this kind of algorithm was to find the best material distribution. The shape optimization has been performed with Ansys Workbench Shape Optimization, setting as objective function the weight reduction of the component [29].
- FEA of the optimized component [29].

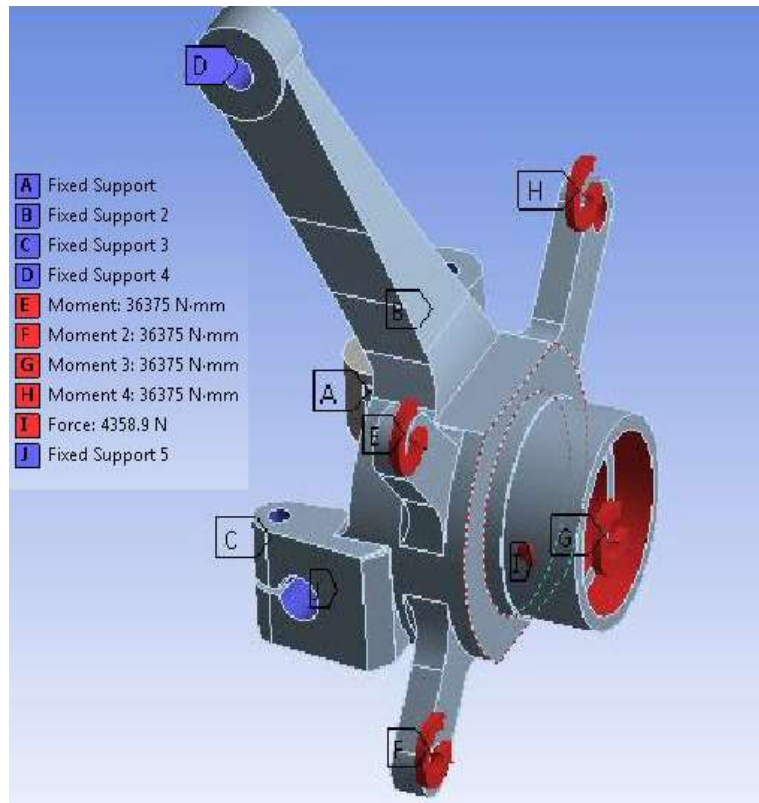


Figure 3.13 – Loading condition and constraints [29].

Figure 3.14 shows the optimized design and the component after re-design.

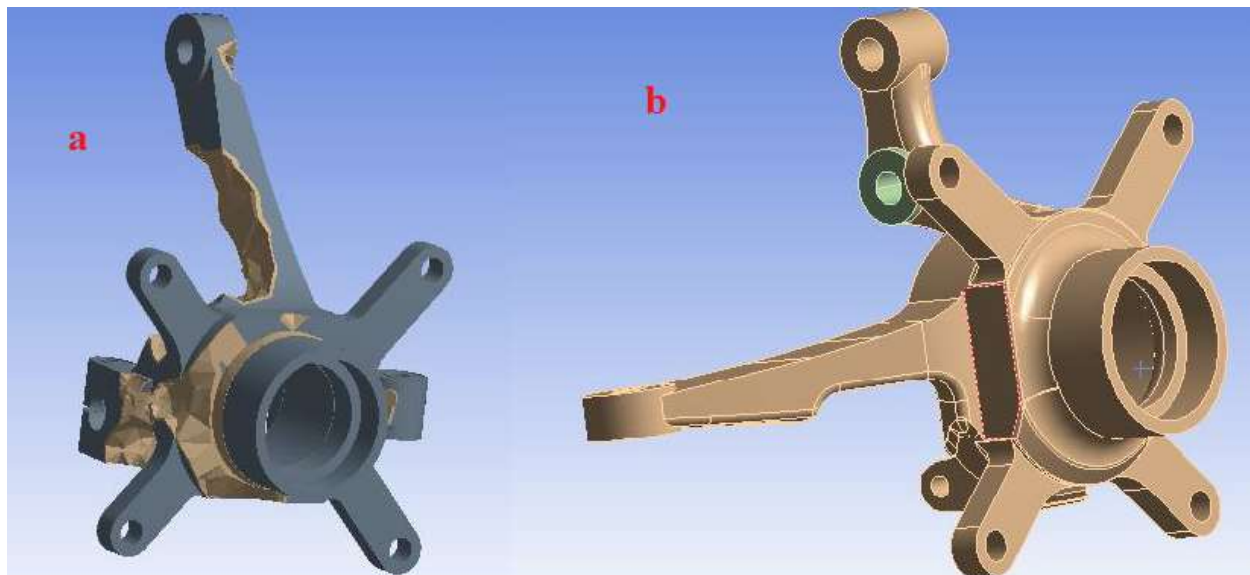


Figure 3.14- (a) optimized component; (b) re-designed component [29].

Table 3.5 shows the results before and after the shape optimization.

	<b>Initial Design</b>	<b>Optimized Design</b>	<b>Reduction</b>
<b>Displacement</b>	0.138 mm	0.150 mm	
<b>Stress</b>	63.814 MPa	65 MPa	
<b>Mass</b>	1.3331 Kg	1.0751 Kg	19.35 %

*Table 3.5 - Comparison between the initial steering knuckle and the optimized one [29].*

The mass reduction could be considered satisfactory since it did not modify significantly the safety factor of the structure [29].

Finally, *Jaswadi et al.* have performed a topology optimization on a rocker arm in order to manufacture this component with AM.

The methodology followed by the authors could be summarized in:

- Meshing: CAD model has been converted into STEP file and then imported in Autodesk Inventor for analysis, using Aluminum alloy as material for the simulations;
- Loading and boundary conditions: the loads were applied to push rod and absorber mounting considering that the vehicle was marching on a flat straight road. The only one point that had constraint is the rocker arm pivot point. Figure 3.15 shows the loading and boundary conditions;
- Topology optimization: during this analysis, the material was progressively removed by using mass target reduction until the final iteration is stopped. The final design was assumed to be optimized to a defined level of efficiency at that mass target. The topology optimization has been performed with Autodesk Inventor's Shape Generator module.
- FEA of the optimized component.

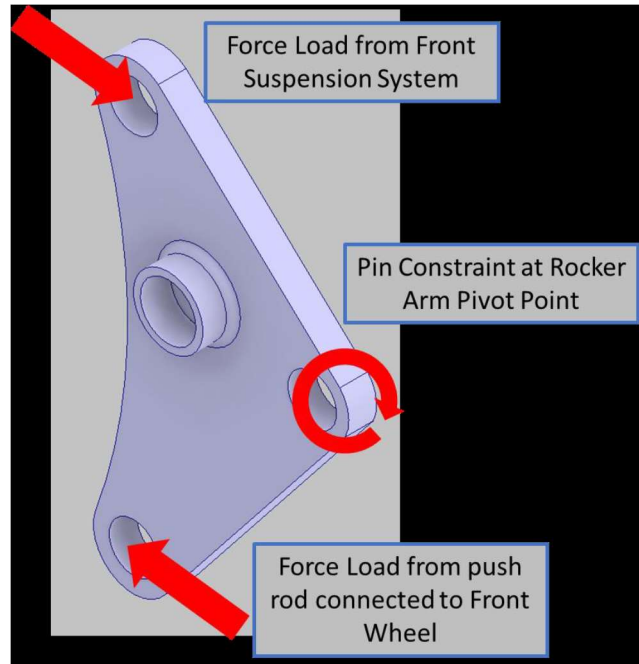


*Figure 3.15 – Model schematics for loading and boundary conditions [30].*

In this work, 4 different optimizations have been performed using the same loading and boundary conditions:

- Reduction 15%;
- Reduction 25%;
- Reduction 35%;
- Reduction 50%.

Figure 3.16 shows the initial design and the optimized designs.

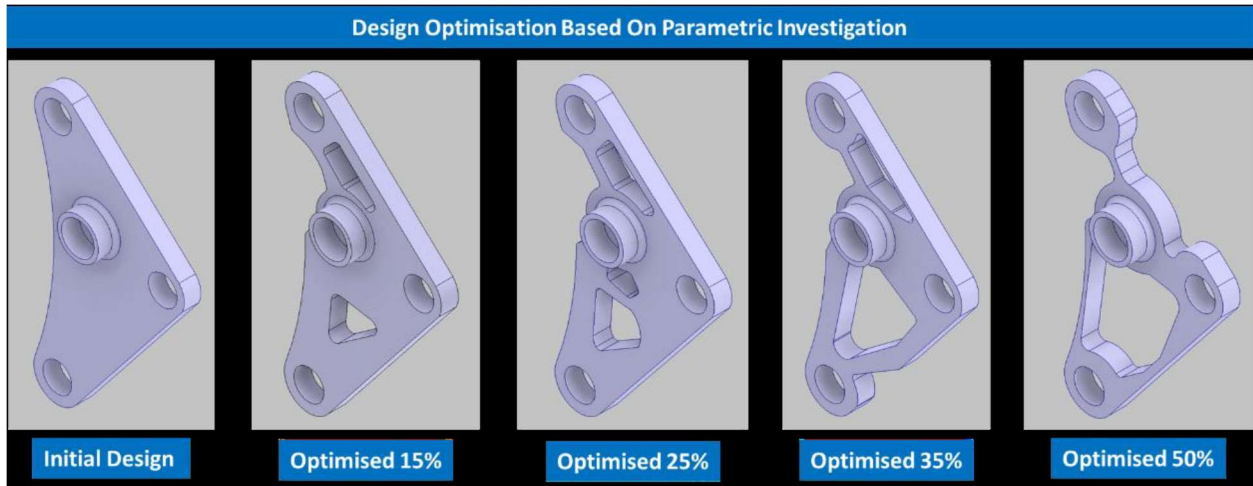


Figure 3.16 – Rocker arm optimization based on weight criteria [1].

Figure 3.17 and 3.18 show the von Mises stress plot and the deformation plot for rocker arm model. The initial ones, 15% and 25% produced similar stress concentration, where the stress peaked at around the pivot mount point. The third case (35%) showed new local stress concentration especially around the lower mount point. The last simulation (50%), showed local stress concentration around the pivot point, as the first 2 models, and to the upper neck area between the central support column and the pivot mount points [30].

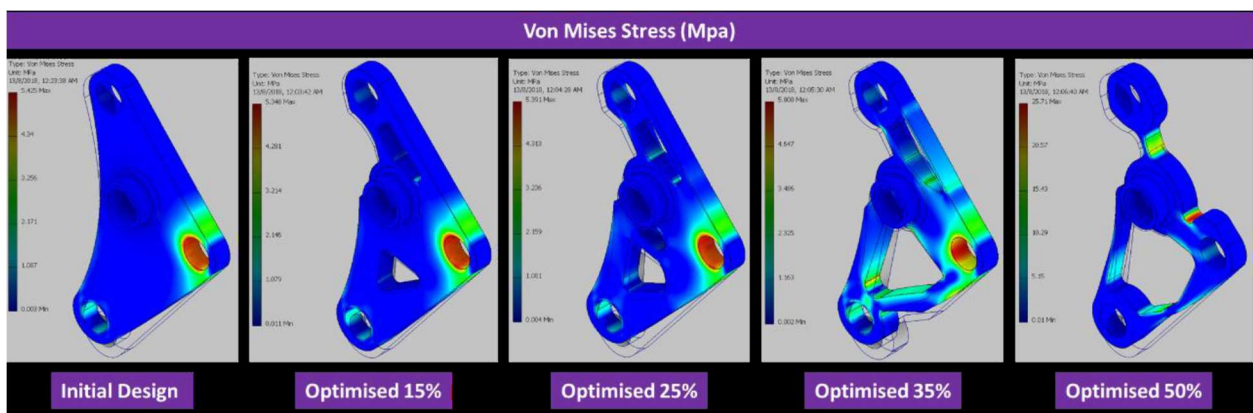


Figure 3.16 – Von Mises stress plot for different models [30].

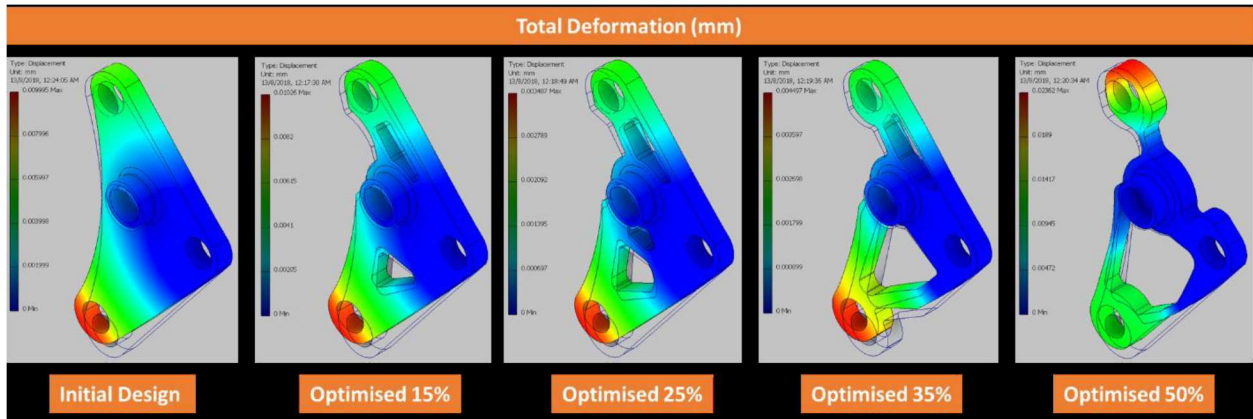


Figure 3.17 – Deformation plot for different models.

Stress value for the first three models was almost the same, while the last model recorded an increase as much as 5 times higher compared to the other models [30].

Finally, the 35% mass reduction model offered the best result in terms of maximum stress value, maximum deformation and weight reduction compared with other models.

In the end, it can be said that the aim of all the researchers was the mass reduction of the component; in fact, they all tried to find some methods in order to achieve the mass reduction in improve the performances of the vehicle and decrease the fuel consumption. In addition to this, some researchers focused on the combination of the weight reduction derived from the topology optimization of a component and the possibility to print it with Additive Manufacturing. In this way it would be possible to reduce production waste, to have a more automated process and to manufacture component with more complex geometries in an easier way.

## 4. Results

This chapter is organized in the following way:

- Preliminary Finite Element Analysis (FEA): the results of a preliminary FEA will be observed and commented in order to realize which kind of stresses the component is facing;
- Topology optimization of the complete component: the shape of the optimized component will be shown;
- Finite element Analysis of the optimized component: the results of a final FEA will be shown in order to determine if the component can resist to the applied loads.

All the results will be shown as percentages and not as absolute values. Furthermore, since three loading conditions and twenty-two different steps have been considered, for sake of brevity, only the results for the following loading conditions in the following order will be shown, being the most significant ones:

- Braking;
- Fatigue;
  - Cornering 2;
  - Braking 2;
  - ax+ay 1;
- Buckling.

As already said, the first and the last ones are two different loading conditions, while Cornering 2, Braking 1 and ax+ay 1 join the Fatigue loading condition.

The results will be reported as percentage of the total stress for each loading condition and each loading condition has a different stresses percentage from the others.

## 4.1 Preliminary Finite Element Analysis

### **BRAKING**

Figure 4.1 shows the result of the FEA on the component before the optimization in this loading condition. As it can be seen, the stresses in general do not affect the structure in a heavy way. In fact, observing the legend on the side of the figure, it is possible to see that the blue color corresponds at the zero percentage of the stresses, while the red color corresponds to the maximum percentage of the stresses. Of course, the maximum percentage is a lower value than the yield stress, as established in Chapter 2.2.

Figures 4.2, 4.3, 4.4 and 4.5 are enlargements of the bushings zones where the loads are applied. In fact, as said in Chapter 2.2, in this loading condition points 5, 55, 15 and 10 have been bounded; as it is possible to observe from the following figures, the highest stresses are concentrated in these points.

In this case, the use of Topology Optimization finalised to Additive Manufacturing is highly recommended because there is a huge part of the component that does not have a structural function.

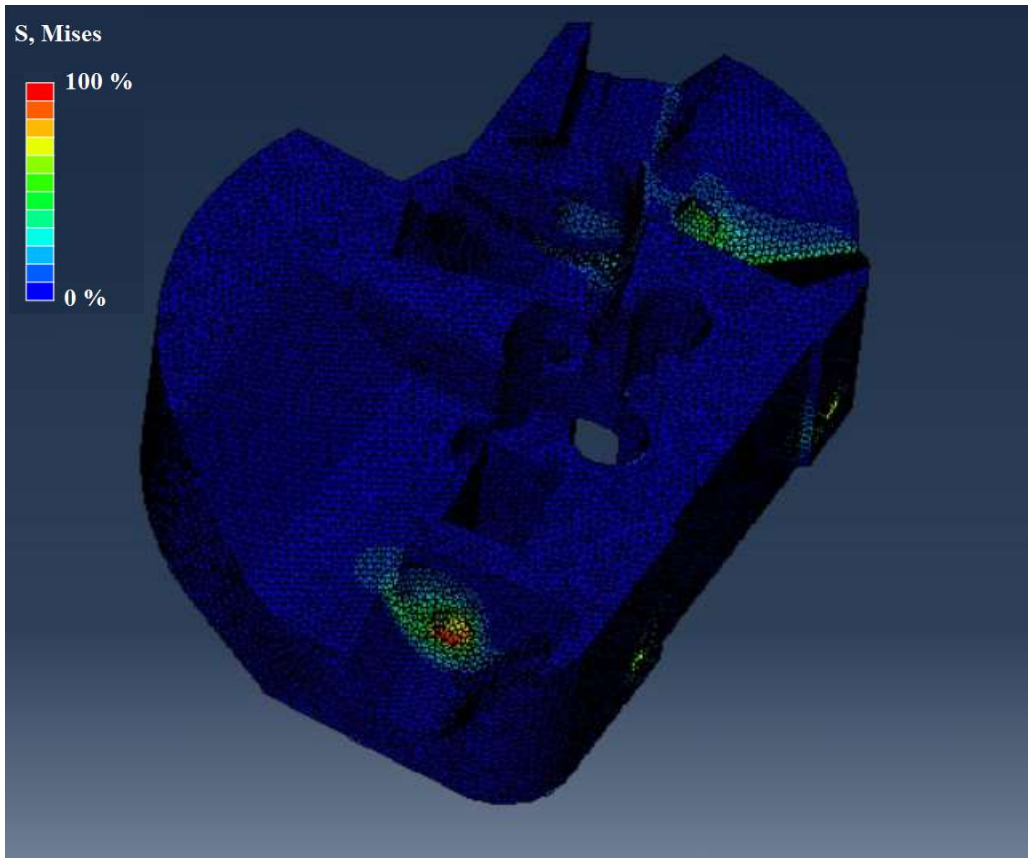


*Figure 4.1 – FEA result, general view.*

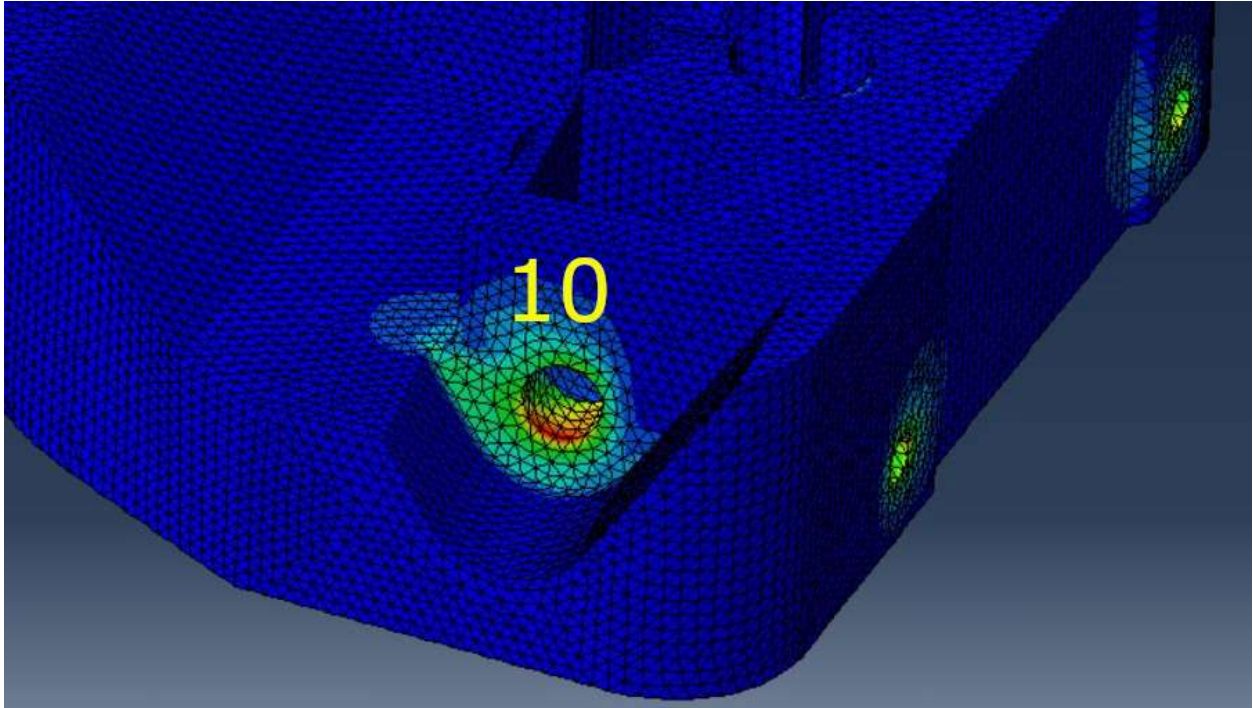


*Figure 4.2 – FEA results, view 1.*

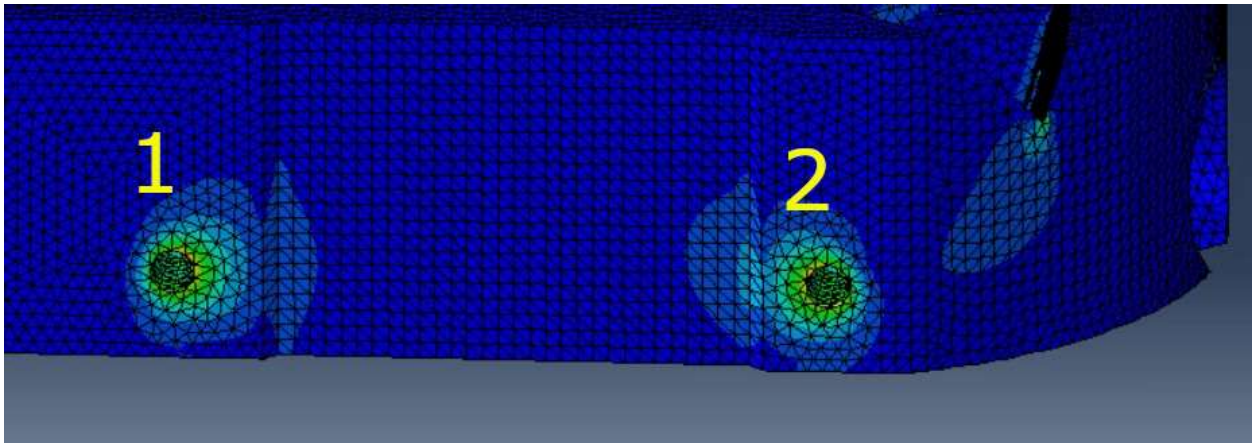


*Figure 4.3 – FEA results, view 2.*

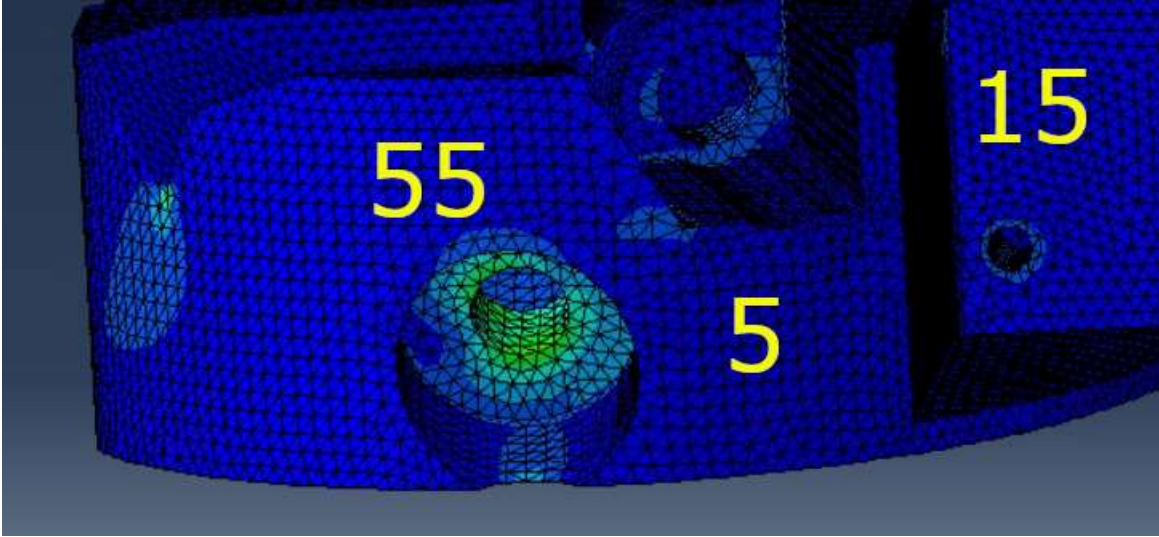


*Figure 4.4 – FEA results, view 4.*

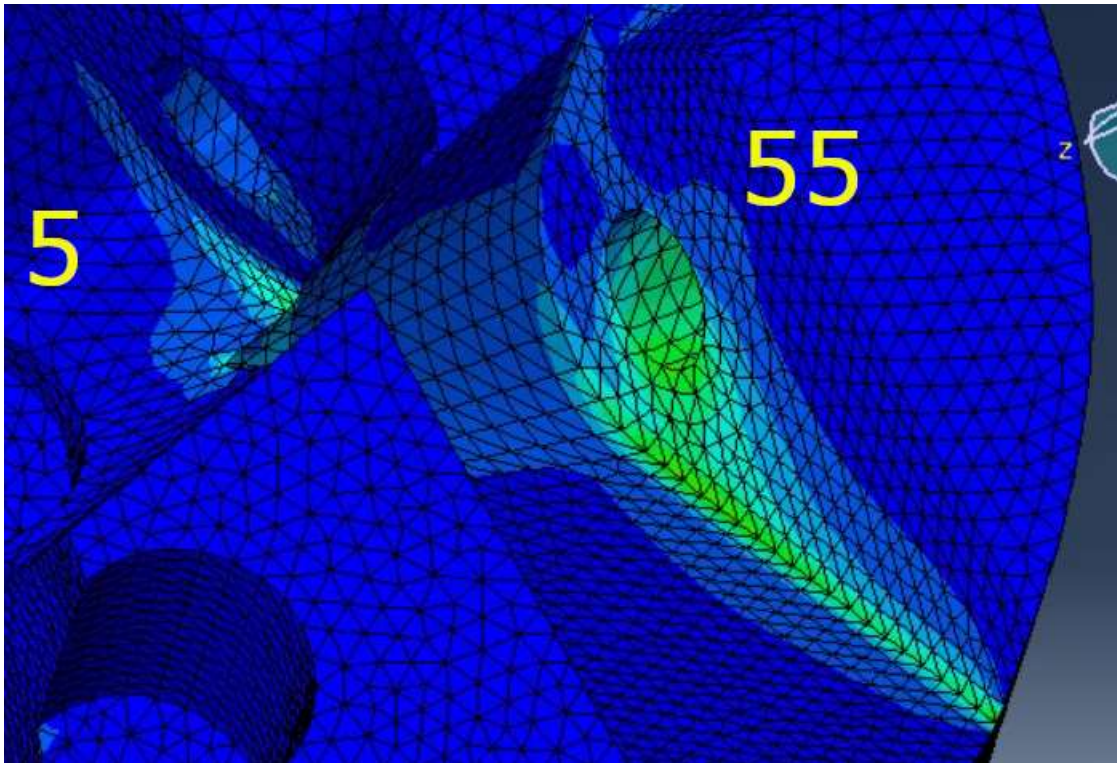


*Figure 4.5 – FEA results, view 4.*

## CORNERING 2

Figure 4.6 shows the result of the FEA of the component before the optimization in the Fatigue loading condition in this precise step. As it can be seen, the stresses in general do not affect the structure in a significant way. In this case and in the following two cases, the maximum percentage is a lower value than the fatigue stress, as established in Chapter 2.2. Figures 4.7, 4.8, 4.9, 4.10 and 4.11 are enlargements of the bushings zones where the loads are applied. In fact, as said in Chapter 2.2, in this loading condition point 16 has been bounded; comparing this case with the previous one, in this case point 55 is the most stressed and there are more stresses on point 16, where the constraint is applied.

Even in this case, the use of Topology Optimization finalised to Additive Manufacturing is highly recommended because there is a huge part of the component that does not have a structural function.

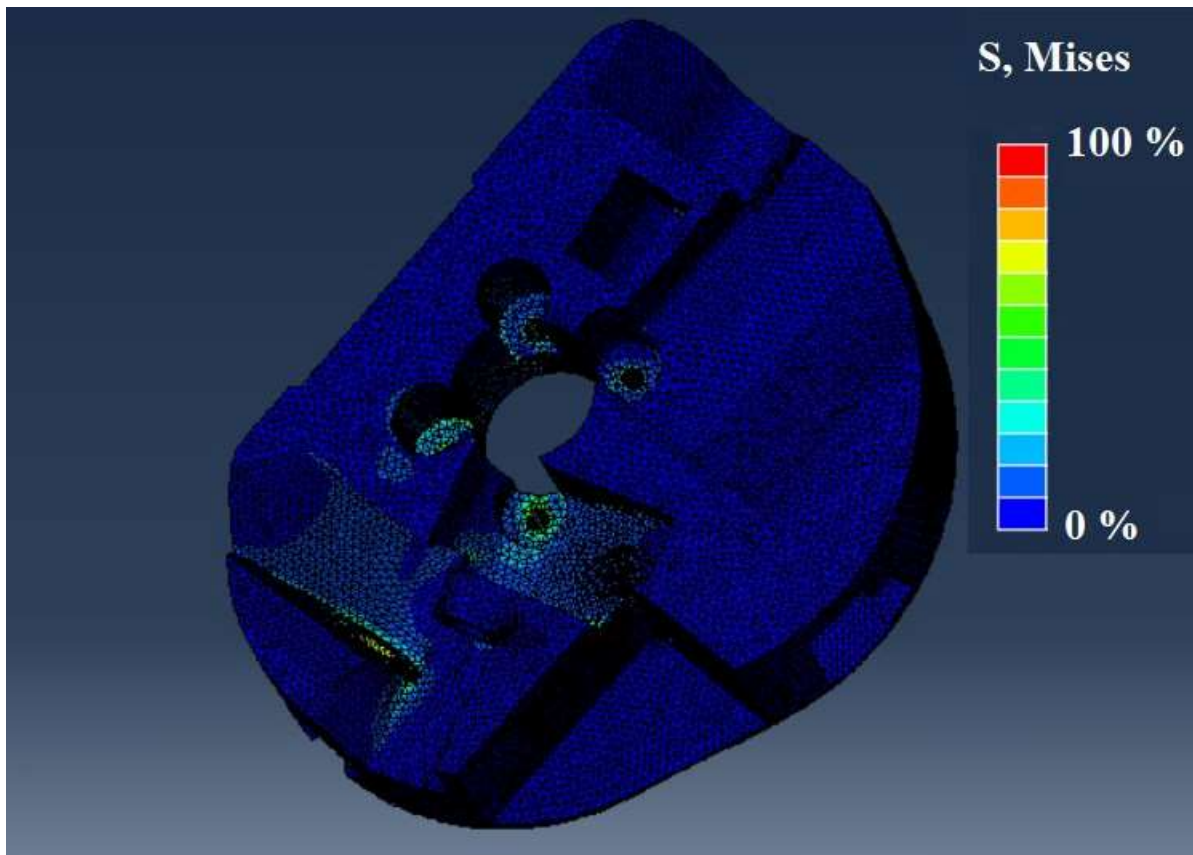


Figure 4.6 – FEA results, general view.

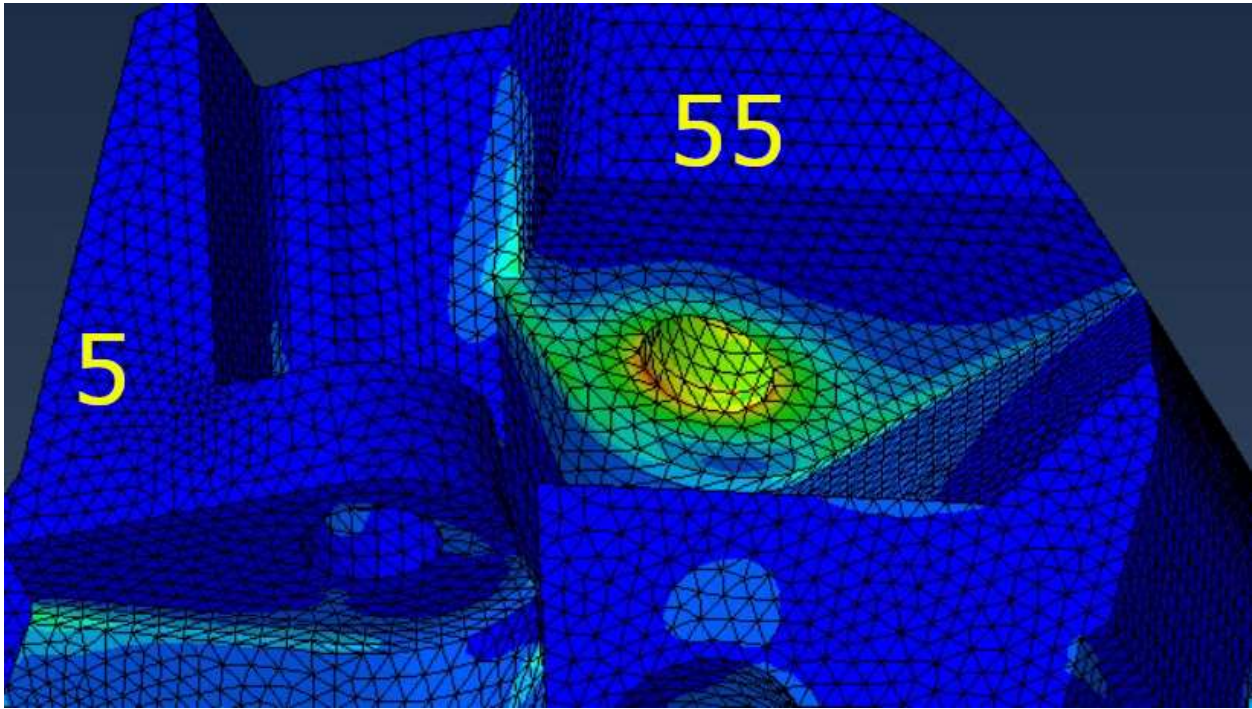


Figure 4.7 – FEA results, view 1.

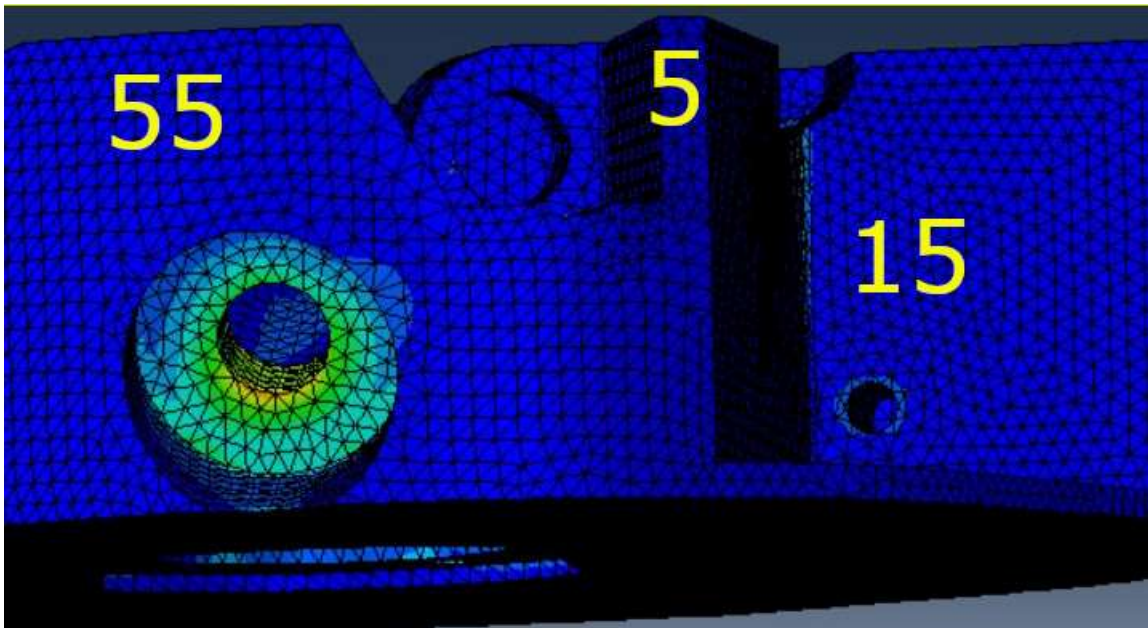
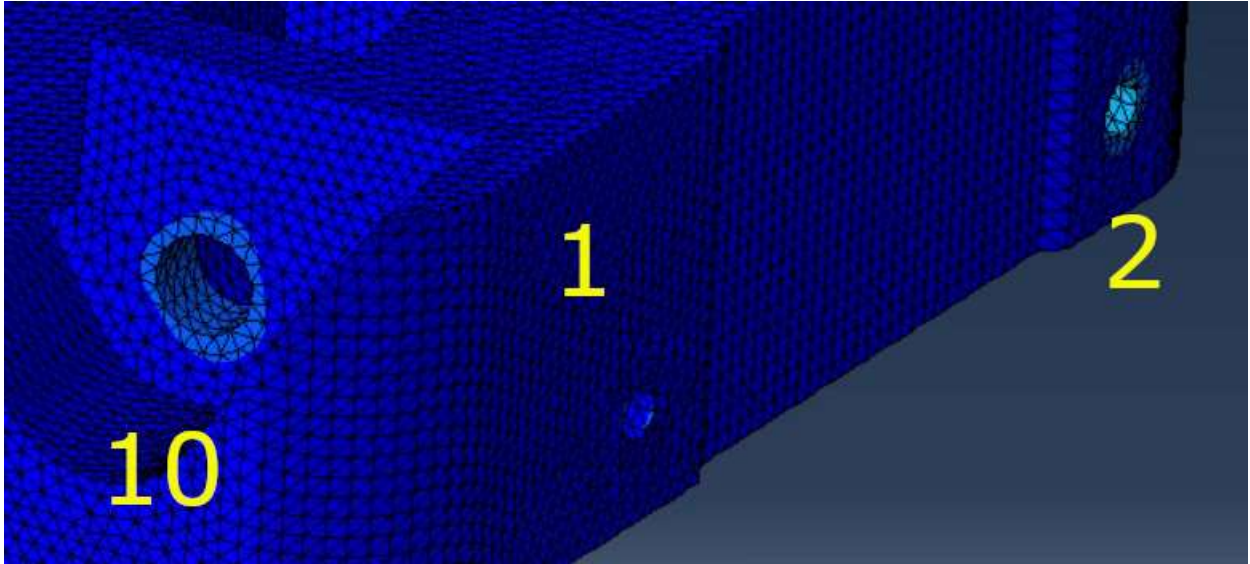
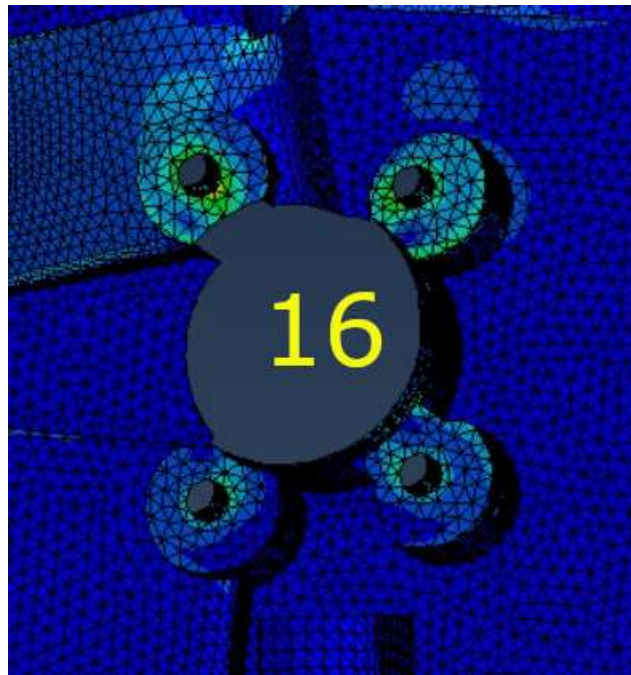


Figure 4.8 – FEA results, view 2.



*Figure 4.9 – FEA results, view 3.*



*Figure 4.10 – FEA results, view 4.*

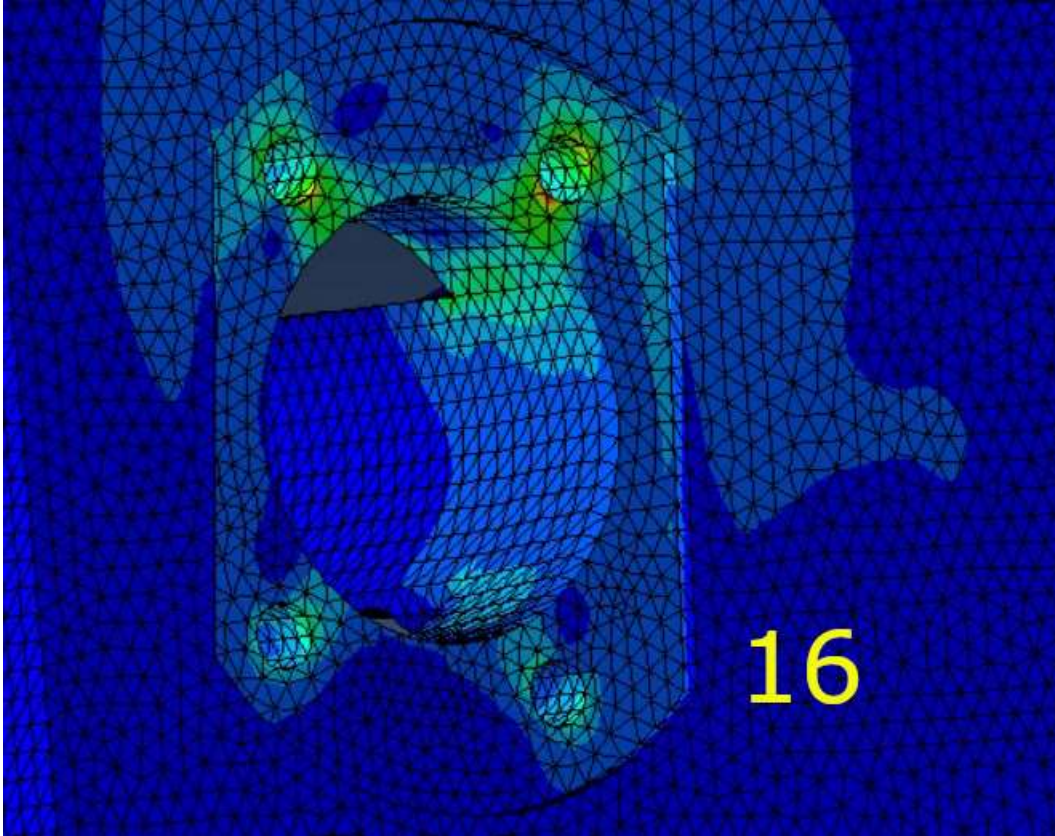


*Figure 4.11 – FEA results, view 5.*

## **BRAKING 2**

Figure 4.12 shows the result of the FEA on the component before the optimization in the Fatigue loading condition in this precise step. As it can be seen, the stresses in general do not affect the structure in an important way. Figures 4.12, 4.13, 4.14 and 4.15 are enlargements of the bushings zones where the loads are applied. In fact, as said in Chapter 2.2, in this loading condition point 16 has been bounded; it is possible to observe that point 5 is the most stressed. In fact, this point will be the most critical one because of its shape.

As already said, also these loads justify the use of Topology Optimization finalised to AM to manufacture this component because there will be a great weight reduction.

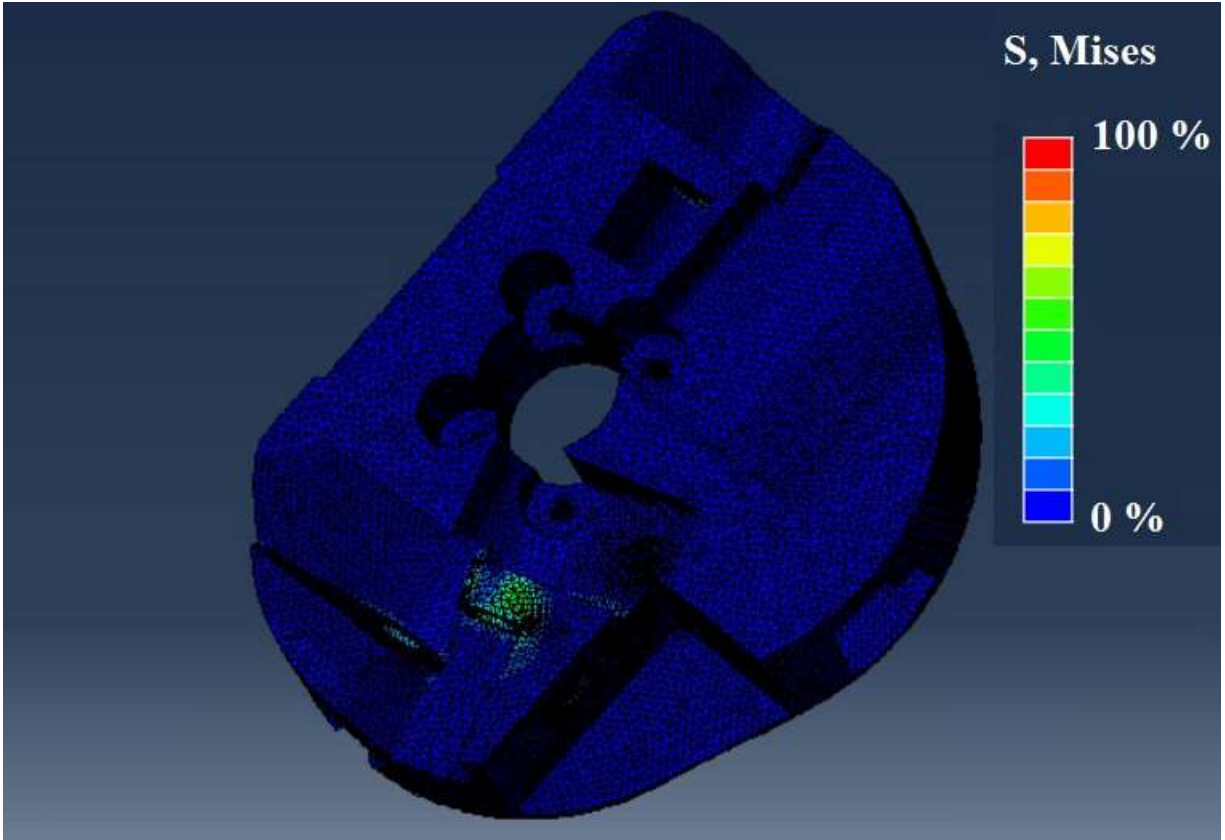


Figure 4.12 – FEA results, general view.

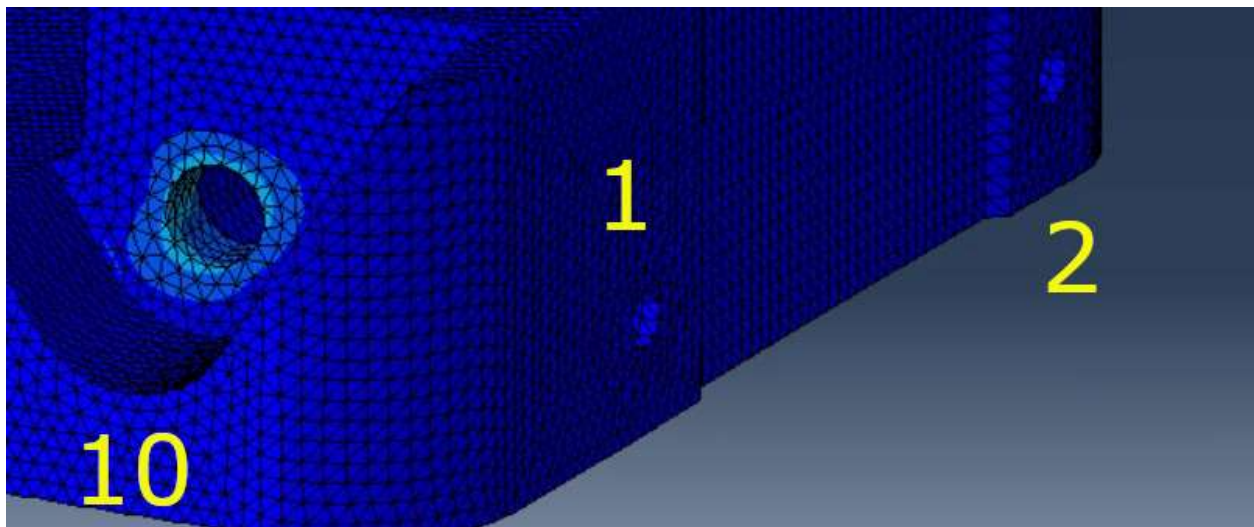
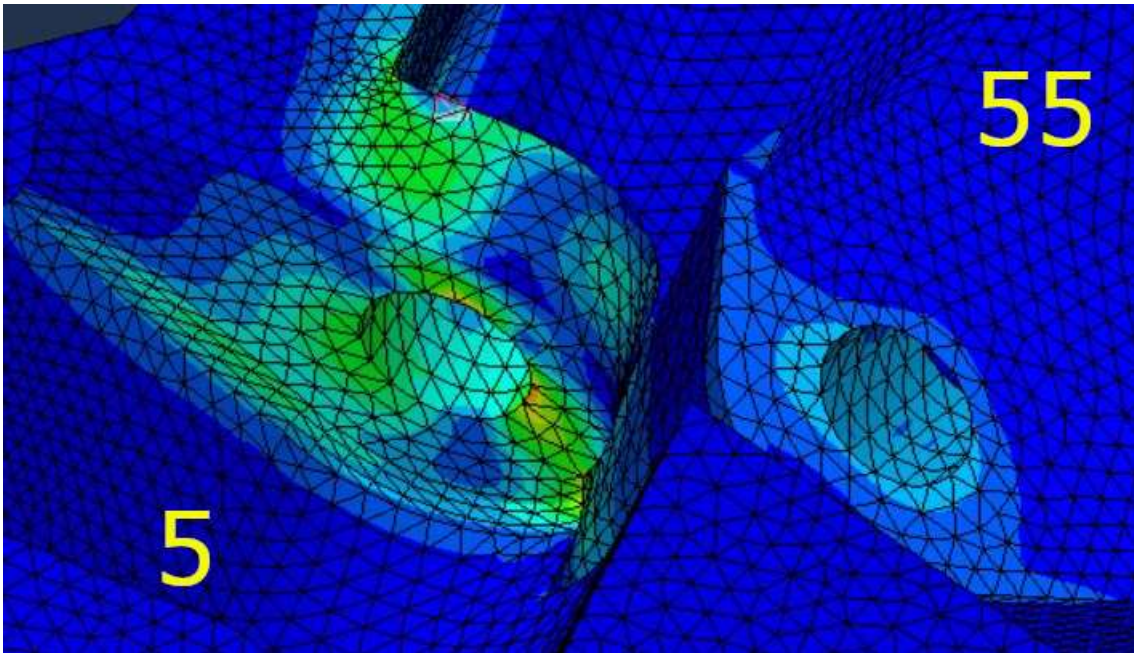
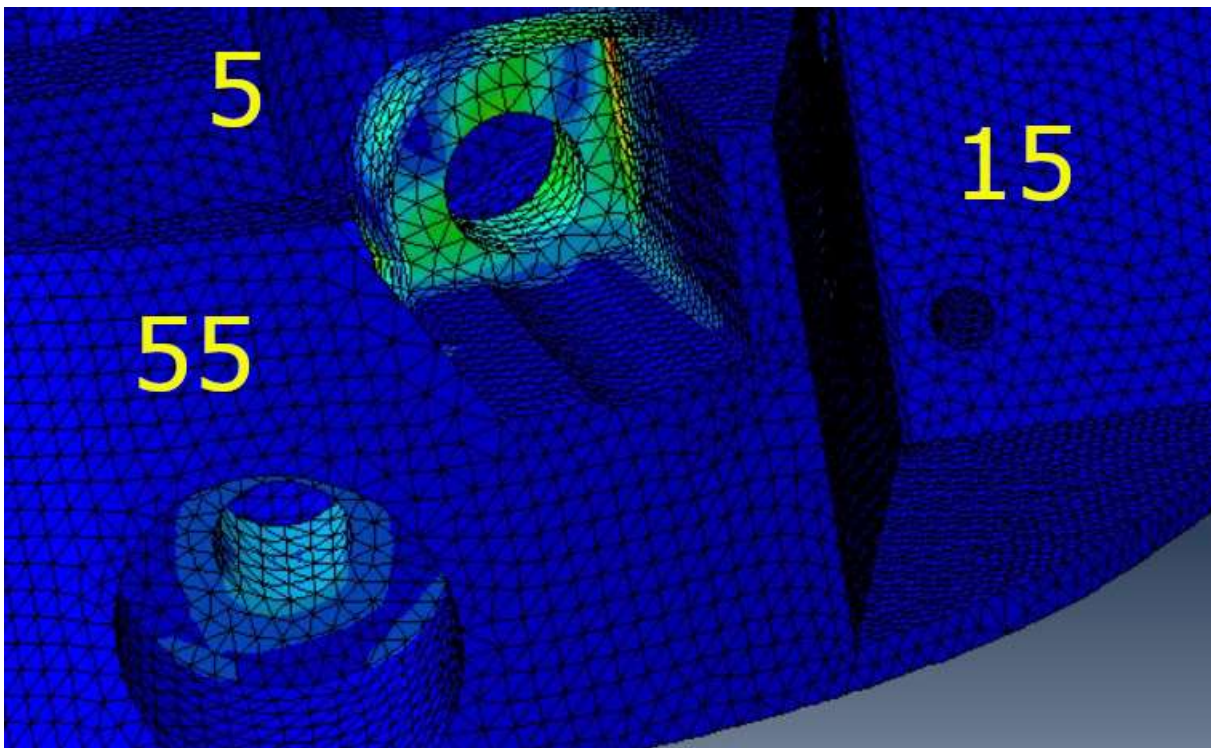


Figure 4.13 – FEA results, view 1.



*Figure 4.14 – FEA results, view 2.*

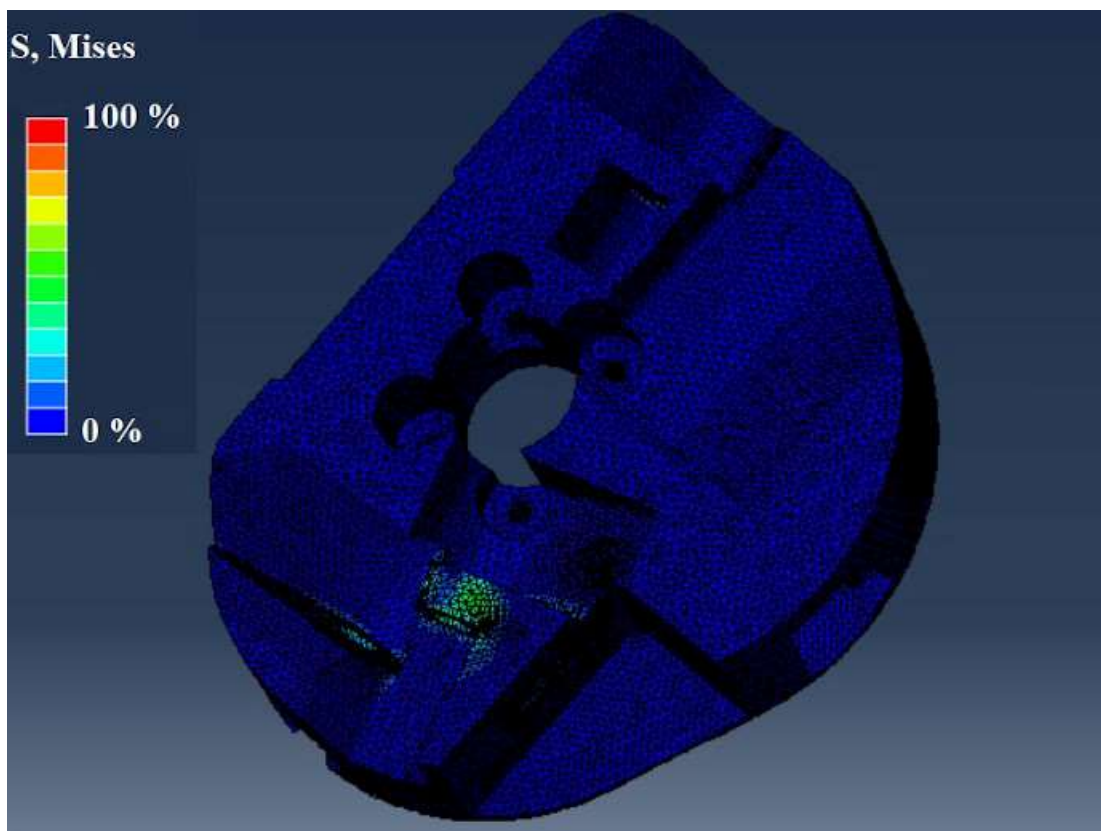


*Figure 4.15 – FEA results, view 3.*

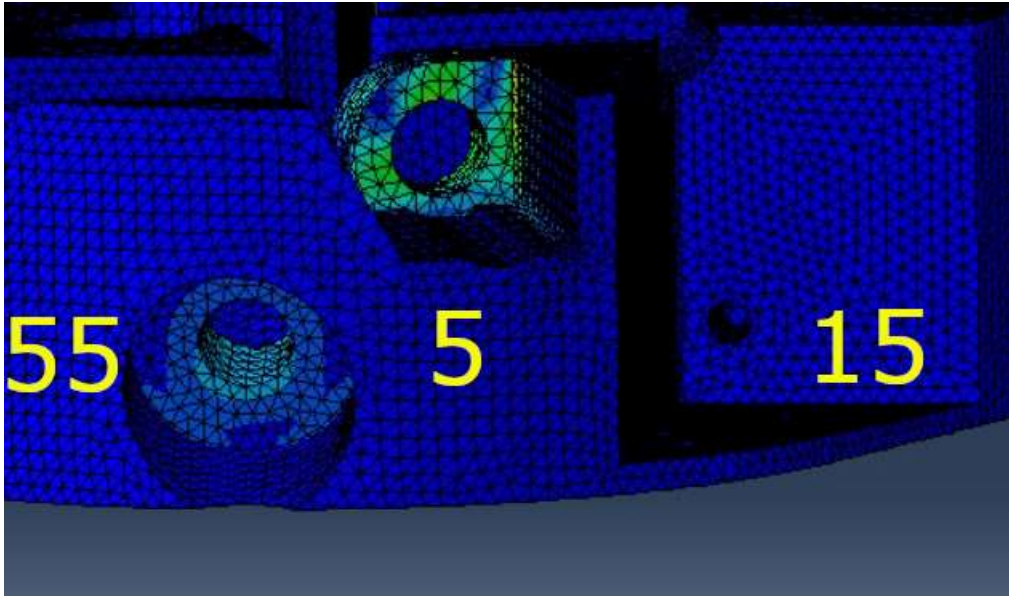
## ax+ay 1

Figure 4.16 shows the result of the FEA on the component before the optimization in the Fatigue loading condition in this precise step. As it can be seen, the stresses in general do not affect the structure in a heavy way. Figures 4.17, 4.18 and 4.19 are enlargements of the bushings where the loads are applied. In fact, as said in Chapter 2.2, in this loading condition point 16 has been bounded; even in this case, point 5 is the most stressed.

As already said, also these loads justify the use of Topology Optimization finalised to AM to manufacture this component because there will be a great weight reduction.



*Figure 4.16 – FEA results, general view.*



*Figure 4.17 – FEA results, view 1.*

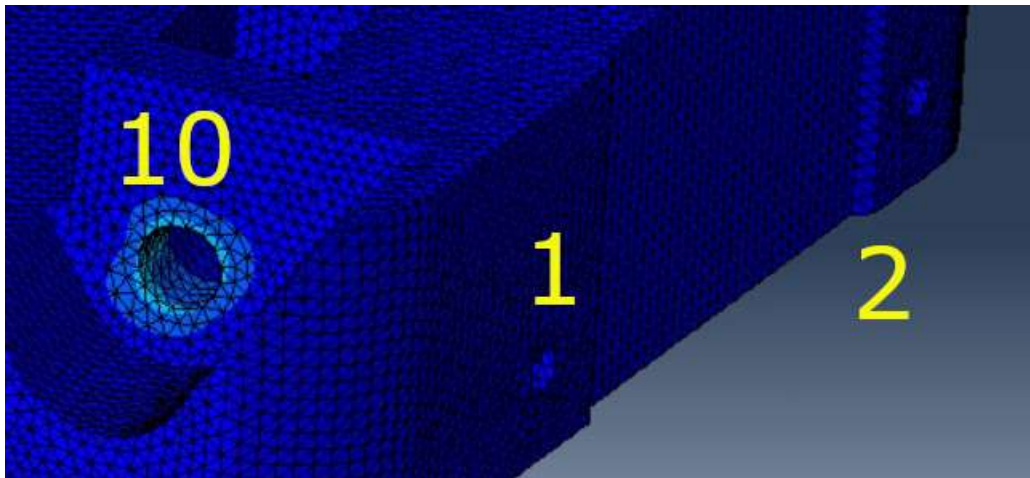


*Figure 4.18 – FEA results, view 2.*

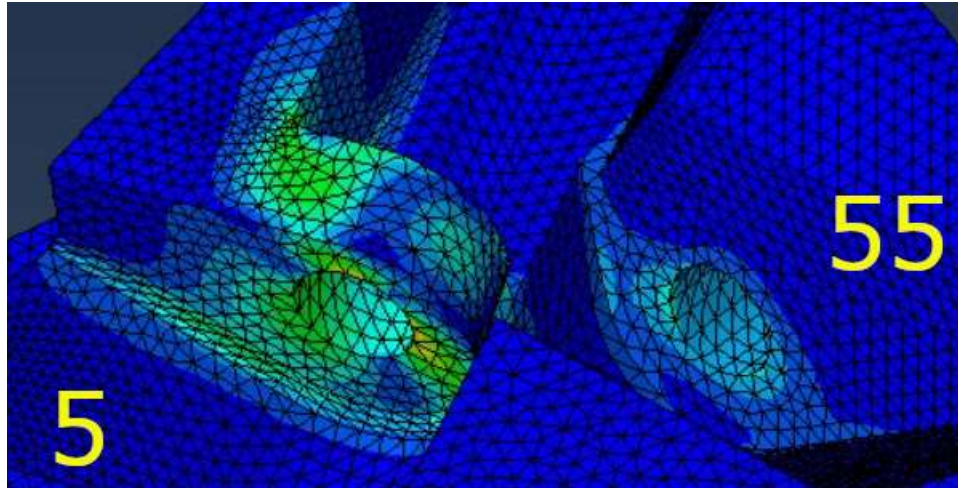


*Figure 4.19 – FEA results, view 3.*

## **BUCKLING**

Figure 4.20 shows the result of the FEA on the component before the optimization in this loading condition. As it can be seen, the stresses in general do not affect the structure in a heavy way. The maximum percentage is a lower value than the yield stress, as established in Chapter 2.2. Figures 4.21, 4.22, 4.23 and 4.24 are enlargements of the bushings. As said in Chapter 2.2, in this loading condition point 16 has been bounded. As it is possible to observe from the following figures, the highest stresses are concentrated in point 15, just because it is the only one loaded.

In this case, the use of Topology Optimization finalised to Additive Manufacturing is highly recommended because there is a huge part of the component that does not have a structural function.

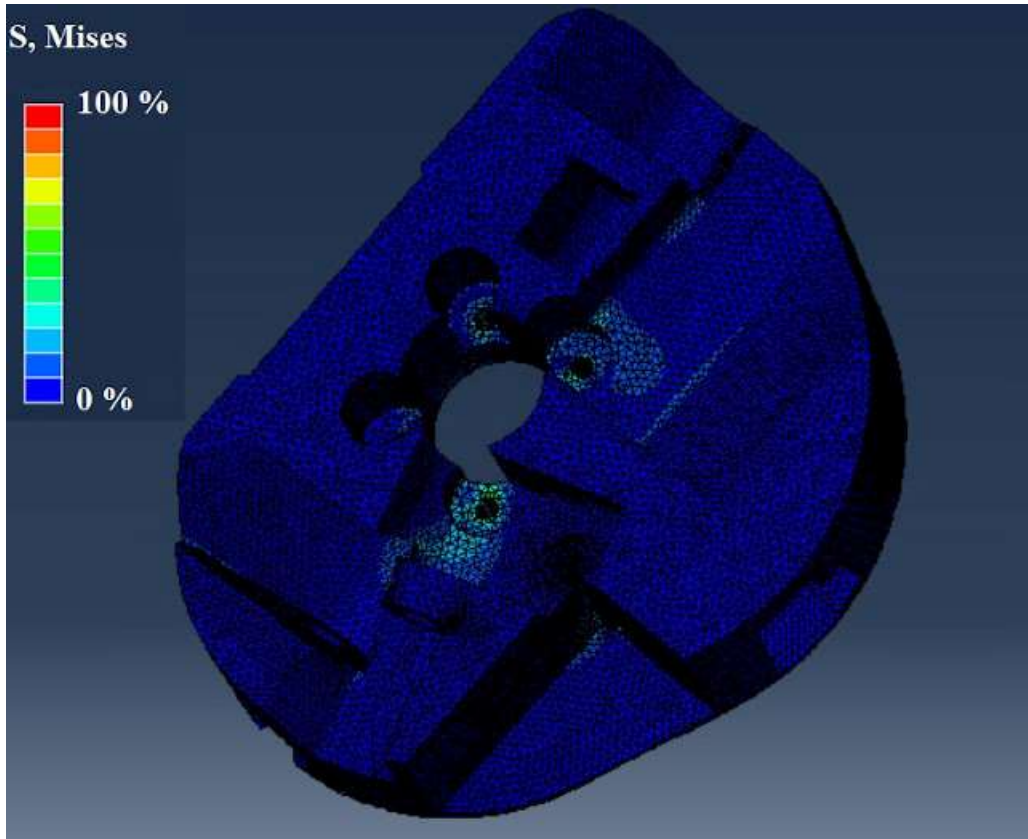
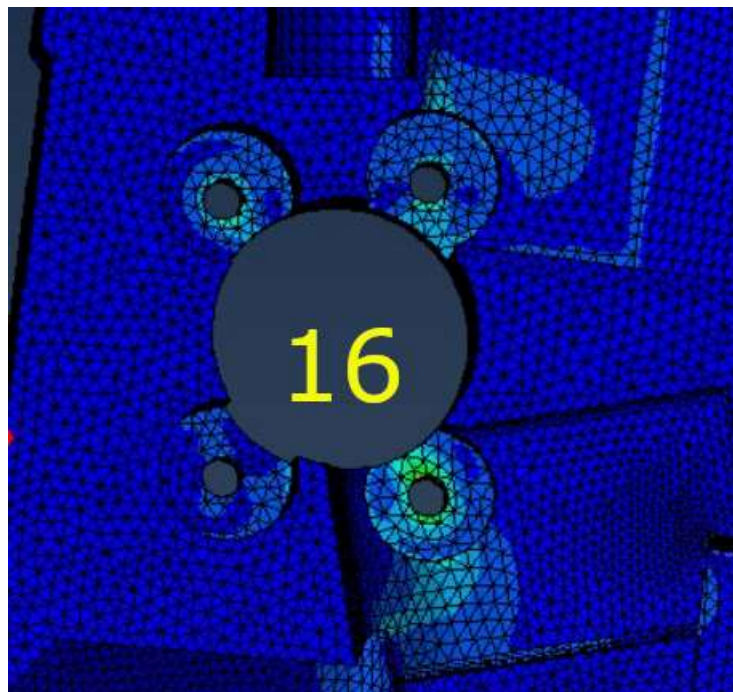
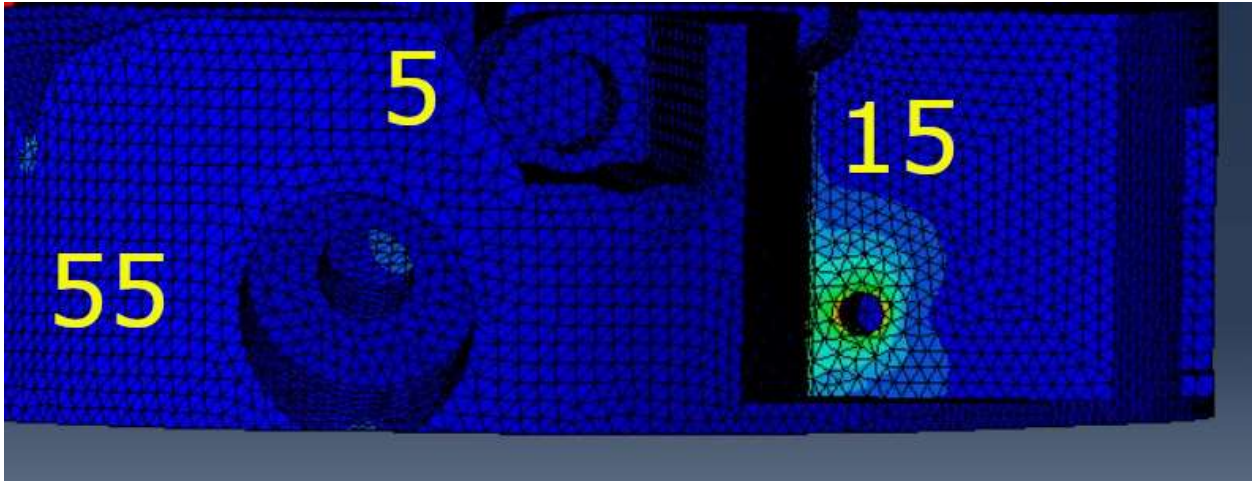


Figure 4.20 – FEA results, general view.



*Figure 4.21 – FEA results, view 1.*



*Figure 4.22 – FEA results, view 2.*

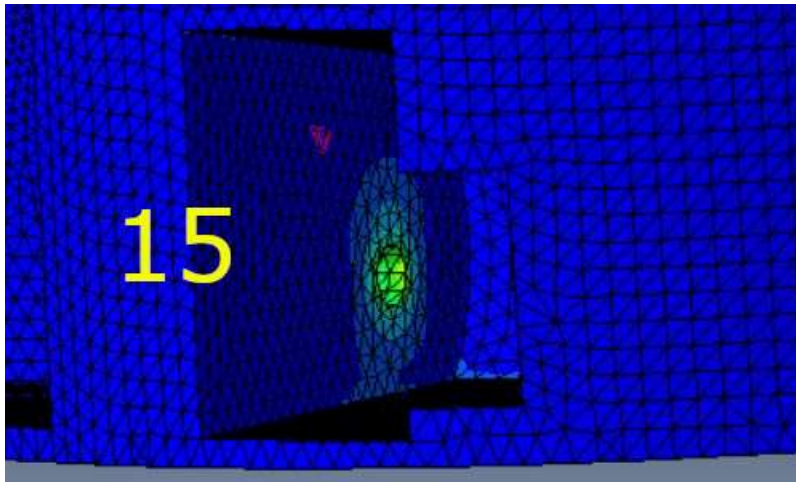


*Figure 4.23 – FEA results, view 3.*

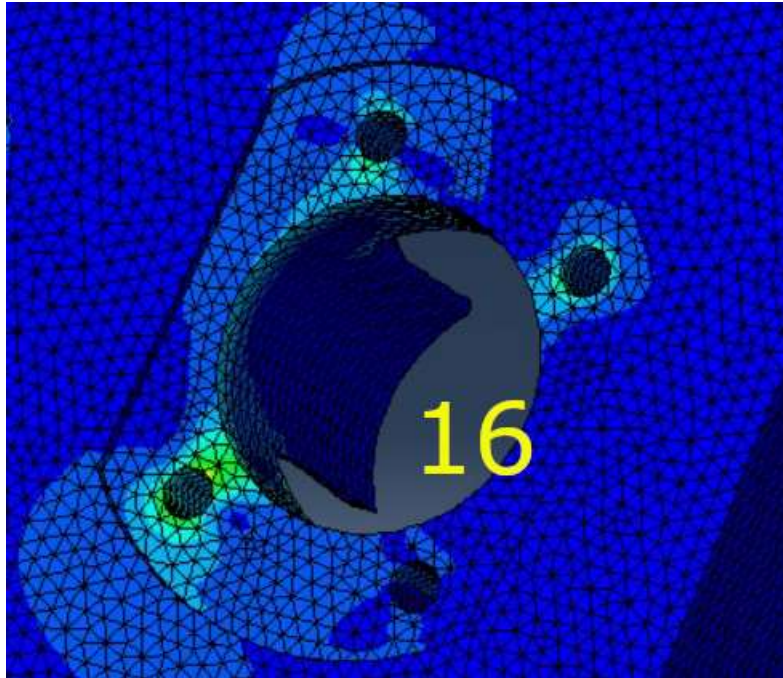


*Figure 4.24 – FEA results, view 4.*

## 4.2 Topology optimization of the complete component

The process has been set with a maximum of 150 cycles; in order to have a result in the fastest way, 48 cores of the server available at McMaster University were used and the process took 13 hours. The convergence of the software has been reached at the 98<sup>th</sup> cycle.

The objective of the optimization is the minimization of the mass of the component. In this process, a mass reduction of 84.3% has been reached; in fact, the initial design space weighted 23 kg while the optimized component weights 3.6 kg.

The optimized component has been exported as a .STL file; the part described by this file had a geometrical poor quality because Abaqus is set with a default density threshold of  $\rho = 0.3$ .

Thanks to the smooth function, a better surface has been obtained. The smoothing process determines which elements are on the surface of the model and uses the ISO value to calculate where on the interior edges of the elements new nodes are created. Increasing the ISO value leads to a decrease of the model volume.

With an ISO value of 0.15, all the holes and the imprecise entities of the surface have been fixed; in fact, with this process, the surface roughness has been improved. Subsequently, the .STL file has been imported in NX Unigraphics Siemens; after that, thanks to the NX Unigraphics, all the triangular faces have been replaced with a unique surface. The resulting component is called “facet body”. Figures 4.25, 4.26, 4.27 and 4.28 show the optimized component from different views.

Comparing the optimized component with the space design, it can be observed that there are huge zones where the material has been eliminated completely. As it can be seen, all the different parts of the optimized component are connected by beams, which absorb all the stresses due to the applied loads.

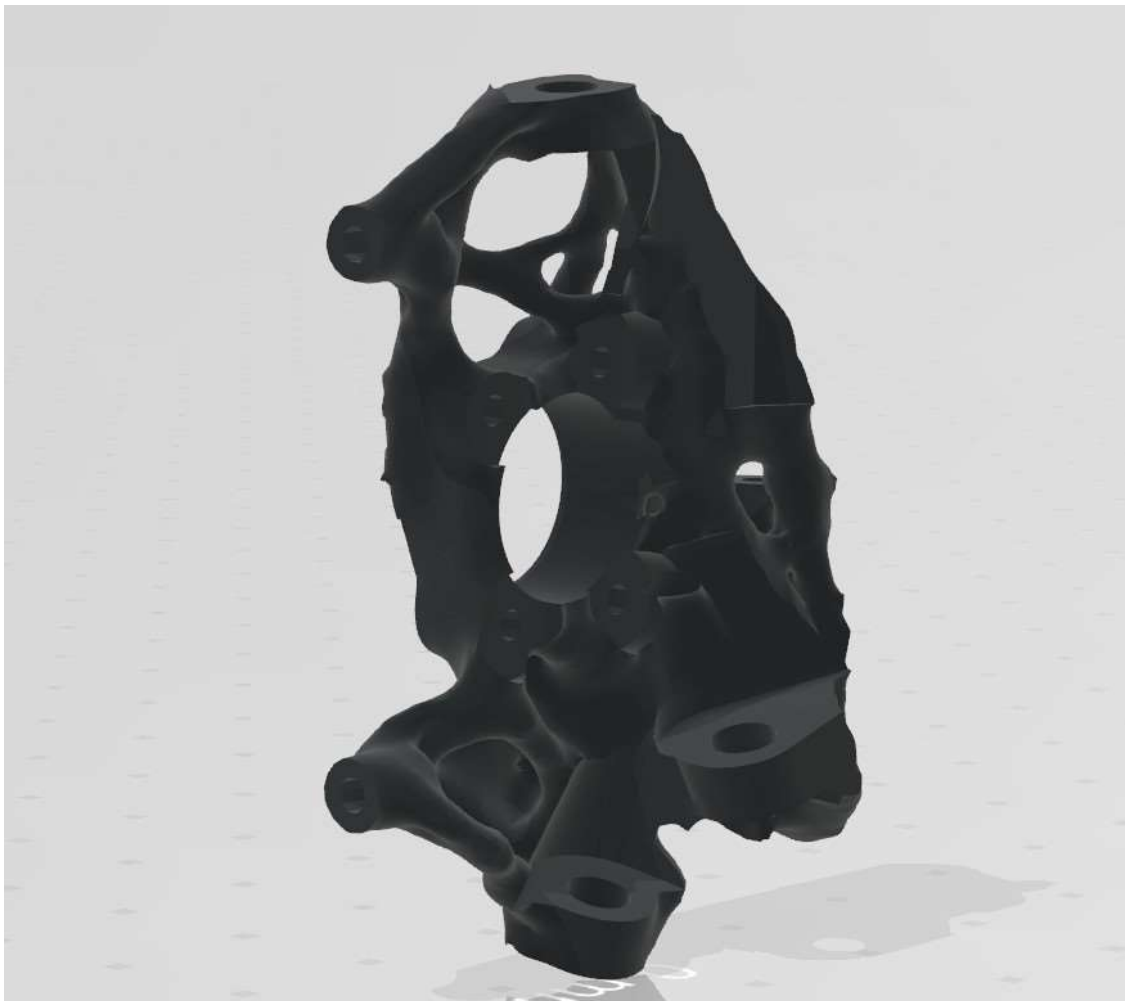


Figure 4.25 – Optimized component, view 1.



Figure 4.26 – Optimized component, view 2.



Figure 4.27 – Optimized component, view 3.



Figure 4.28 – Optimized component, view 4.

### 4.3 Final Finite Element Analysis

To verify the optimized part, a specific Abaqus/CAE plug-in tool has been used; this tool allows to commute a .STL file in a solid part, in order to set again a new analysis.

The steps defined in this analysis are the same of the preliminary one; the only thing that has been modified is the dimension of the mesh elements: for this analysis a dimension of 3 mm has been set.

This final analysis is needed just to verify that the final component resists to all the possible combinations of loads.

## **BRAKING**

Figure 4.29 shows the result of the FEA on the optimized component in this loading condition. As it can be seen, the stresses in general do not affect the structure in a heavy way. In fact, observing the legend on the side of the figure, it is possible to see that the blue color corresponds at the zero percentage of the stresses, while the red color corresponds to the maximum percentage of the stresses. Of course, the maximum percentage is a lower value than the yield stress (240 MPa), as established in Chapter 2.2. As it is possible to observe from figure 4.30, the highest stresses are concentrated near point 2.

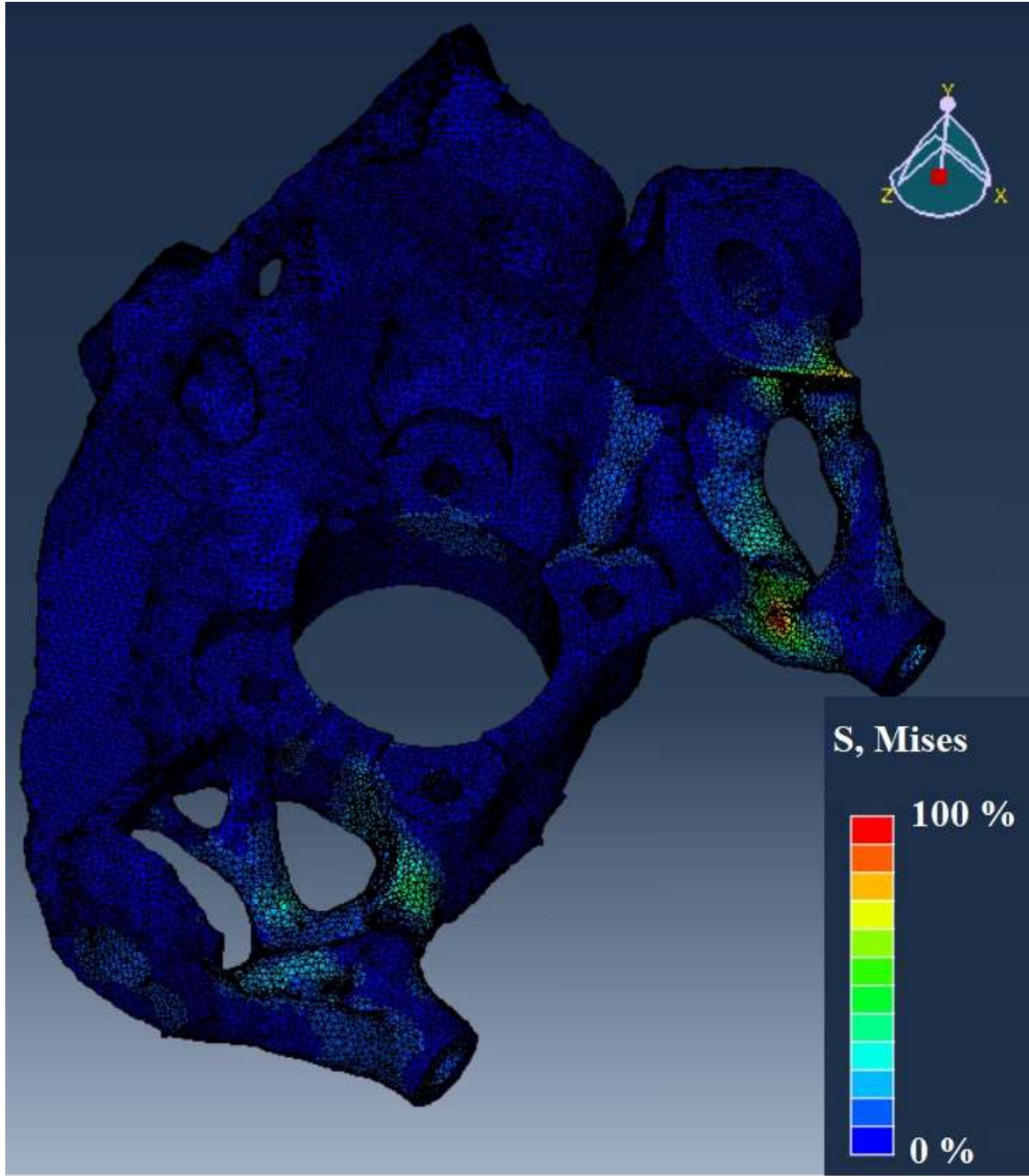


*Figure 4.29 – FEA results, general view.*

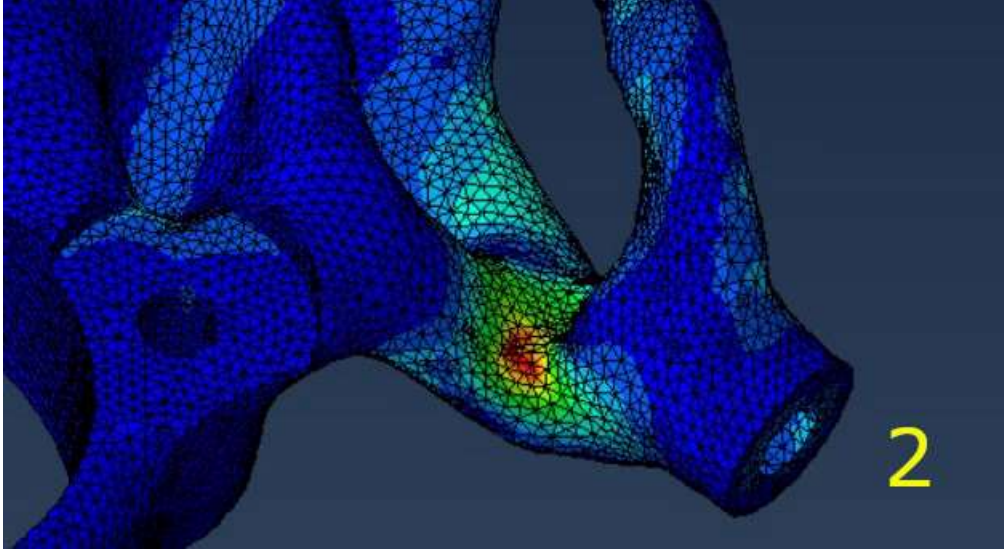


*Figure 4.30 – FEA results, view 1.*

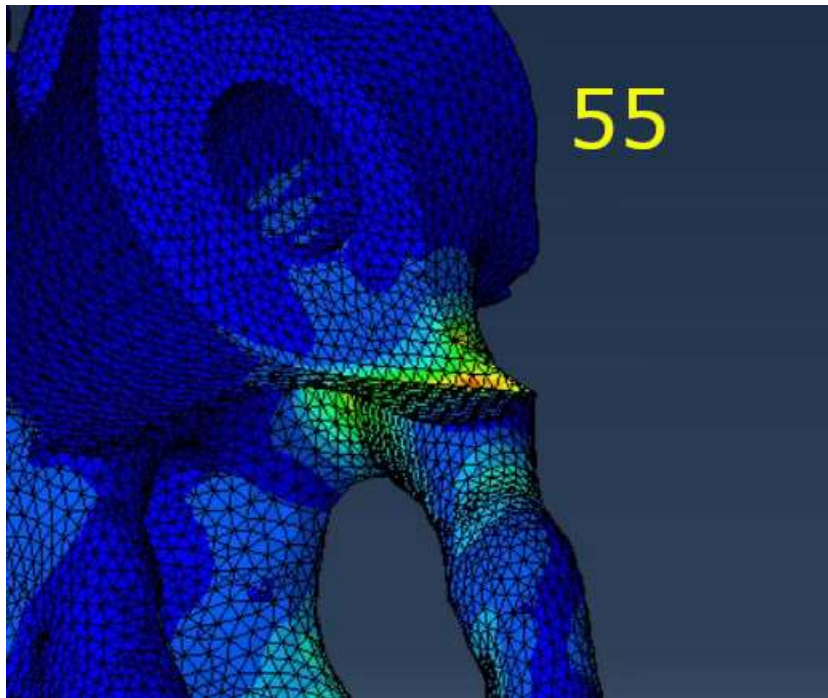


*Figure 4.31 – FEA results, view 2.*

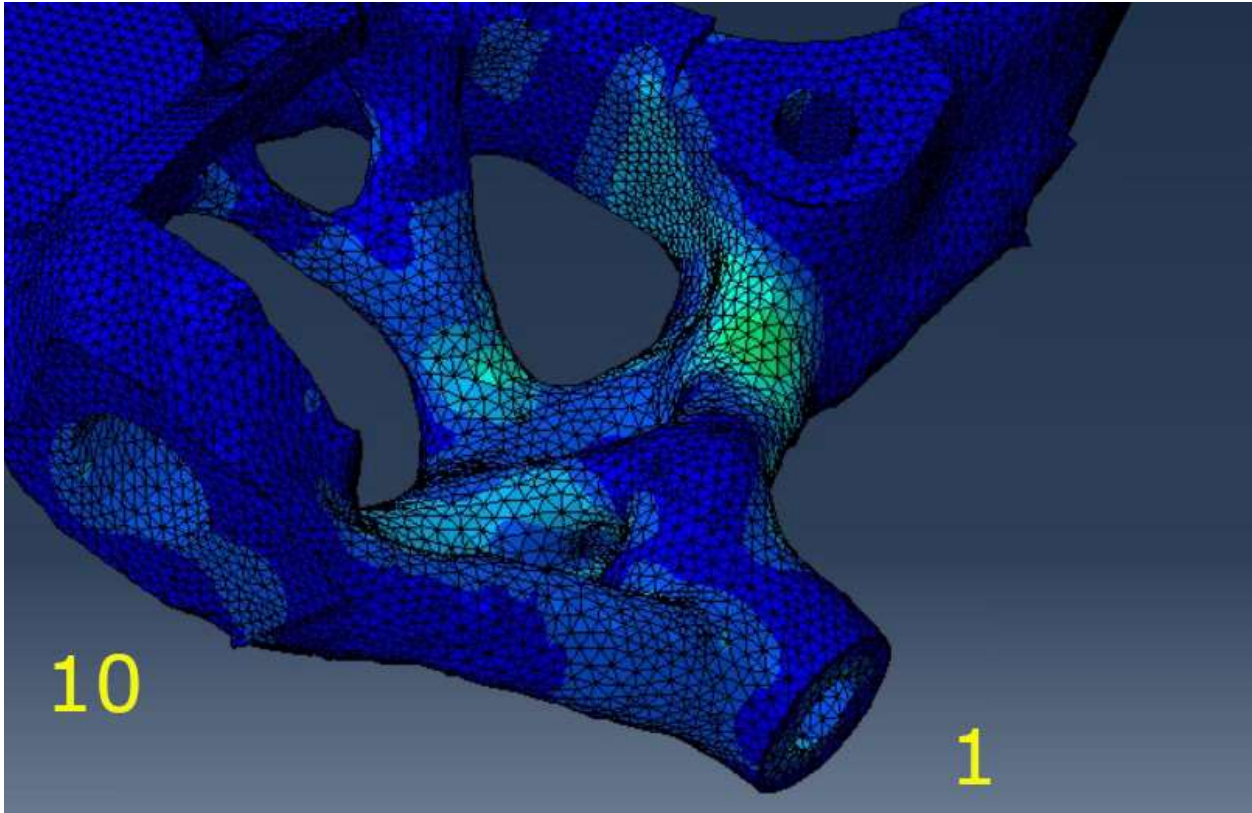


*Figure 4.32 – FEA results, view 3.*

## **CORNERING 2**

Figure 4.33 shows the result of the FEA of the optimized component in the Fatigue loading condition in this precise step. As it can be seen, the stresses in general do not affect the structure in a heavy way. In this case and in the following two cases, the maximum percentage is a lower value than the fatigue stress, as established in Chapter 2.2. Comparing this result with the preliminary one, in both cases all the area around point 55 is the most stressed and there are more stresses on the area around point 16, where the constraint is applied.

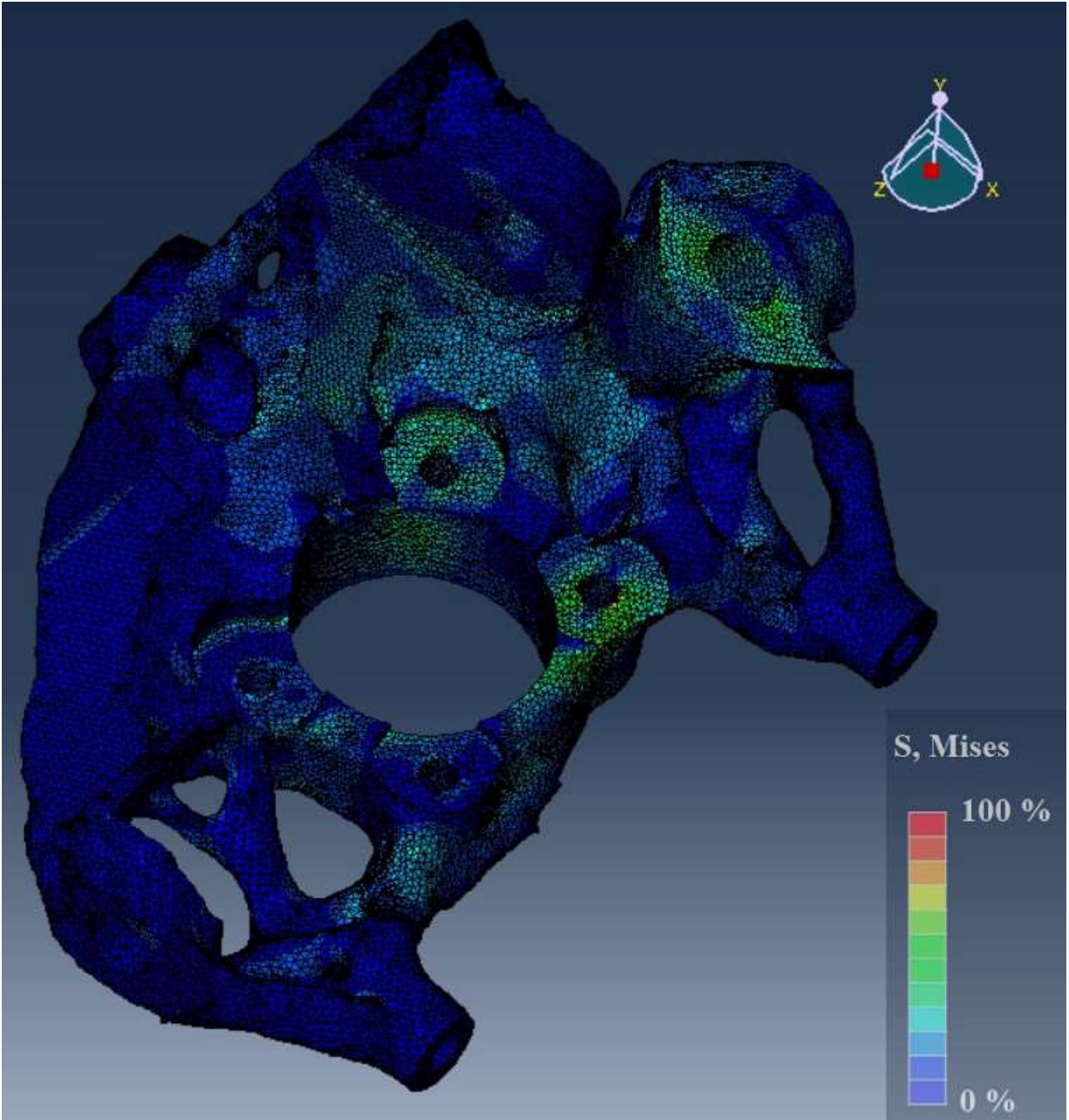


*Figure 4.33 – FEA results, general view.*

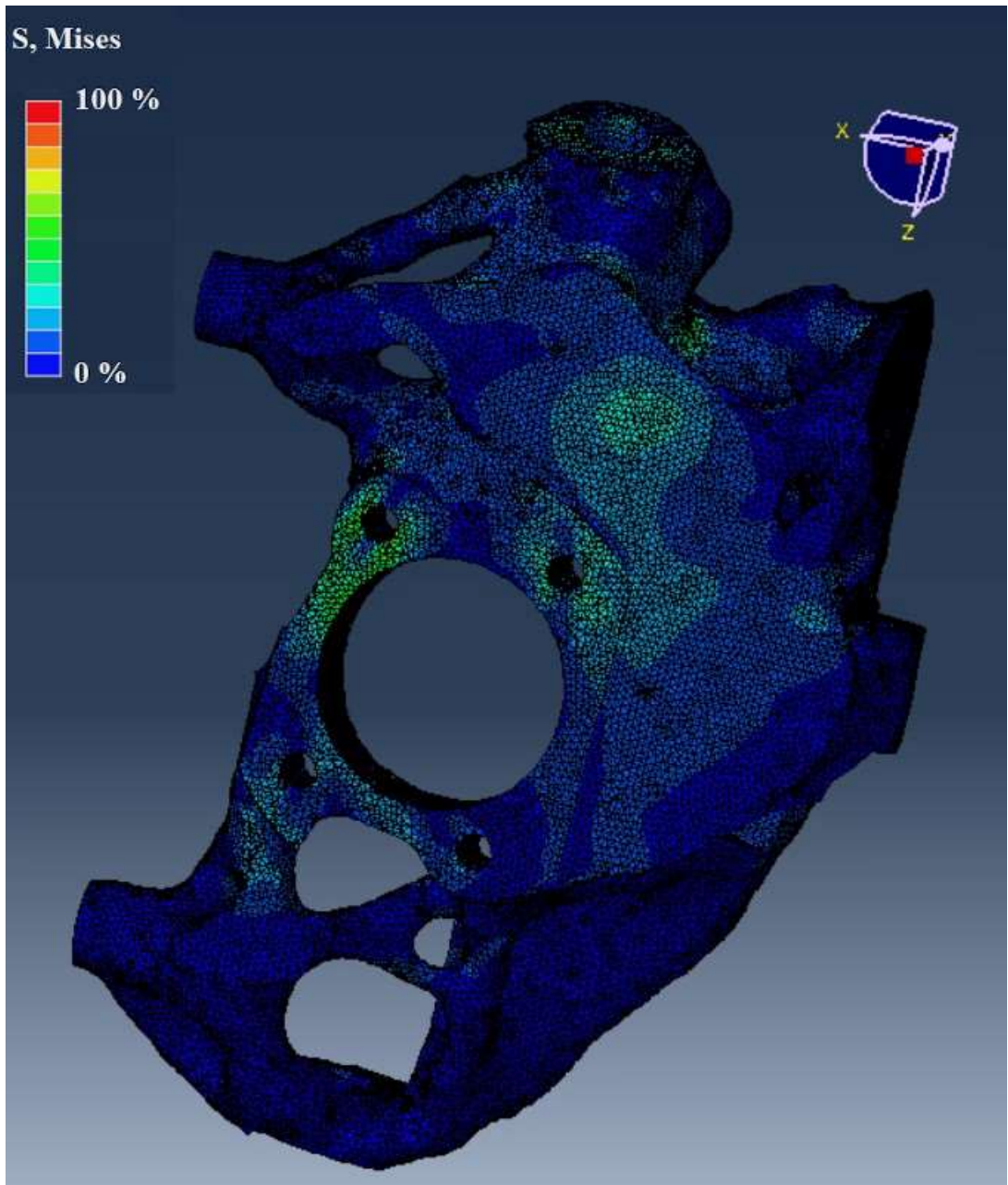
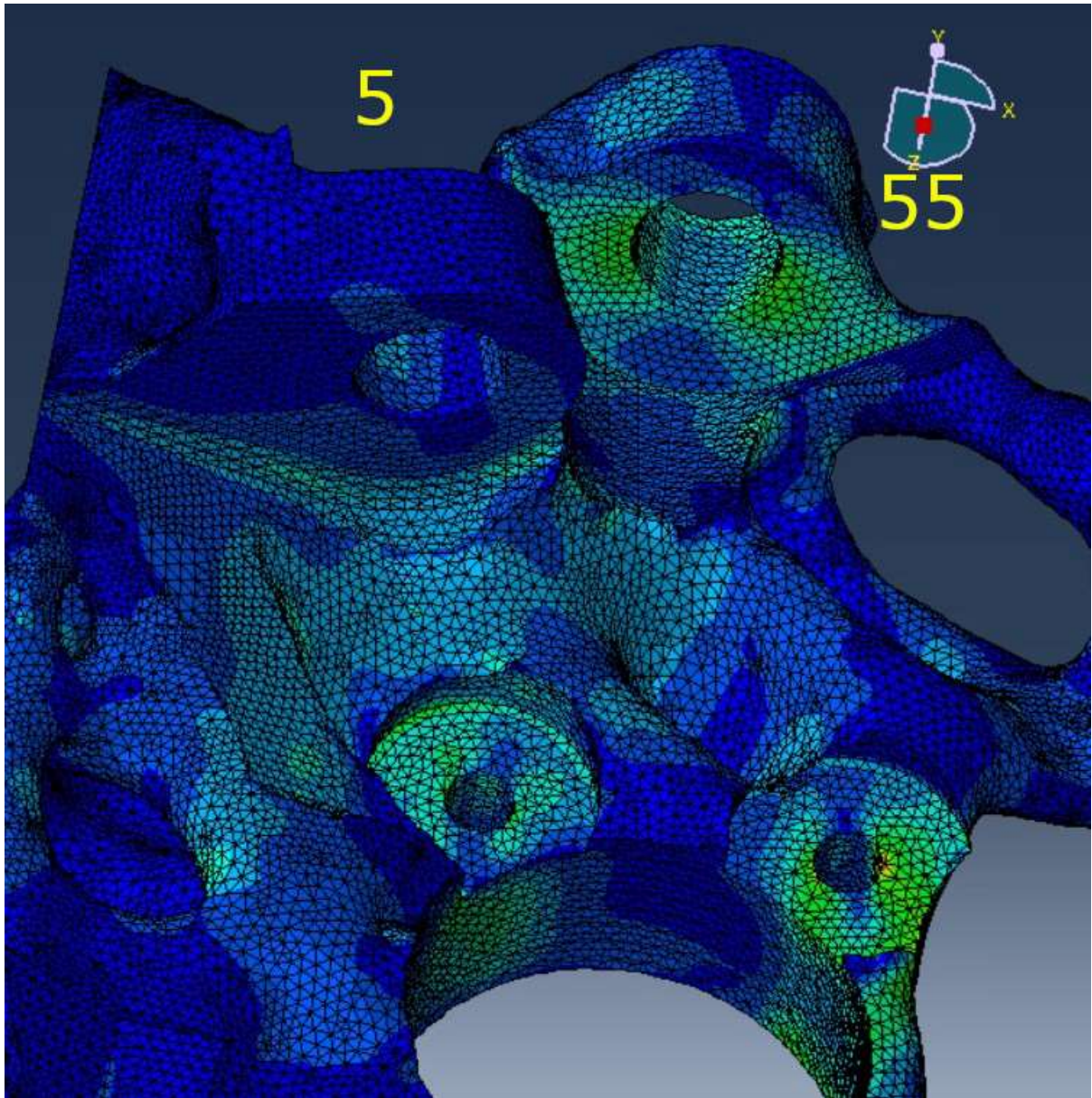
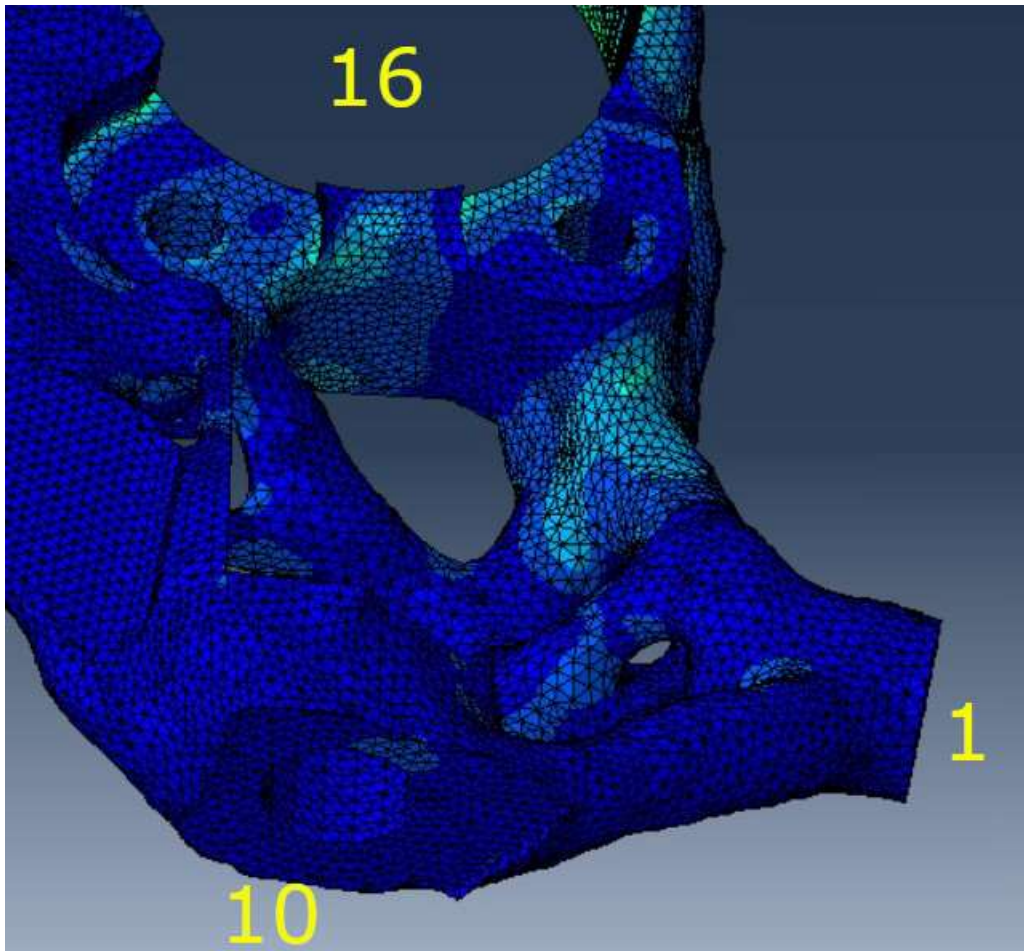


Figure 4.34 – FEA results, general view.



*Figure 4.35 – FEA results, view 1.*



*Figure 4.36 – FEA results, view 2.*

## **BRAKING 2**

Figure 4.37 shows the result of the FEA of the component in the Fatigue loading condition in this precise step; comparing the loads of this step with others, it can be noticed that this step is heavier than the previous ones. The most affected zones are the areas around point 5 and point 55.

As it can be seen from figure 4.39, there are some red elements on the edge of bushing seat; this phenomenon can be explained with the presence of a rigid connection. The distributing coupling makes the structure infinitely rigid: obviously, it is impossible to obtain really an infinite stiffness. In fact, the rigid coupling gives to the structure more stiffness. This phenomenon is smoothed due to the material ductility.

It is possible to observe that point 5 is the most stressed. In fact, this point is the most critical one because of its shape.

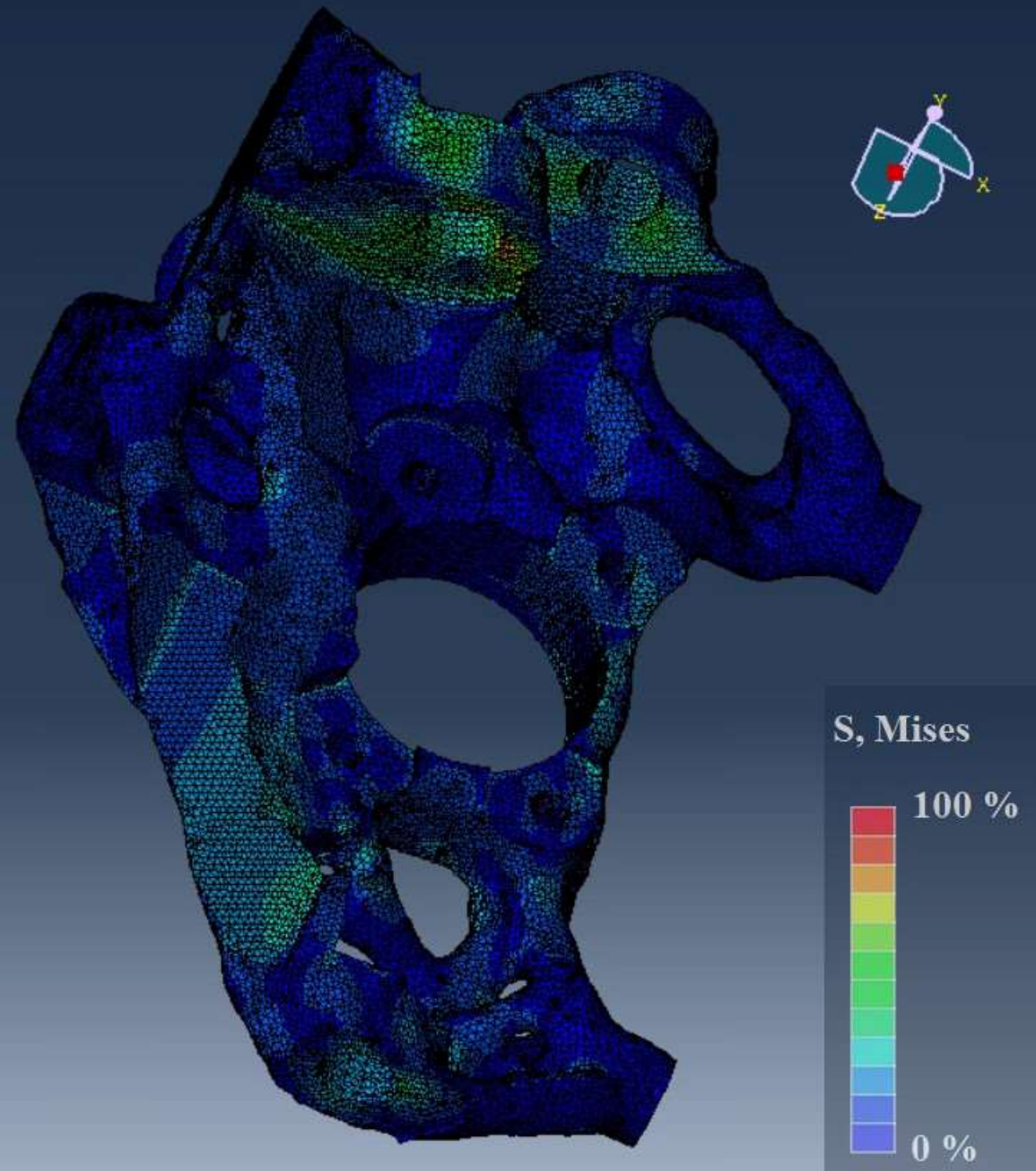
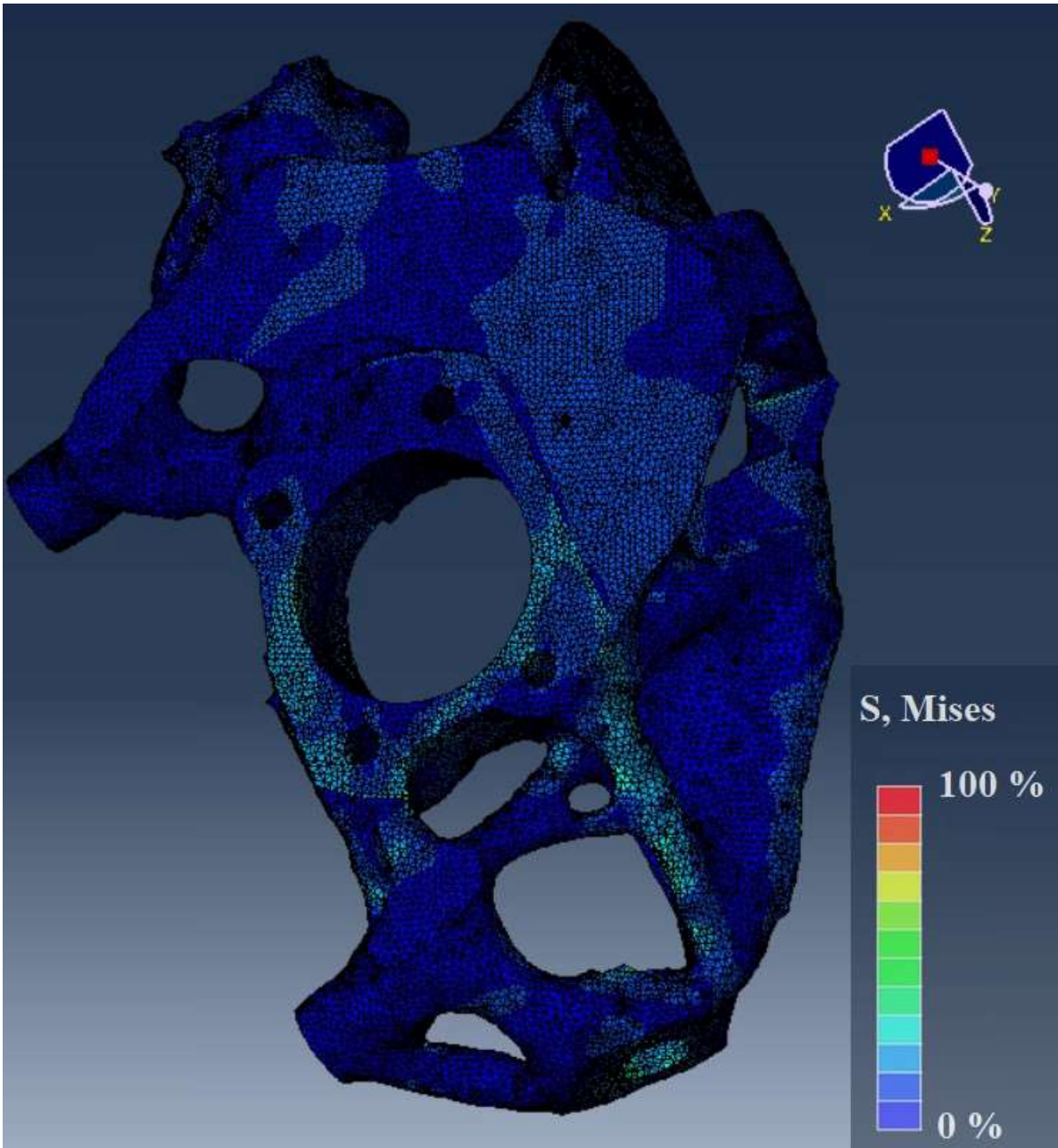
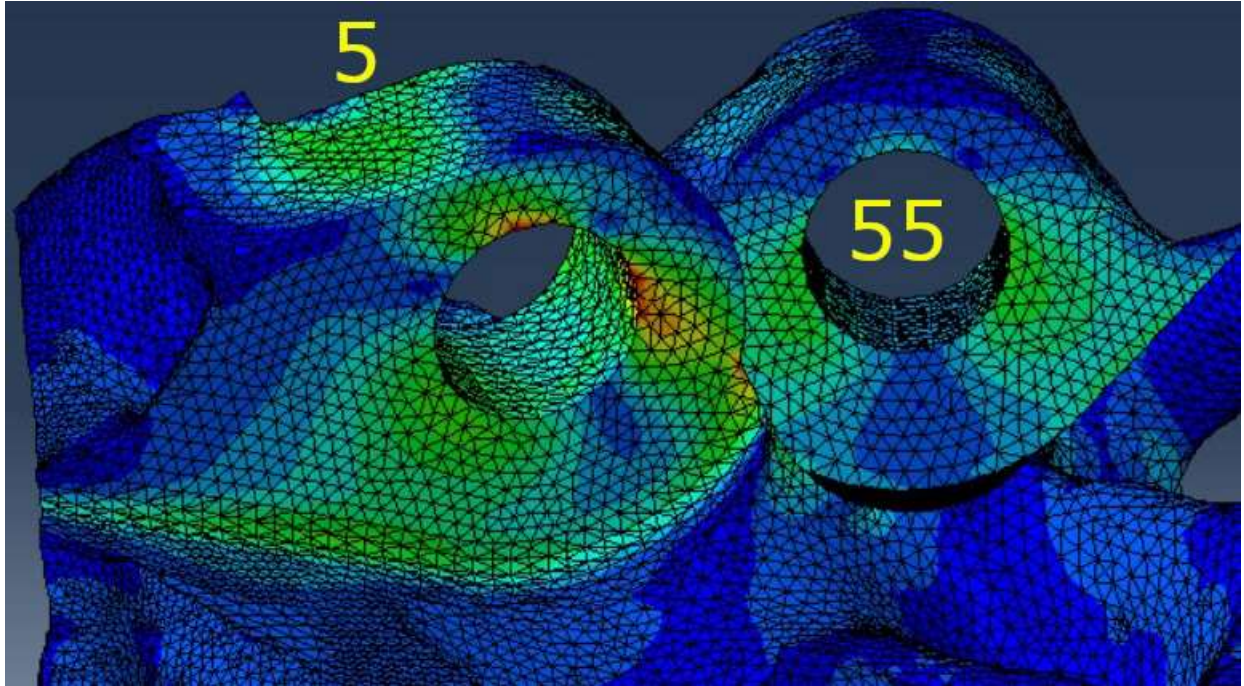


Figure 4.37 – FEA results, general view.



*Figure 4.38 – FEA results, general view.*



*Figure 4.39 – FEA results, view 1.*

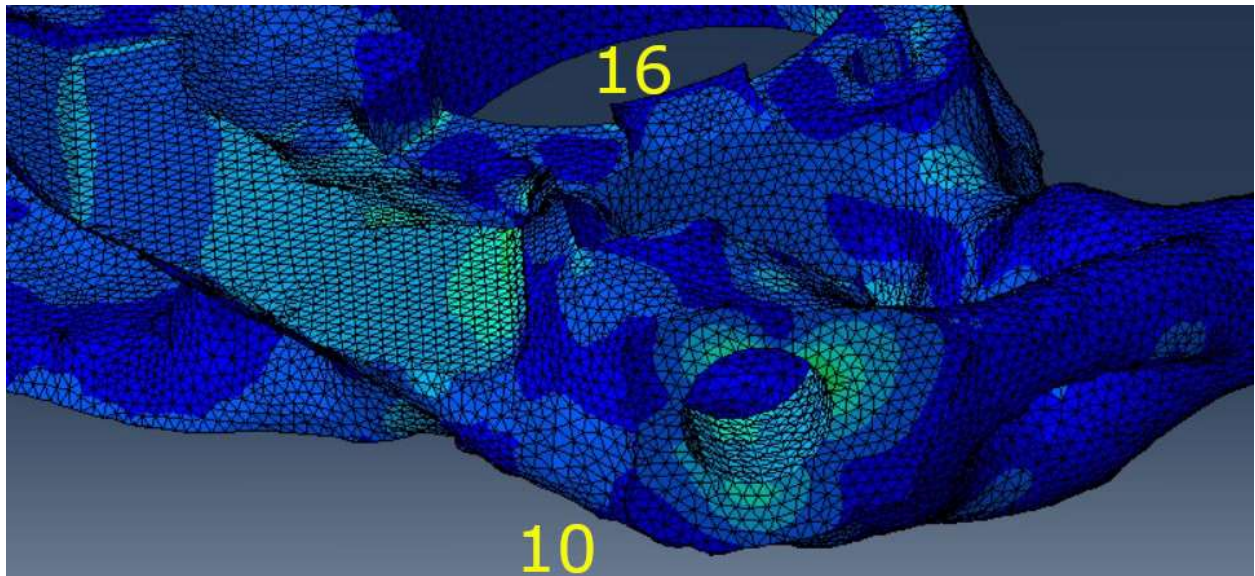


*Figure 4.40 – FEA results, view 2.*

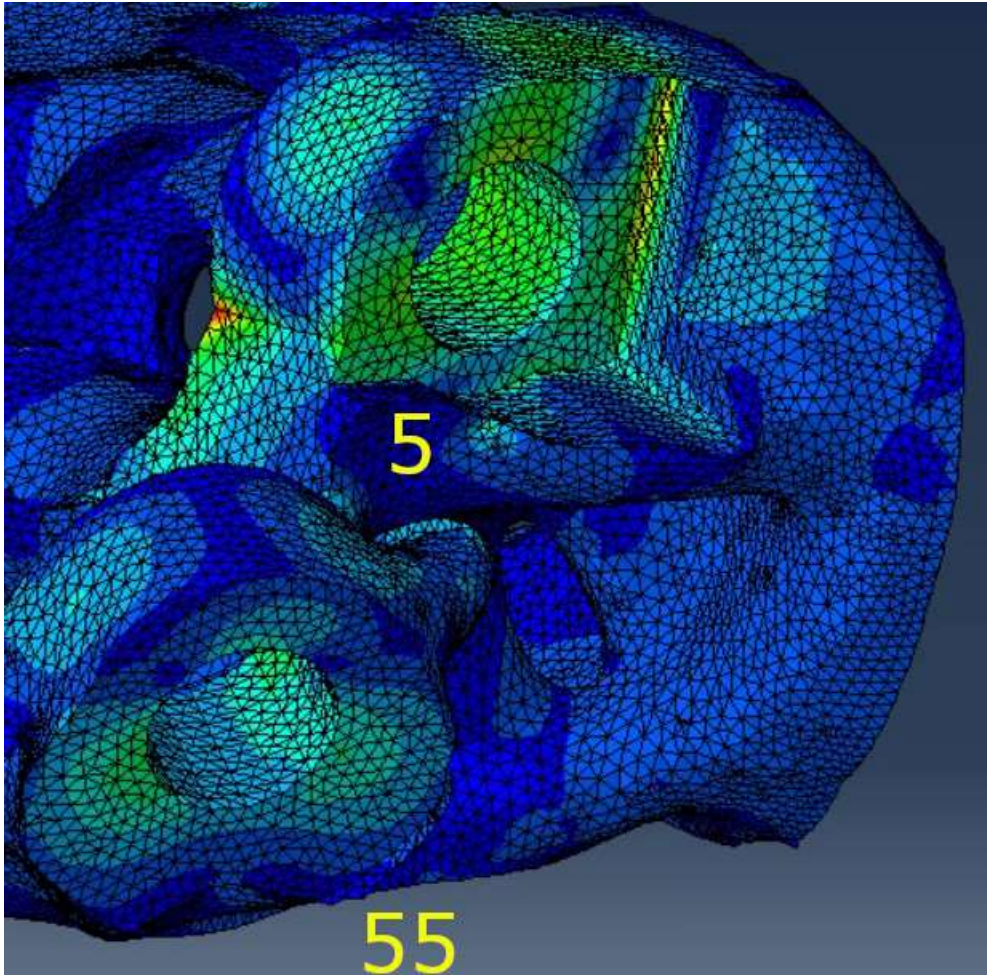


*Figure 4.41 – FEA results, view 3.*

**ax+ay 1**

Figure 4.42 shows the result of the FEA of the component in the Fatigue loading condition in this precise step; in this step the stresses are the highest because this step is the heaviest one. The most affected zones are the areas around point 5 and point 55.

The phenomenon that affects the area around point 5 has been already discussed.

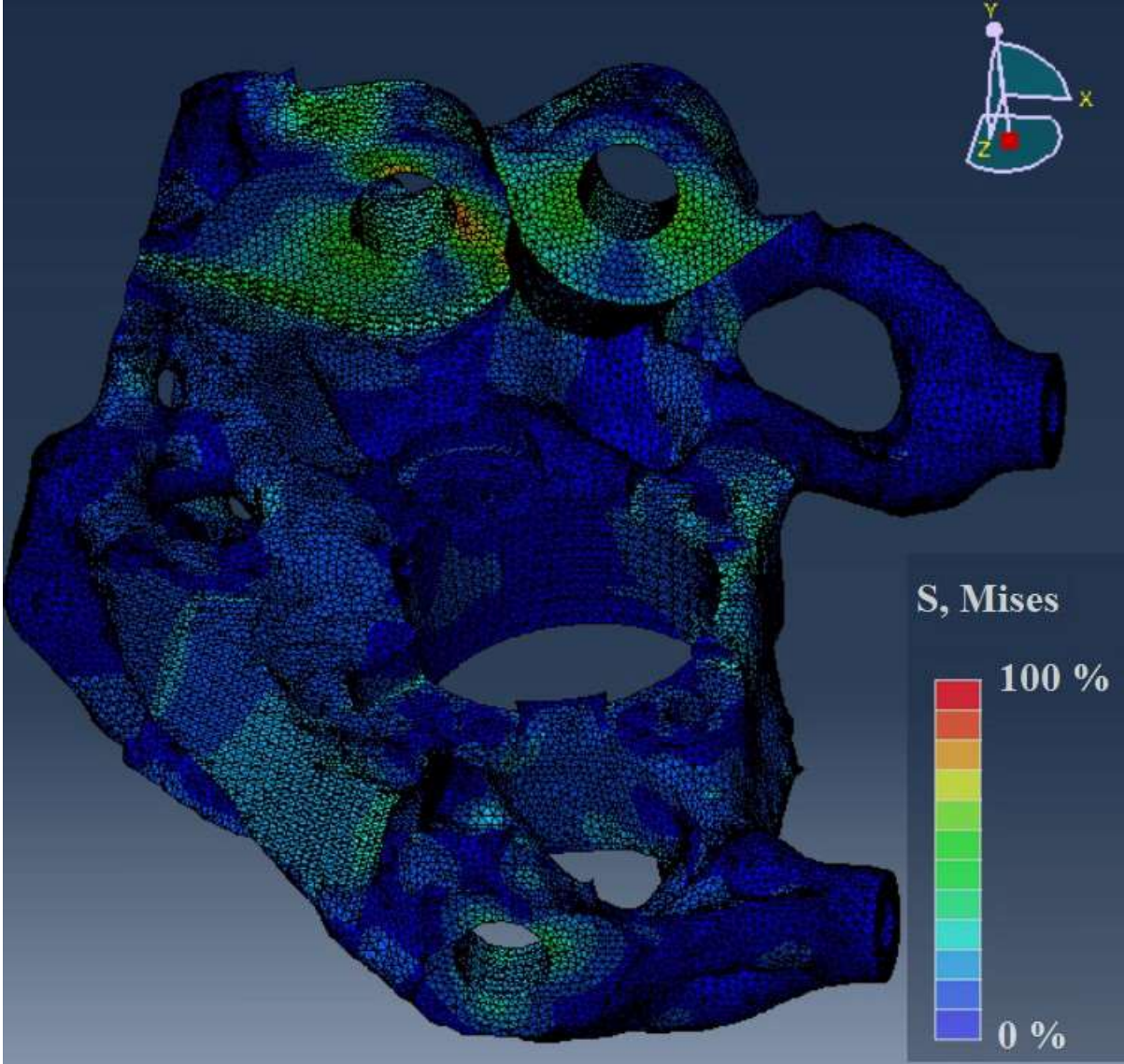


Figure 4.42 – FEA results, general view.

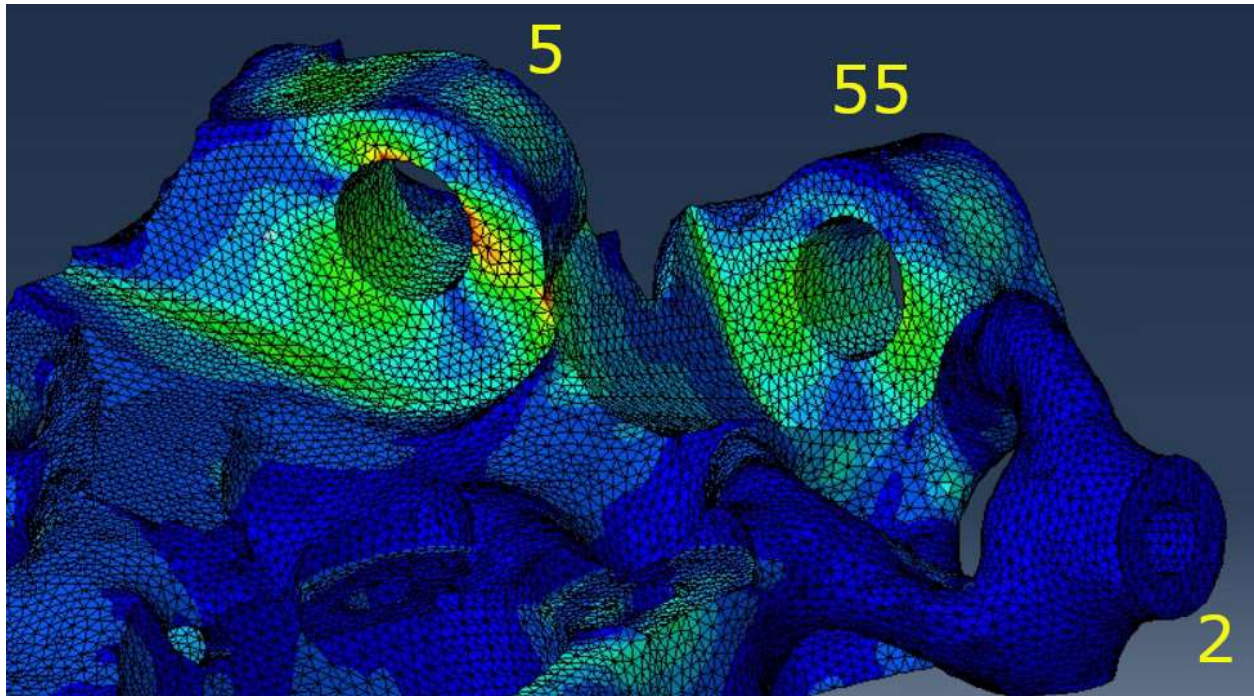


Figure 4.43 – FEA results, view 1.

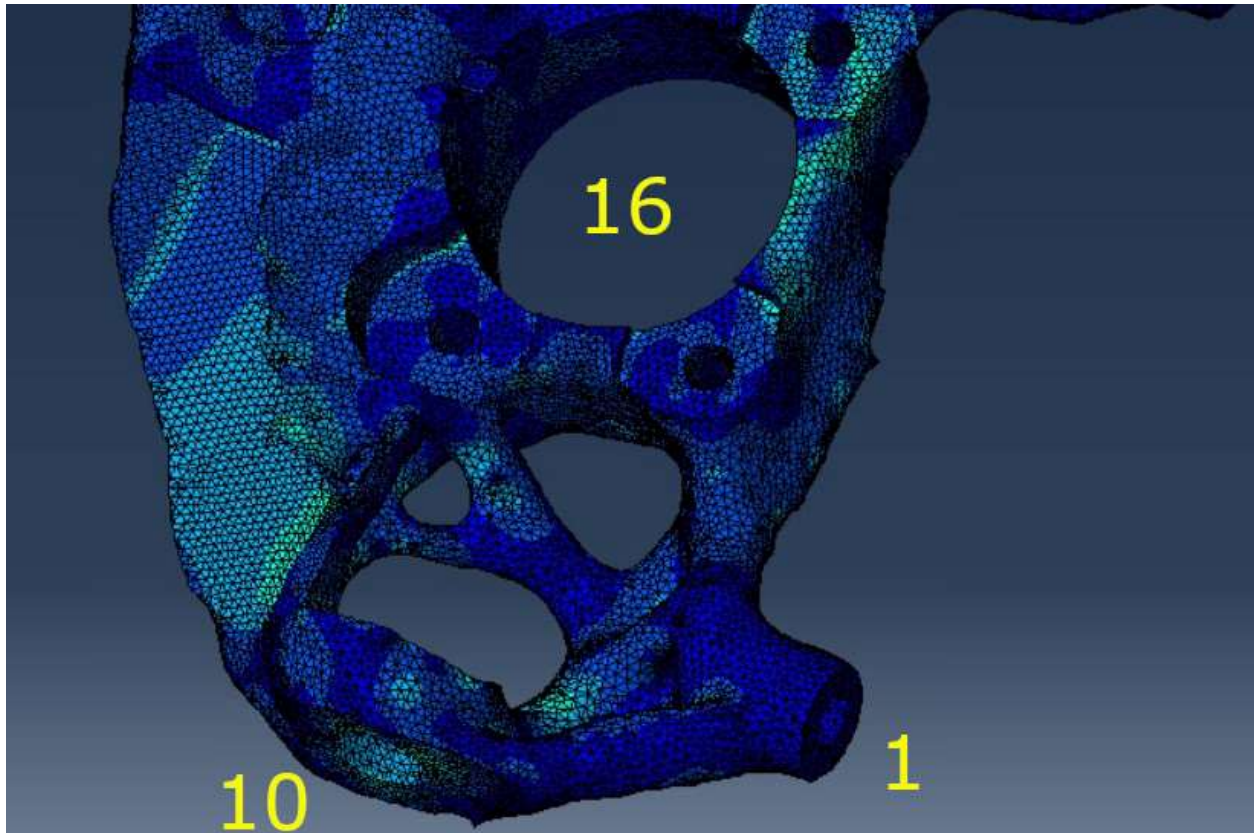
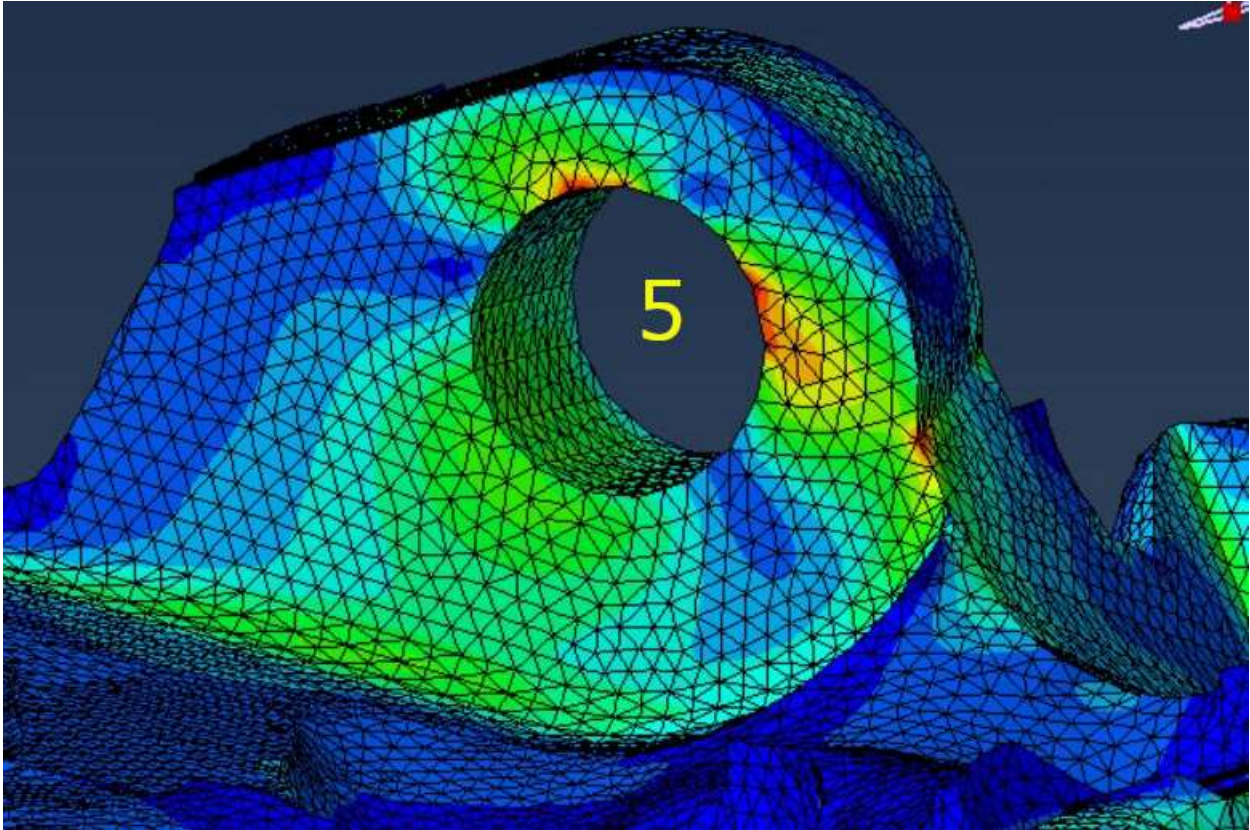


Figure 4.44 – FEA results, view 2.



*Figure 4.45 – FEA results, view 3.*

## **BUCKLING**

Figure 4.46 shows the result of the FEA of the optimized component in this loading condition. As it can be seen, the stresses in general do not affect the structure in a heavy way. The maximum percentage is a lower value than the yield stress, as established in Chapter 2.2. The most stressed zones are the ones around point 15 and point 16: it is possible to explain this because point 15 is the only loaded point while point 16 is the only one bounded.

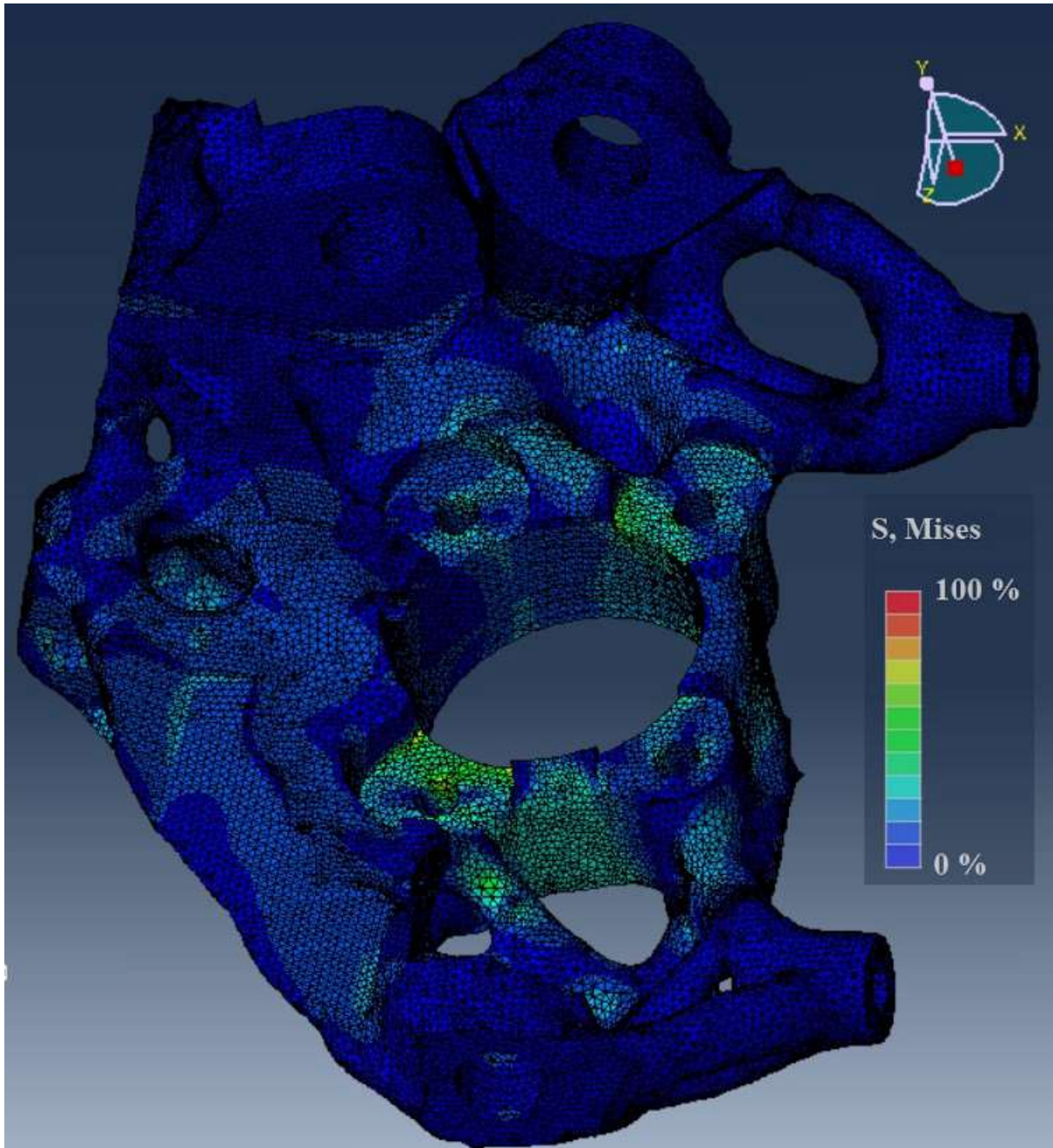


*Figure 4.46 – FEA results, general view.*

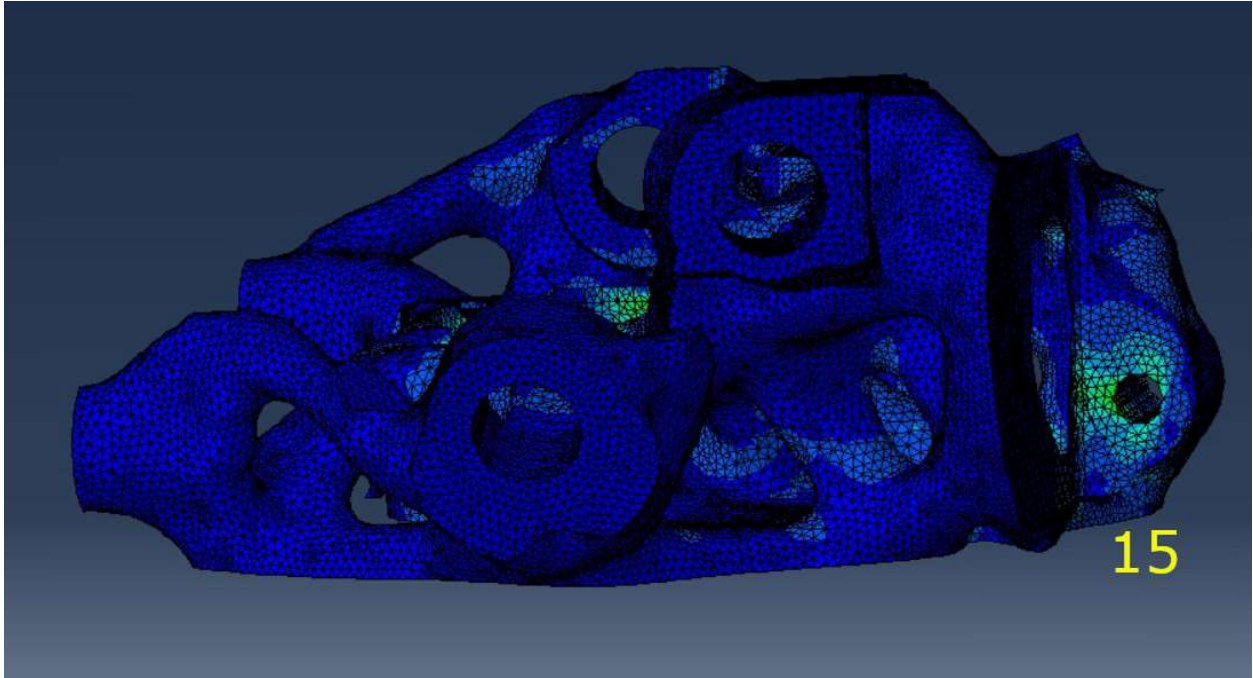


*Figure 4.47 – FEA results, view 1.*

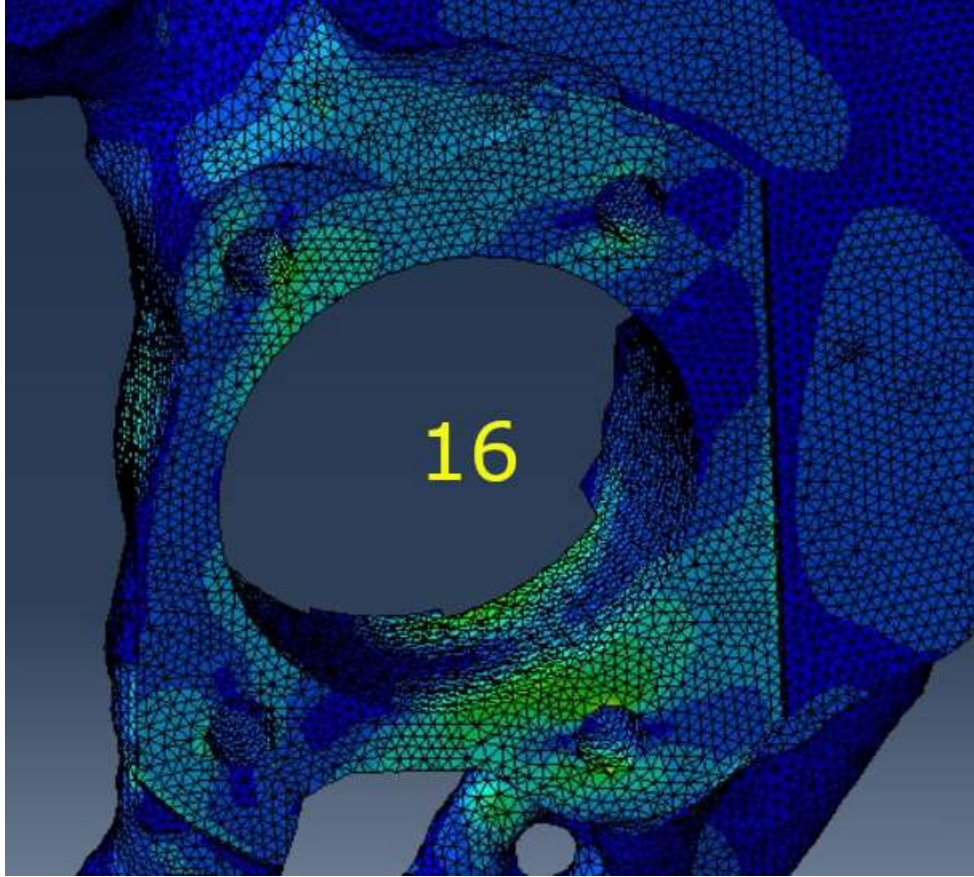


*Figure 4.48 – FEA results, view 2.*

## 5. Conclusions

### 5.1 Conclusions

This work has been performed to show the advantages and disadvantages of a complete series production of an automotive component.

The best advantage is the weight reduction: with topology optimization the weight has been reduced up to 84.3%: the initial component weighted 23 kg while the redesigned one weights 3.6 kg. Since every vehicle needs two front steering knuckles and two rear knuckles, the weight reduction can lead to a reduction of fuel consumption and pollutant emissions. Considering the weight reduction obtained, AM can be considered the best technology to produce this specific component.

Nowadays, the steering knuckle is produced thanks to the traditional manufacturing; the weight of the forged component is 4 kg. Due to AM, the redesign component weights 3.6 kg with a 10% weight reduction.

In conclusion, it is possible to say that the redesigned component leads to undoubted advantages in terms of quality and waste of material. Despite this, it should be taken in account that this component is not ready yet for serial production: nowadays, the effective production time in Additive Manufacturing is still too slow for industrial production. However, for small production, this solution could be seriously considered, for the advantages AM leads compared to conventional manufacturing.

In parallel with this work, another project has been developed: Topology Optimization on the same component has been performed using Maraging Steel instead of AlSi10Mg, in order to compare the results of the Topology Optimizations performed with two different materials.

## 5.2 Future developments

A recommendation for future developments could be to compare different Topology Optimization software available in the market. In this way it is possible to find the best solution, improving design and analyses, decreasing time and costs.

Furthermore, it could be interesting to manufacture some of these parts and test them, in order to compare the simulations with the behavior of the component in real situations. Furthermore, it could be possible to compare the test results of the components made in AlSi10Mg and Maraging steel, in order to establish which material responds better to this load cases.

Finally, an economic analysis may be possible in order to establish which component is more convenient from an economic point of view.

## Bibliography

- [1] D. Herzog, V. Seyda, E. Wycisk, and C. Emmelmann, “Additive manufacturing of metals,” *Acta Mater.*, vol. 117, pp. 371–392, 2016.
- [2] I. Gibson, D. W. Rosen, B. Stucker, and others, *Additive manufacturing technologies*, vol. 17. Springer, 2014.
- [3] G. Chiandussi, “Metodi di ottimizzazione applicati a problemi ingegneristici. Introduzione ai metodi di ottimizzazione,” 2017.
- [4] D. Brackett, I. Ashcroft, and R. Hague, “Topology optimization for additive manufacturing,” in *Proceedings of the solid freeform fabrication symposium, Austin, TX*, 2011, vol. 1, pp. 348–362.
- [5] Gornet, T. W. (2014). *History of additive manufacturing*. Wohlers Associates.
- [6] L. D. Sturm, C. B. Williams, J. A. Camelio, J. White, and R. Parker, “Cyber-physical vulnerabilities in additive manufacturing systems: A case study attack on the .STL file with human subjects”, *J. Manuf. Syst.*, vol. 44, pp. 154–164, 2017.
- [7] P. J. Bartolo, G. Mitchell. “Stereo-thermal-lithography: a new principle for rapid prototyping”, *J. Rapid Prototyping*, vol. 9.3, pp.150-156, 2003.
- [8] B. Lu and X. Tian, “Development Trends in Additive Manufacturing”, *Engineering*, vol. 1, Mar. 2015.
- [9] Autodesk, “<https://www.autodesk.com/redshift/history-of-3d-printing/>”.
- [10] M. Szilvsi-Nagy and G. Mátyási, “Analysis of STL files,” *Math. Comput. Model.*, vol. 38, no. 7, pp. 945–960, 2003.
- [11] K. Muita, M. Westerlund, and R. Rajala, “The Evolution of Rapid Production: How to Adopt Novel Manufacturing Technology,” *IFAC-PapersOnLine*, vol. 48, no. 3, pp. 32–37, 2015.
- [12] D. Bourell *et al.*, “Materials for additive manufacturing,” *CIRP Ann.*, vol. 66, no. 2, pp. 659–681, 2017.

- [13] T. D. Ngo, A. Kashani, G. Imbalzano, K. T. Q. Nguyen, and D. Hui, “Additive manufacturing (3D printing): A review of materials, methods, applications and challenges” *Compos. Part B Eng.*, vol. 143, pp. 172–196, 2018.
- [14] L. Iuliano, M. Galati, *Materiale didattico – Tecniche per la fabbricazione additiva*, 2017.
- [15] C. Y. Yap, C. K. Chua, Z. L. Dong, Z. H. Liu, D. Q. Zhang, L. E. Loh, and S. L. Sing, “Review of selective laser melting: Materials and applications” *Appl. Phys. Review*, vol. 2, 2015.
- [16] R. I. Campbell, D. Bourell, and I. Gibson, “Additive manufacturing: Rapid prototyping comes of age,” *Rapid Prototyp. J.*, vol. 18, Jun. 2012.
- [17] S. Huang, P. Liu, A. Mokasdar, and H. Liang, “Additive manufacturing and its societal impact: A literature review,” *Int. J. Adv. Manuf. Technol.*, vol. 67, Jul. 2012.
- [18] E. Brandl, U. Heckenberger, V. Holzinger, and D. Buchbinder, “Additive manufactured AlSi10Mg samples using Selective Laser Melting (SLM): Microstructure, high cycle fatigue, and fracture behavior,” *Mater. Des.*, vol. 34, pp. 159–169, 2012.
- [19] EOS Gmbh,  
[“https://cdn0.scrvt.com/eos/public/8837de942d78d3b3/4e099c3a857fdddca4be9d59fbb1cd74/EOS\\_Aluminium\\_AlSi10Mg\\_en.pdf”](https://cdn0.scrvt.com/eos/public/8837de942d78d3b3/4e099c3a857fdddca4be9d59fbb1cd74/EOS_Aluminium_AlSi10Mg_en.pdf).
- [20] G. Chiandussi, “Metodi di ottimizzazione applicati a problemi ingegneristici, Introduzione ai metodi di ottimizzazione,” 2018.
- [21] A. Clausen, “Topology Optimization for Additive Manufacturing.” Technical University of Denmark, Kgs. Lyngby, 2016.
- [22] M. P. Bendsoe and O. Sigmund, *Topology Optimization: Theory, Methods and Applications*. Springer, 2004.
- [23] E. Holmberg, B. Torstenfelt, and A. Klarbring, “Stress constrained topology optimization,” *Struct. Multidiscip. Optim.*, vol. 48, no. 1, pp. 33–47, 2013.
- [24] B. Babu, M. Prabhu, P. Dharmaraj, and R. Sampath, “Stress analysis on steering knuckle of the automobile steering system,” *Int. J. Res. Eng. Technol.*, vol. 3, no. 3, pp. 363–366, 2014.

- [25] E. A. Azrulhisham, Y. M. Asri, A. W. Dzuraidah, N. M. Nik Abdullah, A. Shahrum, and C. H. Che Hassan, "Evaluation of fatigue life reliability of steering knuckle using Pearson parametric distribution model," *Int. J. Qual. Stat. Reliab.*, vol. 2010, 2011.
- [26] P. Dumbre, A. K. Mishra, V. S. Aher, and S. S. Kulkarni, "Structural analysis of steering knuckle for weight reduction," *Int. J. Emerg. Technol. Adv. Eng.*, vol. 4, no. 6, pp. 552–557, 2014.
- [27] S. R. Gore, K. K. Gund, P. M. Patane, N. V. Mohite, and C. V. Chimote, "Topology Optimization of Automotive Steering Knuckle using Finite Element Analysis," *Int. J. Current Eng. Technol.*, vol. March 2017, pp. 122-125, 2017.
- [28] S. Srivastava, S. Pande, B. Kapadiya, and S. Salunkhe, "Topology optimization of steering knuckle structure," *Int. J. Simul. Multidiscip. Des. Optim.*, vol. 11, pp. 1–8, Jan. 2020.
- [29] M. P. Sharma, D. S. Mevawala, H. Joshi, D. A. Pate, "Static analysis of steering knuckle and its shape optimization," *J. Mech. Civil Eng.*, pp34-38, 2014.
- [30] R. Jaswadi, M. A. B. Marzuki, and F. Azmi, "Design Optimisation of Automotive Component through Numerical Investigation for Additive Manufacturing," vol. Vol. 6, pp. 19–26, May 2019.
- [31] G. K. Triantafyllidis, A. Antonopoulos, A. Spiliotis, S. Fedonos, and D. Repanis, "Fracture Characteristics of Fatigue Failure of a Vehicle's Ductile Iron Steering Knuckle," *J. Fail. Anal. Prev.*, vol. 9, no. 4, pp. 323–328, 2009.
- [32] G. I. N. Rozvany, "Aims, scope, methods, history and unified terminology of computer-aided topology optimization in structural mechanics," *Struct. Multidiscip. Optim.*, vol. 21, no. 2, pp. 90–108, 2001.